

Characterization of SRP RNA circularization and
Nudix hydrolase activity in the hyperthermophilic
archaeon *Sulfolobus acidocaldarius*

Dissertation

zur Erlangung des Doktorgrades

der Naturwissenschaften

(Dr. rer. nat.)

des Fachbereichs Biologie

der Philipps-Universität Marburg

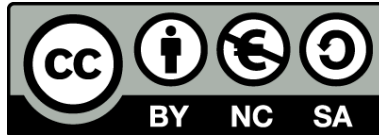
Vorgelegt von

Ruth Breuer

aus Neuwied am Rhein

Marburg (Lahn), September 2022

Originaldokument gespeichert auf dem Publikationsserver der
Philipps-Universität Marburg
<http://archiv.ub.uni-marburg.de>



Dieses Werk bzw. Inhalt steht unter einer
Creative Commons
Namensnennung
Keine kommerzielle Nutzung
Weitergabe unter gleichen Bedingungen
3.0 Deutschland Lizenz.

Die vollständige Lizenz finden Sie unter:
<http://creativecommons.org/licenses/by-nc-sa/3.0/de/>

Die Arbeit zur vorliegenden Dissertation wurde von Oktober 2018 bis September 2022 unter der Betreuung von Herrn Prof. Dr. Lennart Randau an der Philipps-Universität Marburg und dem Max-Planck-Institut für Terrestrische Mikrobiologie Marburg in der Arbeitsgruppe „Prokaryotic RNA Biology“ angefertigt.

Vom Fachbereich Biologie der Philipps-Universität Marburg (Hochschulkennziffer 1180) als Dissertation angenommen am 21.11.2022.

Erstgutachter(in): Prof. Dr. Lennart Randau

Zweitgutachter(in): Prof. Dr. Michael Bölker

Tag der Disputation: 30.11.2022

Erklärung

Ich versichere, dass ich meine Dissertation mit dem Titel „**Characterization of SRP RNA circularization and Nudix hydrolase activity in the hyperthermophilic archaeon *Sulfolobus acidocaldarius***“ selbstständig und ohne unerlaubte Hilfe angefertigt und mich dabei keiner anderen als der von mir ausdrücklich bezeichneten Quellen und Hilfsmittel bedient habe.

Diese Dissertation wurde in der jetzigen oder einer ähnlichen Form noch bei keiner anderen Hochschule eingereicht und hat noch keinen sonstigen Prüfungszwecken gedient.

Marburg, den 29.09.2022

Ruth Breuer

Statement on the contribution to publications in this dissertation

I declare that this thesis was composed by myself and without external assistance. I confirm that the work presented has not been submitted for any other degree or professional qualification. I also declare that I have not made any prior doctoral attempt.

Furthermore, I confirm that no sources other than those indicated have been used and that appropriate credit has been given within this thesis where reference has been made to the work of others.

I confirm that the work submitted is my own, except where explicitly stated otherwise in the text or where work that has formed part of jointly-authored publications has been included. My contribution to this work has been explicitly stated below.

Marburg, 29.09.2022

Ruth Breuer

Teile dieser Arbeit sind in folgenden Artikeln veröffentlicht:

Gomes-Filho JV, **Breuer R**, Morales-Fillooy HG, Pozhydaieva N, Börst A, Paczia N, Soppa J, Höfer K, Jäschke A and Randau L (2022) Identification of NAD-RNAs and ADPR-RNA decapping in the archaeal model organisms *Sulfolobus acidocaldarius* and *Haloferax volcanii* (submitted)

Weitere Publikationen:

Breuer R, Gomes-Filho J-V and Randau L (2021) Conservation of Archaeal C/D Box sRNA-Guided RNA Modifications. *Frontiers in Microbiology* 12:654029. doi:10.3389/fmicb.2021.654029

Table of Contents

I	Abbreviations	I
II	Summary	II
III	Zusammenfassung	III
1	Introduction	1
1.1	Overview of RNA thermal stabilization in Archaea	1
1.2	Structural stabilization by circularization.....	3
1.3	A circular SRP RNA in <i>Thermoproteus tenax</i>	4
1.4	Chemical stabilization via 5'-terminal capping.....	6
1.5	Nudix hydrolases and their implications in RNA decapping.....	9
1.6	Aims of the Project.....	12
2	Results	14
2.1	Circular SRP RNA design and transformation	14
2.2	Identification of the circular SRP RNA.....	14
2.3	Processing of the permuted SRP RNA gene	17
2.4	Replacing the original SRP RNA gene	19
2.5	<i>In silico</i> characterization of potential decapping enzymes	21
2.5.1	Candidate protein identification and sequence analysis	21
2.5.2	Structural predictions.....	21
2.6	<i>In vitro</i> characterization	22
2.6.1	Recombinant protein expression and purification	22
2.6.2	Decapping assays	25
2.6.3	Malachite Green assays.....	28
2.7	<i>In vivo</i> characterization.....	31
2.7.1	Generation of Nudix deletion strains.....	31
2.7.2	Phenotypical analysis.....	33
2.8	Transcriptome Analysis.....	38
3	Discussion	49
3.1	Designing a circular SRP RNA for <i>S. acidocaldarius</i>	49
3.2	Evolutionary implications of a permuted SRP RNA gene	52
3.3	Experimental analysis of the archaeal Nudix family hydrolases	54
3.4	<i>In vivo</i> characterization and transcriptome analysis	60
3.5	Conclusion and Outlook	66
4	Material and Methods	68
4.1	Materials, instruments and consumables.....	68
4.1.1	Chemicals, kits and enzymes	68
4.1.2	Instruments	70

4.1.3	Buffers and Solutions	72
4.2	Strains and Culture Conditions	72
4.2.1	Strains.....	72
4.2.2	Culture conditions for <i>Escherichia coli</i>	72
4.2.3	Culture conditions for <i>Sulfolobus acidocaldarius</i>	73
4.2.4	Growth Curves for <i>S. acidocaldarius</i>	73
4.2.5	Heat shock spotting assay for <i>S. acidocaldarius</i>	74
4.3	Plasmids and oligonucleotides	75
4.3.1	Progenitor plasmid and constructed recombinant vectors.....	75
4.3.2	Oligonucleotides.....	77
4.4	Molecular working with DNA	82
4.4.1	DNA isolation	82
4.4.1.1	Genomic DNA isolation from <i>S. acidocaldarius</i>	82
4.4.1.2	Isolation of plasmid DNA from <i>E. coli</i>	83
4.4.2	DNA quantitation	83
4.4.2.1	Spectrophotometric DNA quantitation and quality control	83
4.4.2.2	Fluorometric quantitation	83
4.4.3	Polymerase chain reaction (PCR)	83
4.4.3.1	Amplification of genomic and plasmid DNA	83
4.4.3.2	Colony PCR	84
4.4.3.3	Site-directed mutagenesis PCR	84
4.4.4	DNA electrophoresis	85
4.4.5	DNA purification	85
4.4.5.1	Purification of PCR reactions.....	85
4.4.5.2	Gel extraction from agarose gels.....	85
4.4.6	Hybridization of DNA oligonucleotides.....	85
4.4.7	Enzymatic modification of DNA	85
4.4.7.1	Restriction	85
4.4.7.2	Dephosphorylation	86
4.4.7.3	Ligation	86
4.4.8	TOPO-Cloning.....	86
4.4.9	Gibson Assembly	86
4.4.10	Transformation	87
4.4.10.1	Preparation of chemically competent <i>E. coli</i> cells	87
4.4.10.2	Transformation of <i>E. coli</i>	87
4.4.10.3	Preparation of electrocompetent <i>S. acidocaldarius</i> cells.....	88
4.4.10.4	Transformation of <i>S. acidocaldarius</i>	88
4.4.11	Gene deletion and gene exchange in <i>S. acidocaldarius</i>	89

4.4.12	Sequencing	90
4.5	Molecular working with RNA	90
4.5.1	Treatment of solutions, glassware and other equipment.....	90
4.5.2	Isolation of total RNA from <i>S. acidocaldarius</i>	90
4.5.3	RNA quantitation	90
4.5.3.1	Spectrophotometric RNA quantitation and quality control.....	90
4.5.3.2	Fluorometric quantitation.....	90
4.5.4	Inverse reverse transcription PCR.....	91
4.5.5	<i>In vitro</i> transcription of differently 5'-capped RNA.....	91
4.5.6	RNA sequencing	91
4.5.6.1	Detection of the circular SRP RNA.....	91
4.5.6.2	Transcriptomic analysis of Nudix deletion strains	92
4.6	Biochemical methods	93
4.6.1	Heterologous production of <i>S. acidocaldarius</i> proteins in <i>E. coli</i>	93
4.6.2	Expression and purification of <i>S. acidocaldarius</i> proteins in <i>E. coli</i>	93
4.6.3	Cell-free <i>in vitro</i> protein synthesis.....	94
4.6.4	Expression and purification of human NudT5	94
4.6.5	SDS-polyacrylamide gel electrophoresis	95
4.6.6	Fluorometric protein quantitation	95
4.6.7	Splicing Assays	96
4.6.8	Decapping assays	97
4.6.9	Malachite Green Assays	97
4.7	Bioinformatical methods	98
4.7.1	Analysis of Illumina RNA-Seq data.....	98
5	References.....	99
6	Appendix.....	114
6.1	Supplementary Material	115
6.2	Abgrenzung der Eigenleistung.....	121
6.3	Curriculum Vitae	122
6.4	Acknowledgements.....	124

I Abbreviations

% (v/v)	percent by volume	l	liter
% (w/v)	percent by weight	LB	lysogeny broth
Δ	gene deletion	μ	micro (10^{-6})
×g	gravitational acceleration	m	meter
5-FOA	5-fluorotic acid	M	molar (mol/l)
6-FAM	6-carboxyfluorescein	max.	maximum
ADPR	adenosine diphosphate ribose	MCS	multiple cloning site
AP	alkaline phosphatase	min.	minute(s)
Ap4A	diadenosine tetraphosphate	mRNA	messenger RNA
APB	acrylamidophenyl boronic acid	n	nano (10^{-9})
approx.	approximately	NAD	nicotinamide adenine dinucleotide
APS	ammonium persulfate	Ni-NTA	nickel-nitrilotriacetic acid
arCOG	archaeal cluster of orthologous genes	NMN	nicotinamide mononucleotide
ATP	adenosine triphosphate	Np _n N	dinucleoside polyphosphate
BLAST	basic local alignment search tool	nt	nucleotide
bp	base pair	N-terminal	amino-terminal
Cas	CRISPR-associated protein	OD	optical density
cDNA	complementary DNA	ORF	open reading frame
CoA	coenzyme A	p	pico (10^{-12})
CRISPR	clustered regularly interspaced short palindromic repeats	PAA	polyacrylamide
C-terminal	carboxy-terminal	PAGE	polyacrylamide gel electrophoresis
CTP	cytidine triphosphate	PCR	polymerase chain reaction
dATP	deoxyadenosine triphosphate	pH	potential of hydrogen
DEPC	diethyl pyrocarbonate	PPase	pyrophosphatase
dGTP	deoxyguanosine triphosphate	pre-rRNA	precursor rRNA
DNA	deoxyribonucleic acid	RBP	RNA-binding protein
DNase	desoxyribonuclease	RNA	ribonucleic acid
dNTP	deoxyribonucleoside triphosphate	RNAP	RNA polymerase
dpCoA	dephospho-coenzyme A	RNase	ribonuclease
dsDNA	double-stranded DNA	RNA-seq	RNA-sequencing
dsRNA	double-stranded RNA	RNP	ribonucleoprotein
DTT	dithiothreitol	rpm	revolutions per minute
DUF	domain of unknown function	rRNA	ribosomal RNA
e.g.	for example ("exempli gratia")	RT	room temperature
EDTA	ethylene-diamine-tetraacetic acid	SDS	sodium dodecyl sulfate
et al	and other ("et alteri")	sec	second(s)
FAD	flavin adenine dinucleotide	sRNA	small RNA
g	gram	SRP	signal recognition particle
GOI	gene of interest	ssDNA	single-stranded DNA
GTP	guanosine triphosphate	TAE	tris-acetate EDTA buffer
h	hour(s)	TBE	tris-borate EDTA buffer
HEPES	2-(4-(2-hydroxyethyl)-1-piperazinyl)- ethanesulfonic acid	TEMEDN,N,N',N'	tetramethylethylenediamine
i.e.	that is ("id est")	T _m	melting temperature
IPTG	isopropyl-β-d-1-thiogalactopyranoside	Tris	tris-(hydroxymethyl)-aminomethane
kb	kilobases	tRNA	transfer RNA
kDa	kilo Dalton	UTP	uridine triphosphate
KO	knock-out	V	Volt
		WT	wild-type

II Summary

Thermophilic archaea inhabit some of the most extreme environments on this planet. In adapting to their habitats, they have evolved numerous mechanisms to ensure the functionality of RNA molecules that are essential for key biological processes. This work describes the characterization of (i) the circularization of the universal signal recognition particle (SRP) RNA and (ii) the activities of a family of hydrolases suspected to play a role in non-canonical RNA decapping. The hyperthermophilic organism *Thermoproteus tenax* possesses a permuted SRP RNA gene whose transcript is processed by the tRNA splicing machinery into a circular SRP RNA proposed to possess elevated thermal stability due to its circular nature. To imitate a proposed genomic rearrangement event, a synthetic, permuted SRP RNA gene was implemented in the related thermophile *Sulfolobus acidocaldarius*, which contains a conventional SRP RNA gene. We show that *S. acidocaldarius* is capable of generating a circular SRP RNA from the synthetic gene variant, however swapping original and permuted gene variants was unsuccessful. Following the discovery of 5'-NAD-RNA in Archaea, this work investigates all four Nudix family hydrolases of *S. acidocaldarius* to uncover their RNA decapping potential. The recombinant proteins were produced and purified, but did not show activity against 5'-NAD-RNA. Instead, the protein SACI_RS00060, a putative ADPR-pyrophosphatase, revealed 5'-ADPR-RNA decapping activity *in vitro* and is suggested to play a role in the protection against thermal degradation of NAD(-RNA). In agreement, SACI_RS00060 also hydrolyzed free ADPR and was renamed Saci_NudT5. Analysis of the substrate preferences of the other Nudix proteins showed that SACI_RS00730 hydrolyzes the dinucleoside polyphosphate Ap4A and SACI_RS00575 exhibits strong preference for guanosine-based substrates. While deletions of the respective Nudix genes did not elicit a distinct phenotype under nutrient limitation or heat stress conditions, transcriptomic analyses of the Nudix deletion strains revealed a large variety of affected cellular processes, most likely due to effects on transcriptional regulators. Notably, the Nudix deletion transcriptomes resemble those of samples taken under heat stress and nutrient-limited conditions. The results of this work predict a connection of at least one Nudix hydrolase to heat stress response in *S. acidocaldarius*. In conclusion, this work provides first insights into specific substrate activities for each Nudix protein and lays the groundwork for the analysis of their impact on the metabolism of *S. acidocaldarius*.

III Zusammenfassung

Thermophile Archaeen bewohnen einige der extremsten Lebensräume unseres Planeten. Durch Anpassung an ihre jeweiligen Habitate haben sie zahlreiche Mechanismen entwickelt, welche die Funktionalität von RNA-Molekülen in lebenserhaltenden biologischen Prozessen sichern. Diese Arbeit widmet sich i) der Zirkularisierung der universellen Signalerkennungspartikel-RNA (signal recognition particle (SRP) RNA) und ii) der Aktivität einer Familie von Hydrolasen welche mutmaßlich eine Rolle bei der Entfernung nicht-kanonischer RNA-Kappen spielen. Der hyperthermophile Organismus *Thermoproteus tenax* besitzt ein permutiertes SRP RNA-Gen, dessen Transkript durch die Aktivität der tRNA-Splicing-Maschinerie zu einer zirkulären SRP RNA mit vermutlich erhöhter thermischer Stabilität verarbeitet wird. Um eine Umlagerung im Genom zu imitieren, wurde ein synthetisches, permutiertes SRP RNA-Gen in den nahe verwandten thermophilen Organismus *Sulfolobus acidocaldarius* eingeführt, der ein konventionelles SRP RNA-Gen besitzt. Wir zeigen, dass *S. acidocaldarius* in der Lage ist eine zirkuläre SRP RNA aus der synthetischen Genvariante herzustellen, der Austausch der ursprünglichen und der permutierten Variante blieb jedoch erfolglos. Im Anschluss an die Entdeckung von 5'-NAD-RNA in Archaeen untersucht diese Arbeit alle vier Nudix-Hydrolasen in *S. acidocaldarius* hinsichtlich ihres Potenzials zum Entfernen von RNA-Kappen. Die rekombinanten Proteine wurden produziert und aufgereinigt, zeigten jedoch keine Aktivität gegenüber 5'-NAD-RNA. Stattdessen zeigte das Protein SACI_RS00060, eine mutmaßliche ADPR-Pyrophosphatase, Aktivität gegenüber 5'-ADPR-RNA *in vitro* und weist somit hin auf eine Rolle beim Schutz gegen die hitzebedingte Degradierung von (NAD-) RNA. SACI_RS00060 hydrolysierte zudem freies ADPR und wurde dementsprechend in Saci_NudT5 umbenannt. Eine Analyse der Substrat-Präferenzen der anderen Nudix-Proteine zeigte, dass SACI_RS00730 das Dinucleosid-Polyphosphat Ap4A hydrolysiert und SACI_RS00575 eine starke Präferenz für Guanosin-basierte Substrate besitzt. Während Deletionen der entsprechenden Nudix-Gene unter Hitze- oder Nährstoffstress keinen eindeutigen Phänotyp hervorriefen, zeigten Transkriptomanalysen der Nudix-Deletionsstämme eine Vielzahl betroffener zellulärer Prozesse auf, vermutlich infolge von Auswirkungen auf ihre Transkriptionsregulatoren. Bemerkenswerterweise ähneln die Transkriptome der Nudix-Deletionsstämme Proben welche unter Hitzestress oder Nährstoffmangel genommen wurden. Die Ergebnisse dieser Arbeit prognostizieren die Verbindung

wenigstens einer Nudix-Hydrolase zur Hitzestress-Antwort in *S. acidocaldarius*. Zusammenfassend liefert diese Arbeit erste Einblicke in die spezifischen Substrataktivitäten jedes Nudix-Proteins und bildet die Grundlage für eine Analyse ihrer Auswirkungen auf den Stoffwechsel von *S. acidocaldarius*.

1 Introduction

1.1 Overview of RNA thermal stabilization in Archaea

Extremophiles have always held a special fascination for the scientific community, ever since it was discovered that even such hostile environments as hot acid springs or deep-sea vents are filled with life. It is intriguing to uncover the metabolic innovations with which extremophiles maintain their integral cellular processes and adapt to highly challenging environments. A large part of extremophilic organisms belongs to the domain of Archaea. Initially believed to belong to the Bacteria, analyses of 16S ribosomal RNA sequences led to the establishment of the Archaea as the third domain of life (Woese & Fox, 1977; Woese et al., 1990). Within this domain, the Thaumarchaeota, Aigarchaeota, Korarchaeota and Crenarchaeota form the TACK superphylum which is known to share several features with Eukaryotes, e.g. regarding their transcription, translation and replication machineries, as well as genomic signatures (Guy & Ettema, 2011). In fact, Eukaryotes are believed to have evolved from an archaeal ancestor, and this relationship was further strengthened by the discovery of the Lokiarchaeota and related Archaea from the Asgard superphylum (Spang et al., 2015; Zaremba-Niedzwiedzka et al., 2017). An organism that quickly established itself as a popular archaeal model organism is the thermoacidophilic organism *Sulfolobus acidocaldarius* which belongs to the Crenarchaeota and naturally occurs in acidic hot springs and thermal soils in the United States of America, El Salvador, Dominica and Italy. Its growth optimum lies in a temperature range of 75-80°C and a pH range of 2-3 (Brock et al., 1972). This work uses the *S. acidocaldarius* strain DSM639 (MW001 variant) which was isolated from Locomotive Spring in the Yellowstone National Park, USA (Brock et al., 1972). The strain DSM639 MW001 is uracil auxotroph, which enables the use of uracil as a positive selection marker and counterselection with 5-fluorotic acid (5-FOA) (Wagner et al., 2012). Furthermore, *S. acidocaldarius* possesses two CRISPR-Cas systems, a Type I-A and a Type III-B system, which can be exploited to generate markerless deletion mutants and are part of a well-established tool box for genetic manipulation in this organism (Daume, 2017; Yingjun Li et al., 2016; Wagner et al., 2012). Growth temperatures for *Sulfolobus* habitats range between 75-85°C and as such remain well below the highest ever reported temperatures to still maintain life, that is 122°C and 130°C for *Methanopyrus kandleri* and the unclassified archaeal “strain 121”, respectively (Kashefi & Lovley,

2003; Takai et al., 2008). Hyperthermophilic archaea are required to adapt their metabolism to these life-threatening conditions and require special mechanisms to stabilize their macromolecules. The following sections will focus on mechanisms of stabilizing RNA molecules.

First, RNA stabilization can be achieved by the formation of structured regions with GC base pairs, which seemingly contradicts the observation of AT-rich genomes for many hyperthermophiles (Gomes-Filho et al., 2018; Klein et al., 2002). Notably, GC-rich regions and RNA duplex formation often pose a key signature for non-coding RNAs (Klein et al., 2002; Miralles, 2010; Schattner, 2002). Notably, to date no protein with a dsRNA-degrading RNase III domain has been identified in Archaea, suggesting RNA duplex formation as a stabilization strategy in these organisms (Gomes-Filho et al., 2018). Furthermore, RNA stability can be achieved by protein binding. In Archaea, two prominent families of RNA-binding proteins (RBPs) are the L7Ae/L30 protein family (L30e in Eukaryotes) and the Lsm protein family (Hfq in Bacteria, Sm/Lsm in Eukaryotes) (Achsel et al., 2001; Kuhn et al., 2002). The L7Ae proteins recognize a structural motif called “kink-turn” (k-turn) and interact with more than one hundred RNA molecules, encompassing many small RNAs (sRNAs) such as C/D box sRNAs, non-coding RNAs like the RNase P RNA and signal recognition particle (SRP) RNA and multiple messenger RNAs (mRNAs), including its own transcript (Daume et al., 2017; Lai et al., 2014; Rozhdestvensky et al., 2003). The Lsm proteins exhibit affinity for single-stranded poly-U or poly-A stretches near the 3' end of various RNAs and interact predominantly, though not exclusively, with non-coding RNAs such as transfer RNAs (tRNAs), ribosomal RNAs (rRNAs) and other sRNAs (Achsel et al., 2001; Fischer et al., 2010; Märtens, Hou, et al., 2017; Märtens, Sharma, et al., 2017). Another notable structural feature to increase stability is the circularization of the RNA molecule. Here, free termini are eliminated through ligation and become inaccessible to enzymatic or thermal degradation (Becker et al., 2017; Danan et al., 2012; Plagens et al., 2015). Increased stability can also be achieved by chemical modification of the nucleobases, either internally by addition of methyl groups and pseudouridylation or at the terminus by addition of a cofactor derivative or nucleoside metabolite as a cap-like structure (Höfer & Jäschke, 2018). Two such features, namely structural stabilization by circularization and stabilization by capping, will be the focus of the following work.

1.2 Structural stabilization by circularization

One mechanism to achieve improved stability of an RNA molecule is its circularization, of which there are several examples to be found in the archaeal domain. Specifically, a majority of circular RNAs occurs in non-coding RNA classes, such as tRNA and rRNA introns and 23S and 16S rRNA processing intermediates (Birkedal et al., 2020; Danan et al., 2012; Jüttner et al., 2020; Tang et al., 2002). In the case of rRNA processing intermediates, the rRNAs are excised as circular pre-rRNAs from a long RNA precursor molecule before being processed into mature rRNAs (Birkedal et al., 2020; Tang et al., 2002). Circular RNA forms are furthermore found among C/D box sRNAs, although their role and evolution, as well as the exact method of circularization, remains to be uncovered (Danan et al., 2012; Randau, 2012; Starostina et al., 2004; Su et al., 2013). Notably, in the hyperthermophilic organisms *Pyrococcus abyssi* and *Saccharolobus solfataricus* the number of circular C/D box sRNAs outweighs the linear forms (Becker et al., 2019). Circular RNA molecules were furthermore identified among coding RNAs, RNase P RNA and non-coding RNAs which potentially target two transposon open reading frames (ORFs), suggesting regulation of their activity (Becker et al., 2019; Danan et al., 2012).

While circular RNA biogenesis can be the result of a self-splicing event or the activity of ATP-dependent RNA ligases, a third mechanism relies on the activity of the tRNA splicing machinery (Becker et al., 2017; Gu et al., 2016; Y. Wang & Wang, 2015). This activity is essential for the processing of intron-containing tRNAs. These are present for example in *S. acidocaldarius* (21/50 tRNA genes) and its close relative, the hyperthermophilic archaeon *Thermoproteus tenax* (46/46 tRNA genes), whose genome contains the same number of tRNA introns as tRNA genes, since several genes carry more than one intron (24 tRNA genes with one intron, 11 tRNA genes with two introns, 11 tRNA genes without introns) (Chan & Lowe, 2009; Sugahara et al., 2008). Due to the essentiality of tRNAs to the translation process, the organism consequently relies on an efficient mechanism for intron excision. To this end, the tRNA genes are transcribed into precursor tRNAs which exhibit a conserved structural feature called the bulge-helix-bulge (BHB) motif, consisting of a central 4 bp-helix, flanked by two 3 nt-bulges (Figure 1.1) (Kaine et al., 1983). The archaeal tRNA-splicing endonuclease recognizes this motif and cleaves at specific positions within the two bulges (Figure 1.1) (Marck & Grosjean, 2003; Thompson & Daniels, 1988).

The free termini are subsequently annealed by the conserved tRNA ligase RtcB and the anticodon loop is formed (Englert et al., 2011). This process of structural motif formation, recognition, cleavage and subsequent ligation occurs for *cis*-splicing as well as *trans*-splicing where tRNA genes are split into gene halves with complementary terminal sequences and scattered throughout the genome, as observed in *Nanoarchaeum equitans* (Randau, Münch, et al., 2005). While the BHB motif is not present in circular C/D box sRNAs whose maturation remains largely elusive, it is found in the processing stem of rRNAs and its structural integrity is essential to their maturation process via the formation of circular pre-rRNA intermediates (Jüttner et al., 2020; Starostina et al., 2004).

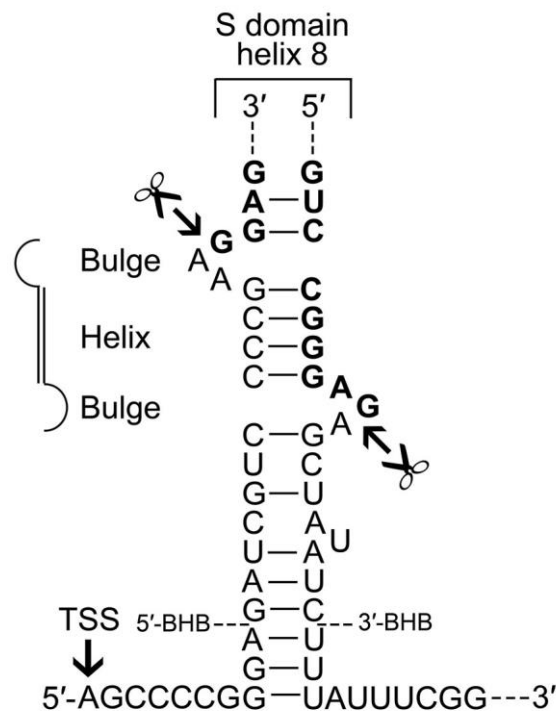


Figure 1.1: Sequence and structure of the bulge-helix-bulge (BHB) motif as present in helix 8 of the S domain of the precursor SRP RNA of *Thermoproteus tenax*. The motif consists of a 4 bp-helix flanked by two 3 nt-bulges. The *T. tenax* tRNA splicing endonuclease cleaves the RNA at specific positions, as indicated in the figure. Figure adapted from Plagens et al., 2015.

1.3 A circular SRP RNA in *Thermoproteus tenax*

In *Thermoproteus tenax* this mechanism is used not only for tRNA-intron removal or rRNA maturation, but also for the processing of the SRP RNA, another essential non-coding RNA. Archaeal signal recognition particles (SRPs) consist of an approx. 300 nt-long SRP RNA as well as the proteins SRP54, SRP19 and L7Ae (Bhuiyan et al.,

2000; Daume et al., 2017). Usually, the RNA component is a linear molecule with eight helical elements (h1 – h8) forming a smaller Alu domain and a larger S domain (Figure 1.2A). The S domain harbors the SRP protein binding sites and is connected to the Alu domain by an extended linker region (Batey et al., 2000; Gundelfinger et al., 1983; Zwieb et al., 2005). The standard termini are located in the duplex region of helix 1. SRP19 binds to the tips of helices 6 and 8 in the S domain, leading to the formation of a strictly conserved tertiary RNA interaction and exposing the SRP54 binding site in helix 8 (Figure 1.2A) (Hainzl et al., 2002; Rose & Weeks, 2001).

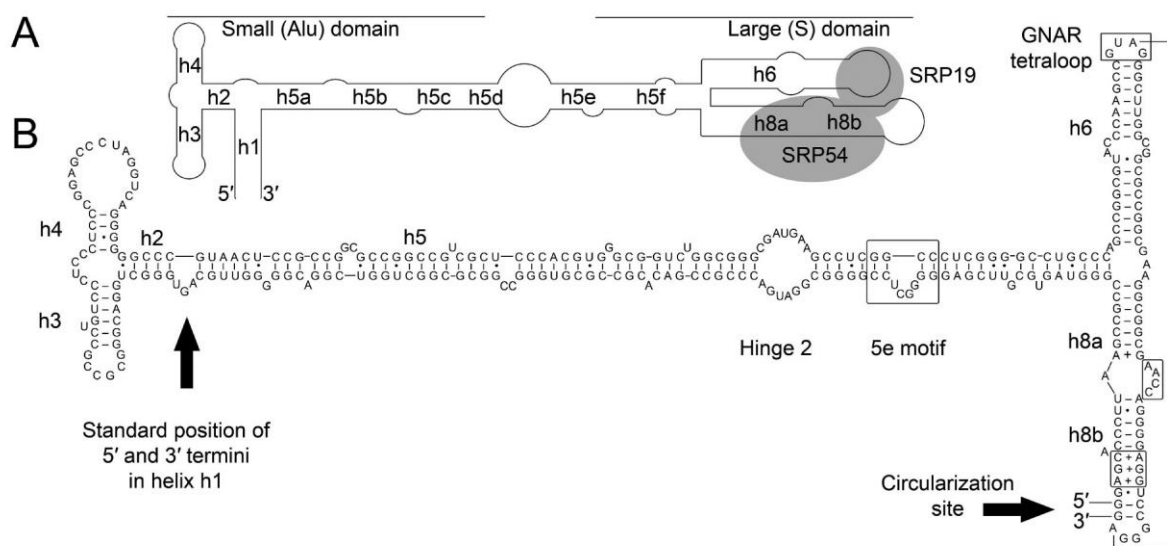


Figure 1.2: The signal recognition particle RNA (SRP RNA) of *Thermoproteus tenax*. (A) Schematic representation of the secondary structure of canonical archaeal SRP RNAs. Indicated are the approximate positions of the helices 1-8, the small and large domains and the protein binding sites of SRP19 and SRP54. The standard 5' and 3' termini are located in helix 1. (B) Sequence and structure of the circular SRP RNA in *T. tenax*. Indicated are conserved features and tertiary interactions. The 5' and 3' termini are located in helix 8, as indicated by a black arrow. Figure from Plagens et al., 2015.

Interestingly, some *Thermoproteus* species (e.g. *T. tenax* and *T. uzoniensis*) do not contain canonical SRP RNAs (Siebers et al., 2011). Instead, the SRP RNA of *T. tenax* exhibits its 5' and 3' termini in helix 8, while helix 1 is missing altogether (Figure 1.2B). Consequently, the SRP RNA gene exhibits a permutation and the 3' portion of the gene is located upstream of the 5' portion (Plagens et al., 2015). As the termini are located close to the functionally important loop in helix 8, restoration of this loop by termini ligation is essential. In fact, lack of SRP RNA circularization impairs SRP

protein binding (Plagens et al., 2015). To this end, the primary SRP RNA transcript contains a 23 nt-long leader sequence which, together with the extended trailer sequence, folds into a BHB motif (Figure 1.1). Furthermore, it was experimentally proven that the tRNA splicing endonuclease from *T. tenax* can cleave this non-tRNA BHB motif *in vitro* (Plagens et al., 2015). Subsequent ligation of the SRP RNA termini leading to circularization of the molecule is assumed to be conducted by the tRNA ligase RtcB (Englert et al., 2011). In the case of the *T. tenax* SRP RNA, circularization is not only essential to restore the functionally important loop in helix 8 and to ensure protein binding, but also to compensate for the loss of helix 1. Helix 1 is assumed to prevent the unfolding of the SRP RNA in the extreme growth conditions of hyperthermophiles and circularization conveys the necessary thermal stability (Plagens et al., 2015; Zwieb et al., 2005).

1.4 Chemical stabilization via 5'-terminal capping

Over the years, many discoveries have been made regarding the chemical modification of RNA and accumulated a set of over 200 known modifications in all domains of life (Boccaletto et al., 2022). The modifications are generally categorized into internal and 5'-terminal modifications, with the former representing the largest and most diverse group (Helm & Alfonzo, 2014; Höfer & Jäschke, 2018). Among all RNA classes, most modifications are carried by tRNAs (Lorenz et al., 2017). In the archaeal domain, the two most abundant internal RNA modifications, 2'-O-methylation and pseudouridylation (Figure 1.3), are conducted in a manner dependent on non-coding RNAs called C/D box and H/ACA box sRNAs, respectively (Ganot et al., 1997; Gaspin et al., 2000; Kiss-László et al., 1996; Ni et al., 1997; Omer et al., 2000). C/D box sRNAs are 50-60 nt-long RNAs named after their conserved sequence motifs termed C/C' boxes (5'-RUGAUGA-3') and D/D' boxes (5'-CUGA-3') (Dennis & Omer, 2005; Kiss-Laszlo et al., 1998). They form a ribonucleoprotein (RNP) complex with the archaeal proteins L7Ae, Nop5 and the methyltransferase fibrillarlin which places the methyl group at the 2'-moiety of the respective ribose of the target nucleotide (Aittaleb et al., 2003; Omer et al., 2002; W. Wang et al., 2001). 2'-O-methylations are suggested to increase the stability of rRNAs and tRNAs by increasing RNA rigidity as well as preventing hydrolysis (Dennis et al., 2015; Yip et al., 2013). Identification of methylation hotspots in the core of the archaeal ribosome, as well as increased

occurrence of both methylation sites and C/D box sRNAs in thermophilic Archaea support this theory (Dennis et al., 2015; Noon et al., 1998). Furthermore, C/D box sRNAs were proposed to function as RNA chaperones, following the discovery that their dual guides often target sequences located in close spatial proximity (Dennis et al., 2015). Archaeal H/ACA box sRNAs exhibit a single stem followed by either a single-stranded H box (5'-ANANNA-3') or an ACA box (5'-ACA-3') (Yip et al., 2013). The H/ACA box RNP consists of the proteins L7Ae, Nop10, Gar1 and the pseudouridine synthase Cbf5 (Baker et al., 2005; Charpentier et al., 2005). Pseudouridylation is another known mechanism to achieve RNA stabilization; not only does its loss in rRNAs impair translation, but it can convert nonsense into sense codons (Karijolich & Yu, 2011; Kierzek et al., 2014; Liang et al., 2009). Nevertheless, in archaeal rRNAs pseudouridylation sites are greatly surpassed by sites of 2'-O-methylations (Decatur & Fournier, 2002; Noon et al., 1998; Ofengand & Bakin, 1997; Yip et al., 2013).

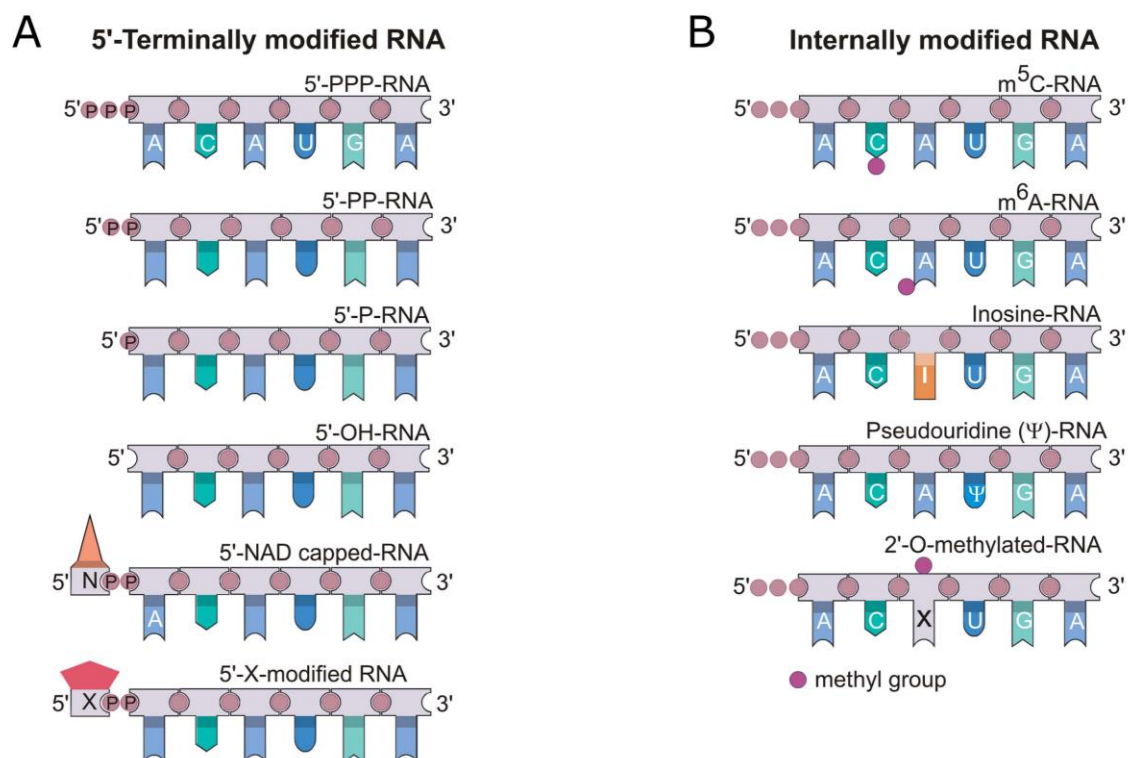


Figure 1.3: RNA modifications in Bacteria and Archaea. A) 5'-terminal modifications found on prokaryotic RNA, with X representing larger molecules, i.e. nucleoside derivatives or sugar metabolites, such as dpCoA, FAD or ADPR. B) Examples for internal modifications found in prokaryotic RNA. Figure adapted from Höfer & Jäschke, 2018.

The first known RNA cap was the 5'-5' linked N⁷-methyl guanosine (m⁷G) cap located at the 5' end of eukaryotic mRNAs, mediating their translation and stability (Furuichi et al., 1975; Furuichi et al., 1977; Wei et al., 1975). As this cap was not found in prokaryotes, they were believed to possess uncapped 5'-triphosphorylated (ppp)-RNA, 5'-monophosphorylated (p)-RNA and 5'-hydroxylated (OH)-RNA (Figure 1.3). This belief was disbanded by the discoveries of RNA 5'-capped with nicotinamide adenine dinucleotide (NAD⁺, from here on NAD) and dephospho-coenzyme A (dpCoA) in *Escherichia coli* and *Streptomyces venezuelae* (Figure 1.3) (Chen et al., 2009; Kowtoniuk et al., 2009). While the 5'-dpCoA-capped RNAs were found among further uncharacterized sRNAs in *E. coli*, NAD was found to be a 5' cap for regulatory sRNAs and mRNAs, but not rRNAs or tRNAs (Cahová et al., 2015). Later, NAD caps were also found on specific mRNAs in yeast, as well as mRNAs and sRNAs in mammalian cells (Jiao et al., 2017; Walters et al., 2017). Furthermore, methylated and non-methylated dinucleoside polyphosphates (Np_nNs) were identified at the 5' ends of *E. coli* RNA and suggested to provide stability against enzymatic degradation (Hudeček et al., 2020). This type of capping was found to be induced by disulfide stress and cap removal was performed by RppH and ApaH (Luciano et al., 2019). A most recent study proved the existence of 5'-ADP-ribose (ADPR)-capped RNAs in human cells, where ADPR is added post-transcriptionally by several transferases onto the 5' end of mRNAs, rendering them unsusceptible to degradation by the eukaryotic 5'→3' exoribonuclease Xrn1 (Weixler et al., 2022). The existence of ADPR-RNAs was predicted a few years earlier when eukaryotic poly ADP-ribose polymerase (PARP) family enzymes were shown to ADP-ribosylate RNA *in vitro* (Munir et al., 2018; Munnur et al., 2019).

The metabolites NAD, NADH, flavin adenine dinucleotide (FAD) and dpCoA were shown to be incorporated as non-canonical initiation nucleotides (NCIN) by the bacterial RNA polymerase (RNAP) *in vitro* and *in vivo* and by the eukaryotic RNA polymerase II *in vitro* (Bird et al., 2016; Malygin et al., 1979). Additionally, it was shown that NCIN capping is initiated only from +1A promoters (A:T at the transcription start site +1) (Bird et al., 2016). The T7 and *E. coli* RNAPs are furthermore able to use dinucleoside polyphosphates (Np_nNs) as NCINs (Hudeček et al., 2020). This repertoire was further expanded by revealing UDP-Glucose and UDP-N-acetylglucosamine as *in vitro* transcription initiation substrates for bacterial RNAP and

the discovery of these caps on eukaryotic, prokaryotic and viral RNA was proven only one year later (Julius & Yuzenkova, 2017; J. Wang et al., 2019). A mechanism for the post-transcriptional incorporation of NAD via enzymes from the NAD biosynthesis pathway has been proposed but remains to be proven (Jiao et al., 2017; Kiledjian, 2018; Wiedermannová et al., 2021). Interestingly, capping of RNA with NAD is not a random but rather a controlled process, as only a specific subset of RNAs are capped and only a low percentage of NAD-capped RNAs are among the highest-expressed RNAs in the cell (Cahová et al., 2015; Frindert et al., 2018). In *E. coli*, NAD caps protect RNA against RNase E-mediated decay and are consequently suggested to promote stability, a concept that was recently challenged (Cahová et al., 2015; Doamekpor et al., 2022). In contrast, the NAD cap does not promote stability on eukaryotic mRNAs. Instead, it targets NAD-capped RNAs for degradation initiation by the decapping enzyme DXO (Jiao et al., 2017). In eukaryotic mRNAs, stability and translation are mediated by the 5'-m⁷G cap which can be removed by Nudix family hydrolases (Furuichi et al., 1977; Wang & Kiledjian, 2001).

A piece to the puzzle was added recently with the discovery of NAD-capped RNAs in Archaea (Gomes-Filho et al., submitted). Using a technique called NAD-captureSeq which enables the chemo-enzymatic capture and sequencing of NAD-capped RNAs, total RNA extracts from *S. acidocaldarius* and *Haloferax volcanii* were investigated and NAD caps identified on archaeal non-coding RNAs (tRNAs, C/D box sRNAs and sRNAs) and mRNAs (Cahová et al., 2015; Gomes-Filho et al., submitted; Winz et al., 2017). In fact, *S. acidocaldarius* revealed itself to be the organism exhibiting the highest concentration of NAD-RNAs detected to date. Just as was reported in Bacteria, in *S. acidocaldarius* and *H. volcanii* the +1 position of all NAD-RNAs presents adenine and analysis of the upstream regions provided evidence for a co-transcriptional NAD-capping process (Gomes-Filho et al., submitted). While the NAD cap fulfills oppositional roles in Bacteria and Eukaryotes, its role in the archaeal RNA metabolism remains elusive.

1.5 Nudix hydrolases and their implications in RNA decapping

The first identified eukaryotic decapping enzyme, Dcp2, is a member of the evolutionary conserved Nudix hydrolase protein superfamily (Dunckley & Parker, 1999). These proteins catalyze the hydrolysis of a wide range of small nucleotide

substrates composed of a nucleoside diphosphate linked to another moiety X (Nudix). The family of Nudix hydrolases comprises functionally versatile proteins that are identified by the conserved Nudix motif with the consensus sequence $GX_5EX_5U/AXREX_2EEXGU$ (U for a hydrophobic residue, X for any residue) (Bessman et al., 1996; McLennan, 2006). Cleavage of the cap structure by Dcp2 (also known as Nudt20) yields m^7GDP and 5'-monophosphorylated RNA (Figure 1.4) and is abolished by mutations of conserved residues in the Nudix motif (Lykke-Andersen, 2002; Van Dijk et al., 2002; Wang et al., 2002). The discovery of more decapping enzymes led to the realization that each of them regulates a specific subset of RNAs, alluding to the complexity of RNA regulation in the cell. Seven additional eukaryotic Nudix proteins, Nudt2, Nudt3, Nudt12, Nudt15, Nudt16, Nudt17 and Nudt19, were shown to decap RNA *in vitro* in a manner similar to Dcp2 (Abdelraheim et al., 2003; Grudzien-Nogalska et al., 2019; Song et al., 2010, 2013).

While these proteins cleave within the pyrophosphate linkage, soon afterwards a new class of decapping enzymes with a different cleaving mechanism was discovered. In addition to proteins from the Nudix hydrolase family, mammalian cells possess the DXO protein (formerly DOM3Z) from the DXO (decapping endonuclease) family of proteins, which exhibits RNA 5'-pyrophosphohydrolase activity, decapping activity and 5'→3' exoribonuclease activity (Jiao et al., 2013). Its homologs in yeast are Rai1 and Dxo1 (Chang et al., 2012; Jiao et al., 2010; Xiang et al., 2009). These proteins release the entire cap structure and preferably act on incompletely capped mRNAs, hence providing a quality control mechanism (Jiao et al., 2010, 2013). Enzymes of the DXO family are identified by four conserved sequence motifs whose residues are centrally located in the active site (Chang et al., 2012). Following the discovery of NAD-capped RNAs in Eukaryotes, it became apparent that DXO removes not only m^7G caps but also NAD caps. In fact, DXO decapping is ~6-fold more efficient on NAD-capped RNA than it is on m^7G -capped RNA (Jiao et al., 2017). Its “deNADing” activity removes the entire NAD moiety yielding 5'-monophosphorylated RNA which is subsequently degraded via the intrinsic 5'→3' exonuclease activity of DXO (Jiao et al., 2017).

The first prokaryotic decapping enzyme was not identified until recently. In Bacteria, the first protein discovered to be involved in NAD-decapping was NudC, a member of the aforementioned Nudix family of hydrolases (Cahová et al., 2015). Initially described as a NAD/H pyrophosphohydrolase, NAD-decapping by NudC results in 5'-

monosphorylated RNA (Figure 1.4) and nicotinamide mononucleotide (NMN), while not being active against 5'-triphosphorylated RNA (Cahová et al., 2015; Frick & Bessman, 1995). Furthermore, processing by NudC requires RNA with at least three unpaired nucleotides at the 5' end, as it is ineffective against RNAs with a paired 5' end (Höfer et al., 2016). As NAD caps confer stability in bacterial RNAs, a deletion of NudC in *E. coli* results in an increase of NAD-capped RNAs (Cahová et al., 2015).

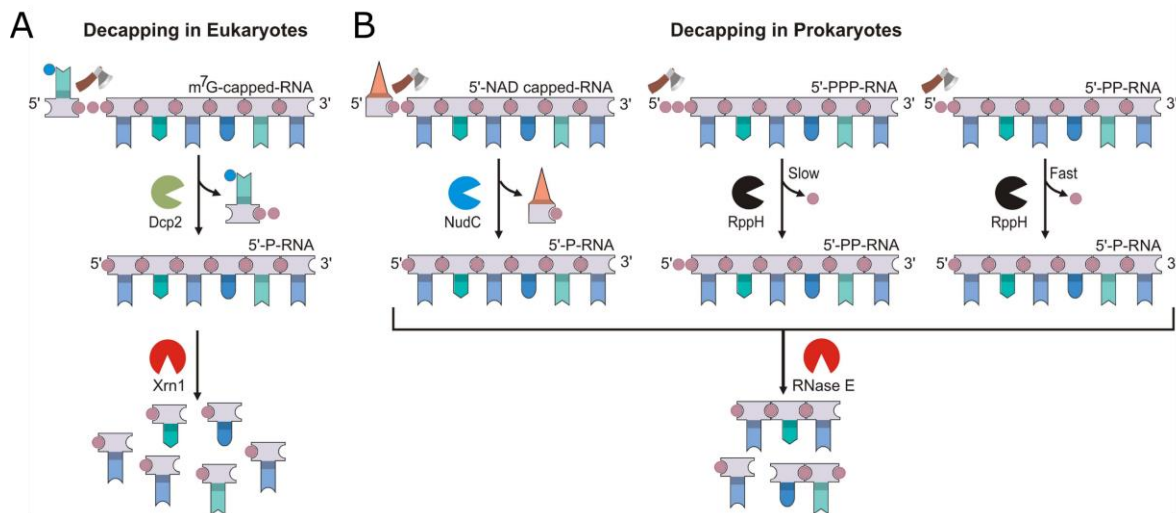


Figure 1.4: Removal of 5'-terminal RNA modifications by Nudix hydrolase family proteins. A) Decapping of m⁷G-capped RNA in Eukaryotes: Dcp2 removes the cap yielding 5'-p-RNA and further degradation is performed by 5'-dependent exonucleases like Xrn1. B) Decapping of 5'-capped RNA in Prokaryotes: NAD-RNA is decapped by NudC yielding 5'-p-RNA; primary transcripts like 5'-ppp-RNA and 5'-pp-RNA are dephosphorylated by RppH into 5'-pp-RNA and 5'-p-RNA, respectively. Subsequent degradation is conducted by RNase E. Figure adapted from Höfer & Jäschke, 2018.

Bacterial RppH is an RNA pyrophosphohydrolase from the Nudix family of hydrolases which converts 5'-triphosphorylated RNA into 5'-monophosphorylated RNA and subsequently triggers RNA degradation by RNase E or RNase J (Figure 1.4) (Deana et al., 2008; Richards et al., 2011). Initially it was shown to be impeded by the NAD cap (Bird et al., 2016; Cahová et al., 2015), however subsequent experiments proved that *E. coli* RppH as well as *Bacillus subtilis* BsRppH act as NAD-decapping enzymes (Frindert et al., 2018; Grudzien-Nogalska et al., 2019). Furthermore, *E. coli* RppH is capable of removing 5'-Np_nN-caps from RNA, as long as the cap itself has not been methylated (Hudeček et al., 2020). Interestingly, *E. coli* RppH also showed decapping activity with eukaryotic m⁷G-capped RNA *in vitro* (Song et al., 2013). Even though treatment with any of the three identified decapping enzymes NudC, RppH or DXO

converts NAD-capped RNA into 5'-monophosphorylated RNA, the mechanism by which they do so is very distinct. A recent review on non-canonical RNA capping outlines four classes of decapping enzymes: I) proteins which remove the intact cap structure, such as DXO/Rai1 enzymes, II) NudC/Nudt12-like proteins which cleave within the pyrophosphate bond of cap and RNA and also hydrolyze the free metabolite, III) RppH-like proteins which cleave only capped RNA but do not hydrolyze the free metabolite, and IIII) ApaH-like proteins which are capable of decapping dinucleoside polyphosphate-capped RNA and hydrolysis of the free compound but do not belong to the aforementioned protein families (Doamekpor et al., 2022). Notably, Nudix family hydrolases may also possess dual activities, as seen in the enzyme CDP-Chase from *Bacillus cereus*. CDP-Chase, a CDP-choline pyrophosphatase, possesses phosphatase activity and 3'→5' exonuclease activity mediated by two different active sites. The protein forms an asymmetric dimer with an enclosed Nudix site on one monomer and a large open cavity on the other, mediating CDP-choline hydrolysis and RNA exonuclease activity, respectively (Duong-Ly et al., 2011).

1.6 Aims of the Project

The circular SRP RNA variant of *T. tenax* is proposed to have evolved via genome rearrangement and recruitment of the tRNA splicing pathways and might offer a selective advantage at elevated temperatures. To investigate this scenario, a permuted variant of the SRP RNA gene from *S. acidocaldarius* is created using the *T. tenax* SRP RNA gene as a model. The permuted SRP RNA gene variant is introduced into *S. acidocaldarius* cells and a combination of inverse reverse transcription PCR and RNA-seq is employed towards its detection. Additionally, it is attempted to exchange the original gene for its permuted variant. Furthermore, *in vitro* splicing assays with a synthetic RNA substrate are employed to verify that the tRNA splicing endonuclease from *S. acidocaldarius* is indeed capable of processing a non-tRNA BHB motif.

Following the recent discovery of NAD-capped RNAs in Archaea, their regulation in *S. acidocaldarius* remains to be uncovered. To this end, all of the potential decapping enzymes from the Nudix family are identified via sequence alignment with the known NAD-decapping enzymes NudC, RppH and DXO. The potential archaeal decapping enzymes are recombinantly produced and assayed for their substrate specificity,

including *in vitro* decapping assays with 5'-NAD-RNA, as well as Malachite Green assays to test the enzymes' capabilities in hydrolyzing specific metabolites. Furthermore, the genes encoding the putative decapping enzymes are individually deleted from the *S. acidocaldarius* genome and the phenotypes and transcriptomes of the deletion strains are profiled.

2 Results

2.1 Circular SRP RNA design and transformation

To engineer a permuted SRP variant, the original SRP RNA gene of *S. acidocaldarius* was modified *in silico* using the SRP RNA of *T. tenax* as a model. Specifically, helix 1 and thereby the standard 5' and 3' termini were deleted and new termini introduced in helix 8b (Figure 2.1B). Consequently, the gene was permuted, i.e. the 3' portion of the gene was relocated upstream of the 5' portion (Figure 2.1A). Furthermore, two intron sequences were added to the termini which form a BHB motif with the 5' and 3' terminal sequences. For transcription, a 40 nt-long region of the original SRP RNA gene encompassing the native promoter was added upstream of the permuted SRP RNA gene (Figure 2.1A). The entire sequence, i.e. the permuted SRP RNA gene plus the native promoter, was synthesized and cloned into the plasmid pSVAaraFX-Stop, an *S. acidocaldarius* expression plasmid and *E. coli* shuttle vector (Berkner et al., 2007). After processing, the modified SRP RNA should harbor the same sequence as the original SRP RNA with the exception of the missing helix 1. To introduce a unique identifier into the sequence of the modified SRP RNA, site-directed mutagenesis of a single nucleotide was performed to change the sequence of the functional loop from GGAA to GGGA (the sequence of the functional loop from *T. tenax*) (Figure 2.1B). The plasmid was transformed into *S. acidocaldarius* with the standard electroporation protocol and cells were plated on Gelrite plates containing Brock medium, NZ-Amine and Dextrin. Single colonies were picked and inoculated in Brock medium supplemented with NZ-Amine and Dextrin and cultures were grown under standard growth conditions to the late logarithmic phase.

2.2 Identification of the circular SRP RNA

Cell pellets from 2 ml late-log cultures were harvested and total RNA was extracted and reverse transcribed. The resulting cDNA served as the template for a polymerase chain reaction (PCR) with inversely oriented primer pairs with complementarity to different regions of the modified SRP RNA (see Table 4.11 in Materials). PCR products were separated by agarose gel electrophoresis and analyzed by sequencing and revealed themselves to be sequences from the original SRP RNA.

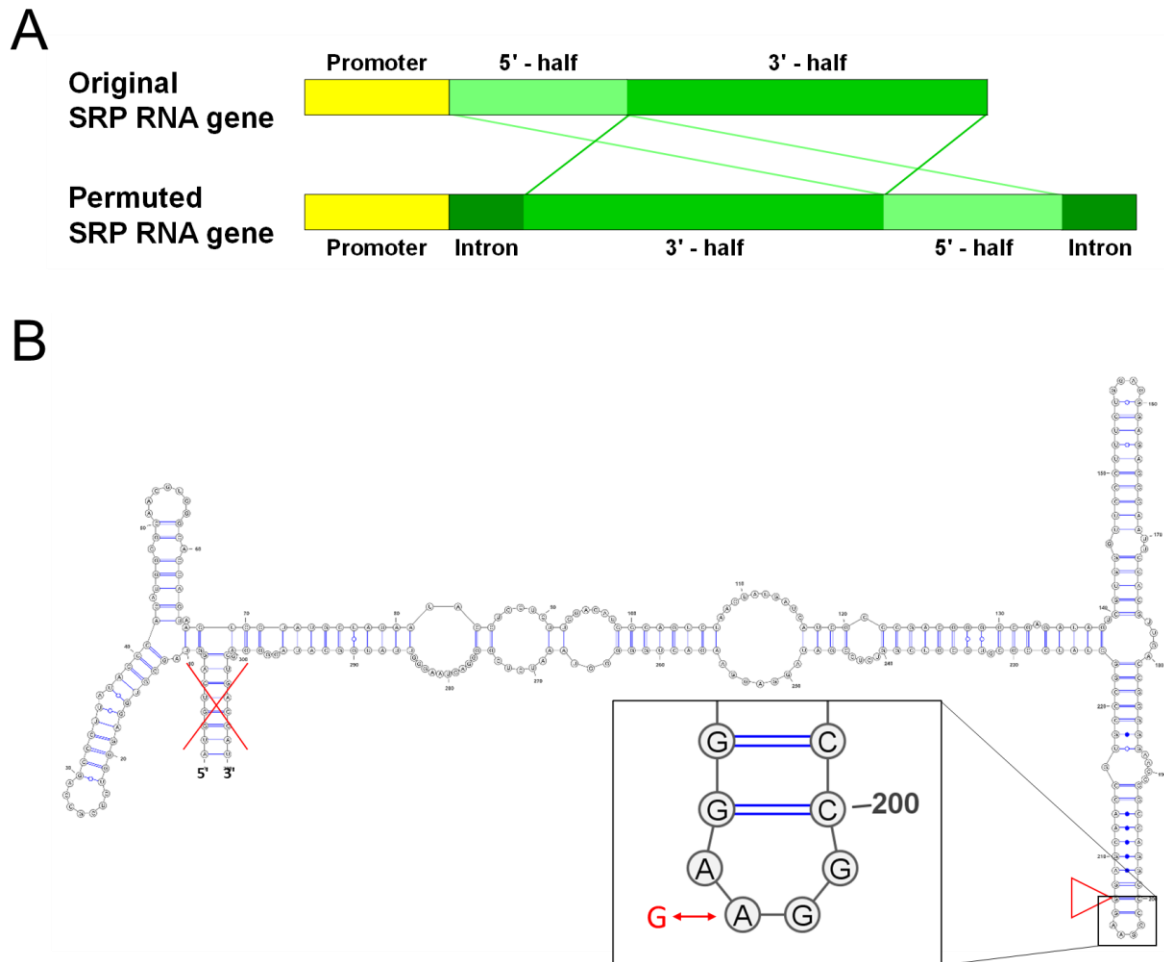


Figure 2.1: Permutation of the SRP RNA gene from *S. acidocaldarius*. A) Schematic representation of the permutation process. The 3' half of the gene is relocated upstream of the 5' half and complementary leader and trailer sequences are added upstream and downstream of the gene. The native promoter is maintained. B) Sequence and structure of the native SRP RNA from *S. acidocaldarius*. Modifications represented in red encompass the following: removal of helix 1 and elimination of the standard termini, introduction of new termini in helix 8 and nucleotide exchange in the functional loop of helix 8.

In preparation for RNA-sequencing, total RNA from late-log *S. acidocaldarius* cultures was extracted, digested with DNase I and treated with Terminator 5'-Phosphate-Dependent Exonuclease (TEX). This 5' → 3' exonuclease selectively digests 5'-monophosphorylated RNA but does not affect the *S. acidocaldarius* SRP RNA as evident from a previous RNA sequencing dataset. TEX-treated RNA was used for the creating of cDNA libraries and the sequencing run was performed using an Illumina® MiniSeq System. In the dataset, the coverage of the wild-type SRP RNA amounts to max. 15.000 reads while showing the usual profile of the wild-type SRP RNA from a TEX-treated sample with increased reads towards the 3' end of the SRP RNA (Figure

2.2A). The coverage of the circular SRP RNA amounts to max. 100 reads. The sequence of the circular SRP RNA matches the original sequence but in two regions: the region of the removed helix 1 and the functional loop carrying the nucleotide exchange as a unique identifier. Consequently, these regions are enriched in the coverage plot (Figure 2.2B). The sequences of both these regions are unique to the circular SRP RNA and do not exist elsewhere in the genome of *S. acidocaldarius*. The circularization junction of the modified SRP RNA was searched for manually and a total of 10 reads with this sequence and the unique identifier was identified from the dataset (Figure 2.2C). Furthermore, alignment to the plasmid sequence revealed reads covering the 3' end of the permuted SRP RNA gene, followed by the 3' intron sequence and the downstream plasmid sequence, likely resulting from transcribed, pre-splicing SRP RNA precursors. Additionally, reads from the 5' end, encompassing the sequence downstream of the promoter and the 5' intron, were identified.

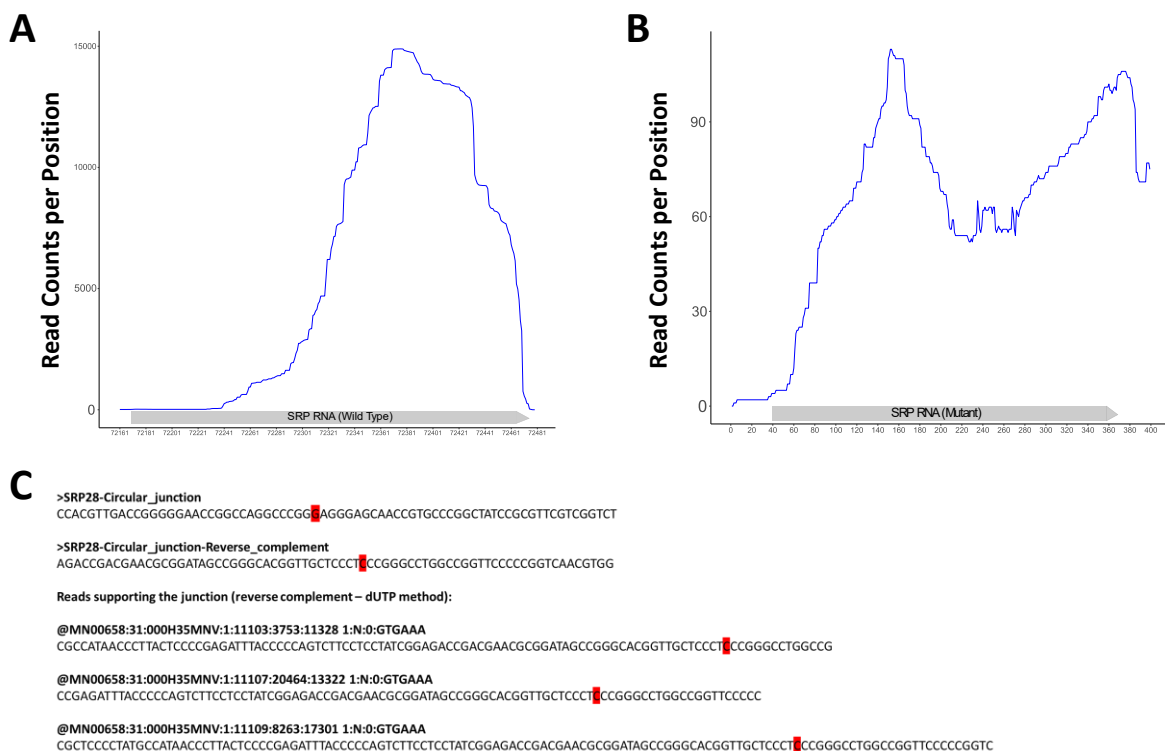


Figure 2.2: RNA-sequencing of total RNA from *S. acidocaldarius*. A) Coverage plot of the wild-type linear SRP RNA. B) Coverage plot of the modified circular SRP RNA. C) Reads covering the functional loop of helix 8 and carrying the unique identifier (marked in red) were identified manually. Shown are 3 out of 10 reads. Coverage Plots and reads provided by José Vicente Gomes-Filho.

2.3 Processing of the permuted SRP RNA gene

As the intron sequences of the permuted SRP RNA gene were tailored to form a BHB motif, it was strongly suggested that the processing of the plasmid-borne SRP RNA was conducted by the tRNA splicing machinery. To test this hypothesis, the two subunits of the *S. acidocaldarius* tRNA splicing endonuclease were identified by sequence similarity to the tRNA splicing endonuclease from *T. tenax*. The genes encoding the catalytic subunit endA (SACI_RS04105) and the structural subunit SACI_RS03165 were cloned each with an N-terminal His_{6x}-tag into the first and second multiple cloning site of the *E. coli* expression vector pRSFDuet-1, respectively, and the plasmid was transformed into the *E. coli* expression strain Rosetta 2 DE3 pLysS. Expression was induced with IPTG and proteins were purified via Ni-NTA chromatography. Elution fractions were analyzed via SDS-PAGE (Figure 2.3) and protein sample concentration was fluorometrically quantified.

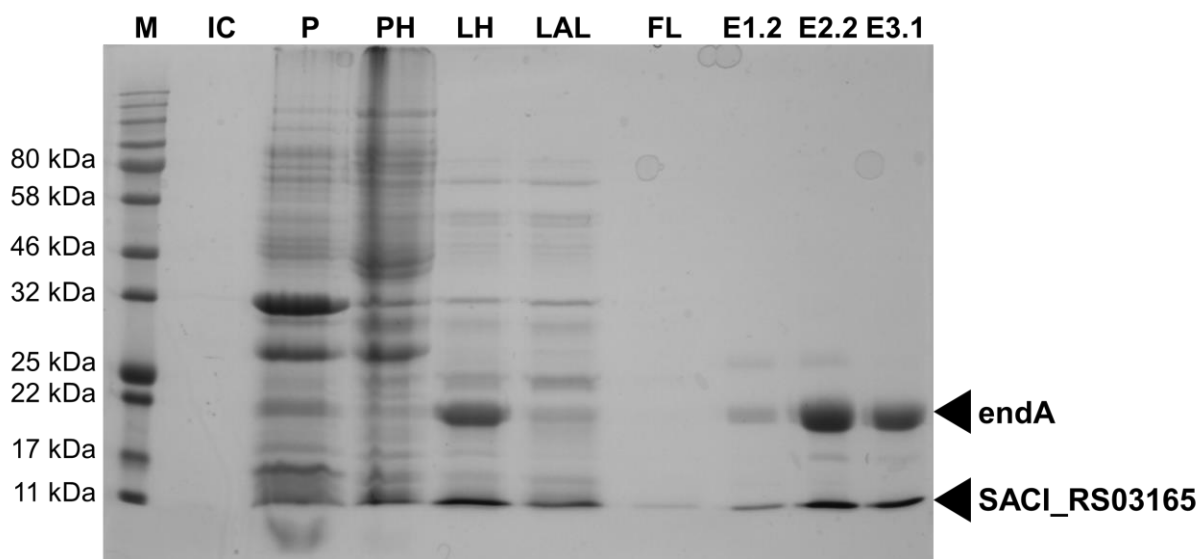


Figure 2.3: Recombinant production of the tRNA splicing endonuclease from *S. acidocaldarius*. The protein subunits were recombinantly expressed in *E. coli* Rosetta 2 DE3 pLysS cells and purified using Ni-NTA chromatography. The purification samples and elution fractions were analyzed via SDS-PAGE. Black arrows indicate the bands representing the two subunits endA (20 kDa) and SACI_RS03165 (10 kDa). M = marker, IC = induction control, P = pellet, PH = pellet after heat treatment, LH = lysate after heat treatment, LAL = lysate after column loading, FL = flowthrough, E1.2 = elution buffer 1 fraction 2, E2.2 = elution buffer 2 fraction 2, E3.1 = elution buffer 3 fraction 1.

To test the ability of the tRNA splicing endonuclease from *S. acidocaldarius* towards splicing non-tRNA BHB motifs, the His-purified protein complex was incubated with an RNA substrate specifically designed for this assay. The 42 nt-long RNA oligo corresponds to the sequences of the 5' and 3' halves of the BHB motif of the precursor SRP RNA connected by a GUAG loop to enable BHB formation upon self-hybridization (Figure 2.4A). Additionally, the 5' end of the RNA oligo was fluorescently labelled with fluorescein (6-FAM). 0.3 μ M hybridized RNA substrate and tRNA splicing endonuclease (concentrations indicated in Figure 2.4B) were incubated for 30 min. The reaction temperature was lowered to 65°C to prevent degradation of the RNA substrate due to the presence of divalent cations in the reaction and protein buffers. Splicing of the RNA BHB substrate at the indicated positions (Figure 2.4A) was expected to result in a 13 nt-long 5' fragment which was visualized via Urea-PAGE. A two-times molar excess of protein was sufficient to process approx. half of the RNA substrate in a 30 min reaction (Figure 2.4B).

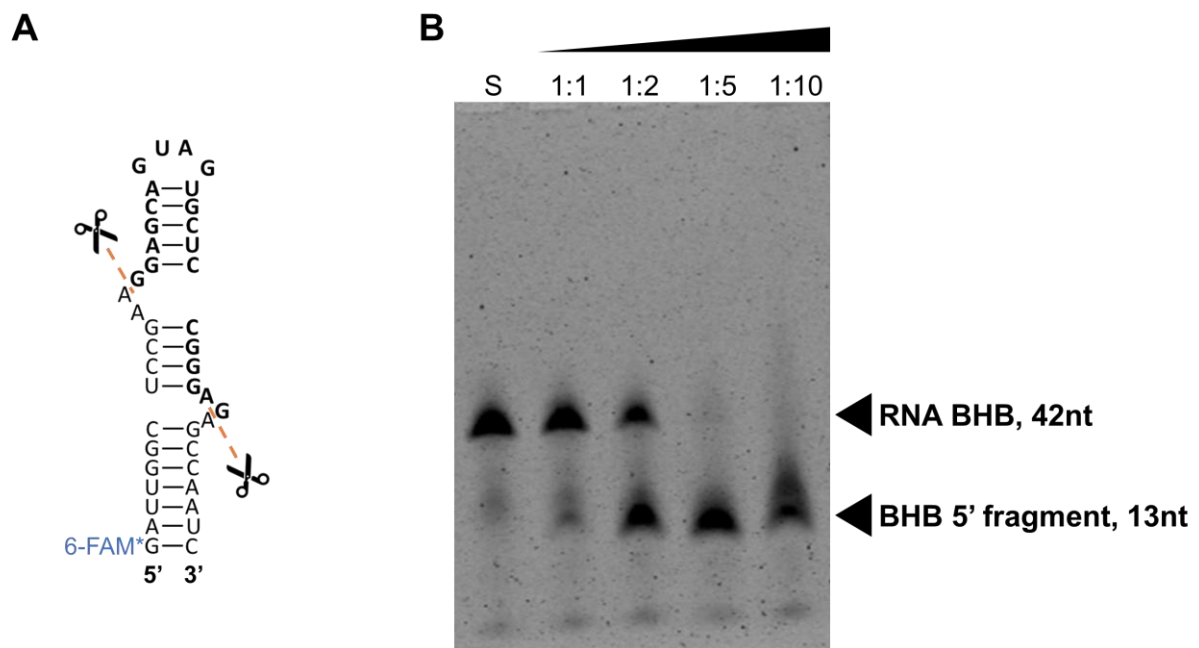


Figure 2.4: Splicing assay with the tRNA splicing endonuclease from *S. acidocaldarius* and a synthetic RNA BHB substrate. A) Sequence and structure of the synthetic RNA substrate. The BHB is formed upon self-hybridization. The splicing sites are indicated in the figure. The 5' terminus is fluorescently labelled with 6-FAM. B) Analysis of the splicing reactions by Urea-PAGE. The 42 nt-long RNA substrate is incubated with increasing concentrations of tRNA splicing endonuclease. Processing of the substrate at the indicated positions will yield a 13 nt-long, fluorescently labelled 5' fragment, as indicated by a black arrow.

2.4 Replacing the original SRP RNA gene

As the *in vitro* splicing assays confirmed the ability of the *S. acidocaldarius* tRNA splicing machinery to process the permuted SRP RNA gene into a circular SRP RNA, it was attempted to replace the original with the permuted SRP RNA gene variant. To this end, an exchange plasmid was created based on the dual marker vector pSVA431 (Wagner et al., 2012). Briefly, the exchange plasmid carries the uracil cassette *pyrEF* and *lacS* from *Sa. solfataricus*, flanked by the gene of interest (GOI), i.e. the original SRP RNA gene, and a donor DNA fragment consisting of the 500 bp left flank (LF) of the GOI, the native promoter, the permuted SRP RNA gene and the 400 bp right flank (RF) of the GOI (Figure 2.5A). After plasmid methylation and digestion, the linear fragment consisting of marker cassette and homologous regions was transformed into *S. acidocaldarius* via electroporation. First, the linear fragment was integrated into the *Sulfolobus* genome via homologous recombination between the GOI and the right flank, induced by uracil selection (Figure 2.5A). Positive integration clones were identified via Blue-White screening by the presence of the *lacS_{SSO}* cassette and grown in liquid medium (Figure 2.5B). Secondly, the cultures were plated on plates containing 5-FOA to induce a second crossover and looping out of the region between the two left flanks, i.e. the marker cassette and the gene of interest. To date, the integration of the marker cassette and the permuted SRP RNA gene into the intended locus was successful, however removal of the original gene variant and the marker cassette, leaving behind only the permuted variant, could not be achieved. Screening of clones after counterselection revealed either one of two scenarios: I) a crossover had occurred restoring the original locus, or II) the locus remained unchanged, i.e. retained both SRP RNA gene variants plus the marker cassette, most likely due to failure to induce a crossover (Figure 2.5C).

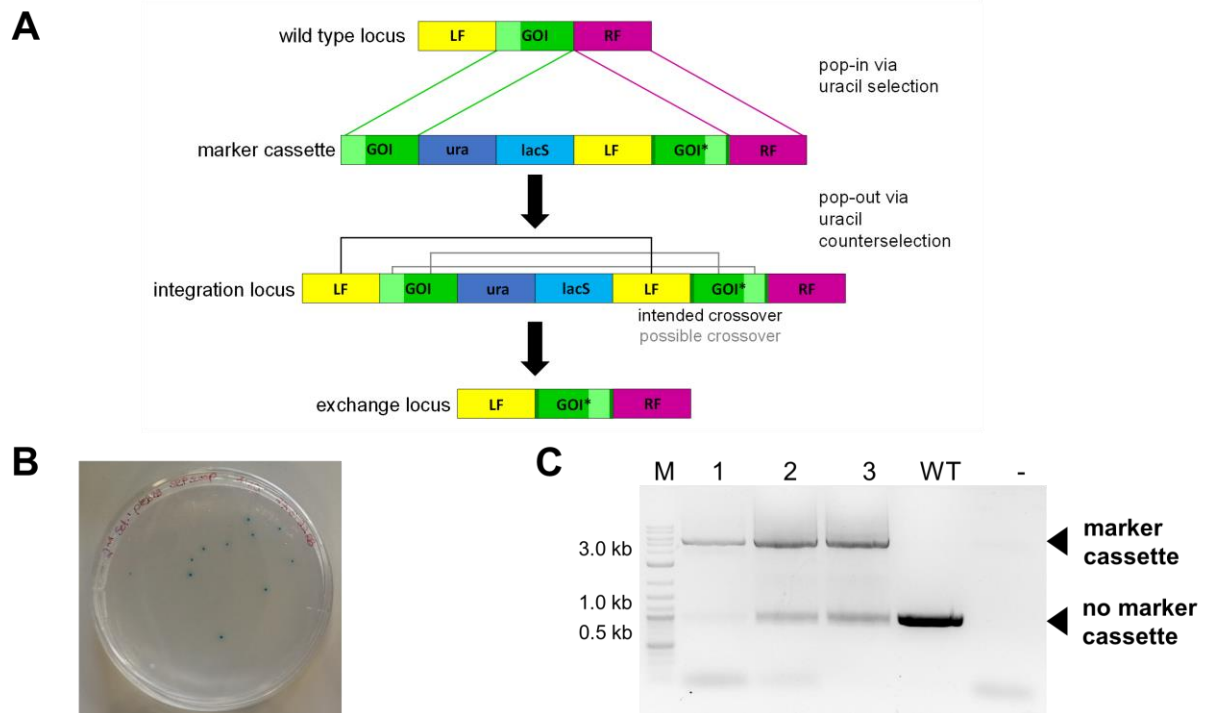


Figure 2.5: Exchanging the SRP RNA gene in *S. acidocaldarius* via homologous recombination. A) Schematic representation of the pop-in / pop-out method using a linear marker cassette fragment and indication of crossover scenarios between the homologous regions. B) Confirmation of the integration of the marker cassette fragment with Blue-White screening. C) PCR analysis of 3 colonies after treatment with 5-FOA. The 5 kb band represents the locus carrying the marker cassette after successful pop-in and the 1 kb band represents the locus without the marker cassette. This can be either the wild-type locus or the modified locus after successful pop-out. WT = wild type, negative control = water.

2.5 *In silico* characterization of potential decapping enzymes

2.5.1 Candidate protein identification and sequence analysis

A total of four putative decapping enzymes were identified using BsRppH from *Bacillus subtilis* and RppH from *Yersinia pestis* as template sequences. The alignment of all four candidate decapping proteins SACI_RS00730, SACI_RS00060, SACI_RS02625 and SACI_RS00575 with *E. coli* NudC and *B. subtilis* BsRppH revealed the presence of the Nudix motif (Figure 2.6A). Furthermore, all proteins possess the conserved glutamic acid residues in the Nudix motif which are crucial to Nudix activity (see next section). As *E. coli* NudC and *B. subtilis* BsRppH have been experimentally proven to actively decap 5'-NAD-capped RNAs, it is suspected that either: I) at least one of these four archaeal Nudix enzymes possesses decapping activity on NAD-RNA, or II) all four enzymes are active and each enzyme regulates a different subset of capped RNAs. Another notable feature is the residue at position 16 following the G of the Nudix motif. The residue at this position was shown to suggest a possible substrate for the respective Nudix proteins and therefore serves to identify and distinguish different subsets of Nudix hydrolases. In SACI_RS00060, a proline at this position suggests ADP-ribose (ADPR) hydrolysis activity, while in SACI_RS00575, the tyrosine hints at specificity for dinucleoside polyphosphate substrates (Dunn et al., 1999). Members of the DXO family of decapping enzymes were not identified in *S. acidocaldarius*.

2.5.2 Structural predictions

The four archaeal Nudix proteins SACI_RS00730, SACI_RS00060, SACI_RS02625 and SACI_RS00575 constitute an expected molecular weight of 17 kDa, 20 kDa, 18 kDa and 18 kDa, respectively. Figure 2.6 panels B-E show the predicted structures for all four proteins modelled by AlphaFold (source: UniProt database) (Jumper et al., 2021; Varadi et al., 2022). As expected, the proteins exhibit a similar structure in which the Nudix motif is present as an α -helix located on the outer part of the structure, next to a clearly visible substrate pocket. In the active site, three conserved glutamic acid residues act as ligands to magnesium ions and are directed towards the inside of the pocket. The indicator residue at position 16 after the G of the Nudix motif is located on the opposite end of the pocket. SACI_RS00060, the largest of the four proteins, furthermore exhibits an extended structure which is not present in the other three proteins (Figure 2.6E).

2.6 *In vitro* characterization

2.6.1 Recombinant protein expression and purification

The genes encoding the putative decapping enzymes SACI_RS00730, SACI_RS00060 and SACI_RS00575 were cloned into the high-copy plasmid pRSFDuet-1 with an N-terminal His_{6x}-tag and expressed in the *E. coli* expression strain Rosetta 2 DE3 pLysS. This strain is particularly suited to express archaeal proteins, as it carries the pRARE2 plasmid with genes coding for tRNAs rarely used by *E. coli*. Expression of the proteins SACI_RS00730 and SACI_RS00060 was induced with 1 mM IPTG, while SACI_RS00575 expression was induced with 0.1 mM IPTG, as this protein remained in the pellet fraction following induction with higher IPTG concentration (Supplementary Figure S1).

As the Nudix proteins originate from a hyperthermophilic organism, a heat denaturation step was integrated into the purification protocol to denature the native *E. coli* proteins. The proteins were purified using Ni-NTA chromatography. Analysis of the elution fractions via SDS-PAGE revealed bands at sizes of approx. 17 kDa, 22 kDa and 18 kDa for SACI_RS00730, SACI_RS00060 and SACI_RS00575, respectively (Figure 2.7A-C). To obtain Nudix domain-mutant variants of the aforementioned proteins, triple nucleotide exchanges via site-directed mutagenesis were performed, changing the three conserved glutamic acid residues to alanine in each protein's Nudix motif (Figure 2.6A). The plasmids carrying the mutated Nudix genes were transformed into the Rosetta 2 strain and the mutant proteins were expressed and purified following the same procedure as their wild-type counterparts. All proteins were eluted at final concentrations between 0.4-0.75 mg/ml, yielding a total of 2.4-4.5mg per protein.

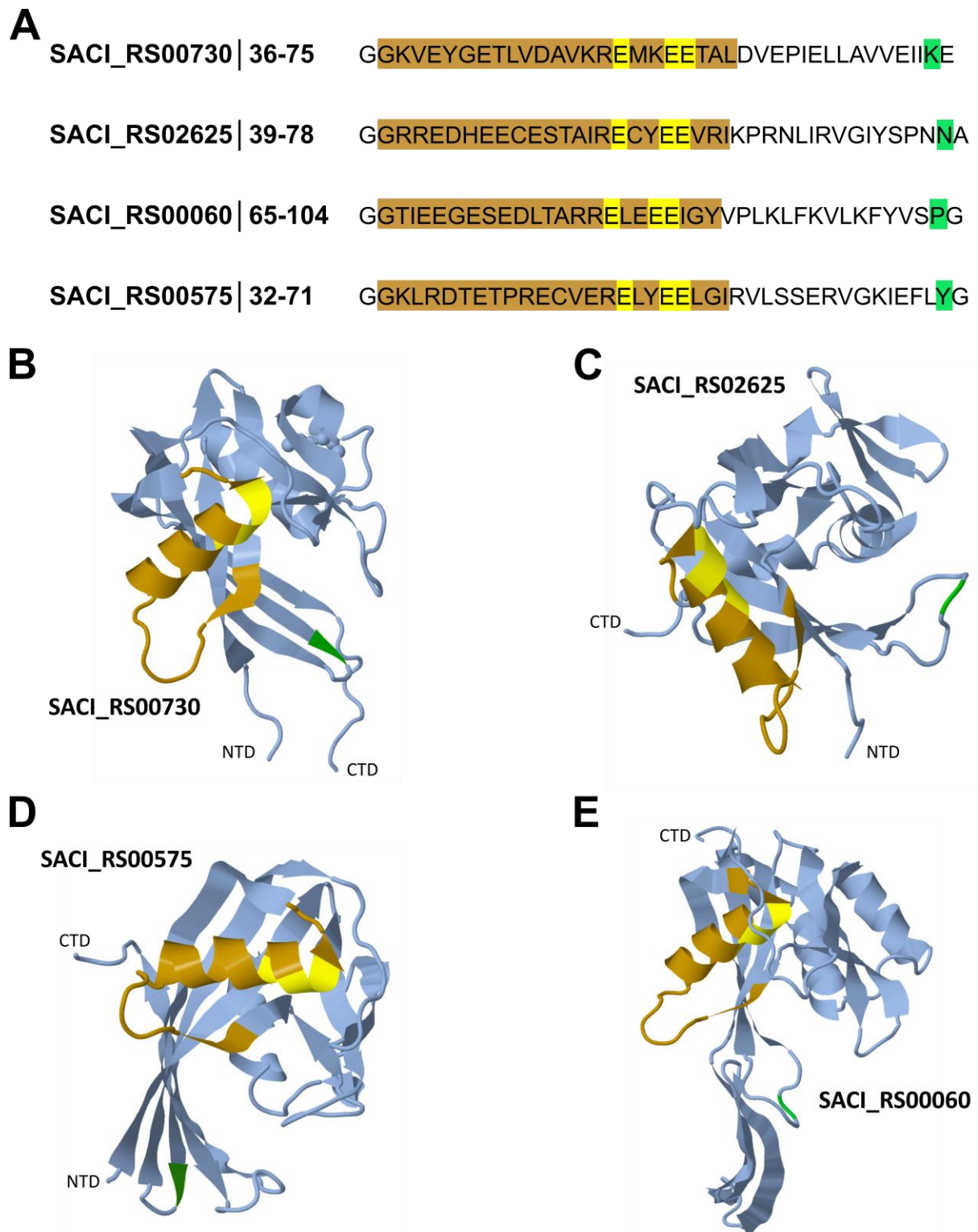


Figure 2.6: Predicted structures of the Nudix family hydrolases from *S. acidocaldarius*. A) Part of the protein sequences of the four Nudix family hydrolases. Presented is the part of the sequence encompassing the Nudix box (brown), the three conserved glutamic acid residues (yellow) and the indicator residue at position 16 after the G of the Nudix box (green). Prediction of the structure of B) SACI_RS00730, C) SACI_RS02625, D) SACI_RS00575 and E) SACI_RS00060. The notable features Nudix box (brown), conserved residues (yellow) and indicator residue (green) are indicated. Structural predictions were generated by AlphaFold and images sourced from the Uniprot database (Jumper et al., 2021; Varadi et al., 2022).

It was not possible to express and purify the protein Saci_RS02625 with this protocol, as the respective gene was not maintained in the plasmid after transformation into *E. coli*, most likely due to toxicity of the gene product. To circumvent this issue, the gene encoding SACI_RS02625 (wild-type and mutant variant) was synthesized and subcloned into the pRSFDuet-1 vector. The proteins were subsequently produced using an *in vitro* protein synthesis system based on *E. coli* cell extract and purified via Ni-NTA chromatography. The elution fractions were analysed by SDS-PAGE and both the wild-type and Nudix domain-mutant protein were visualized as a band at approx. 20 kDa (Figure 2.7D). Both proteins were eluted at a final concentration of approx. 0.37 mg/ml, yielding approx. 0.148 mg for each protein.

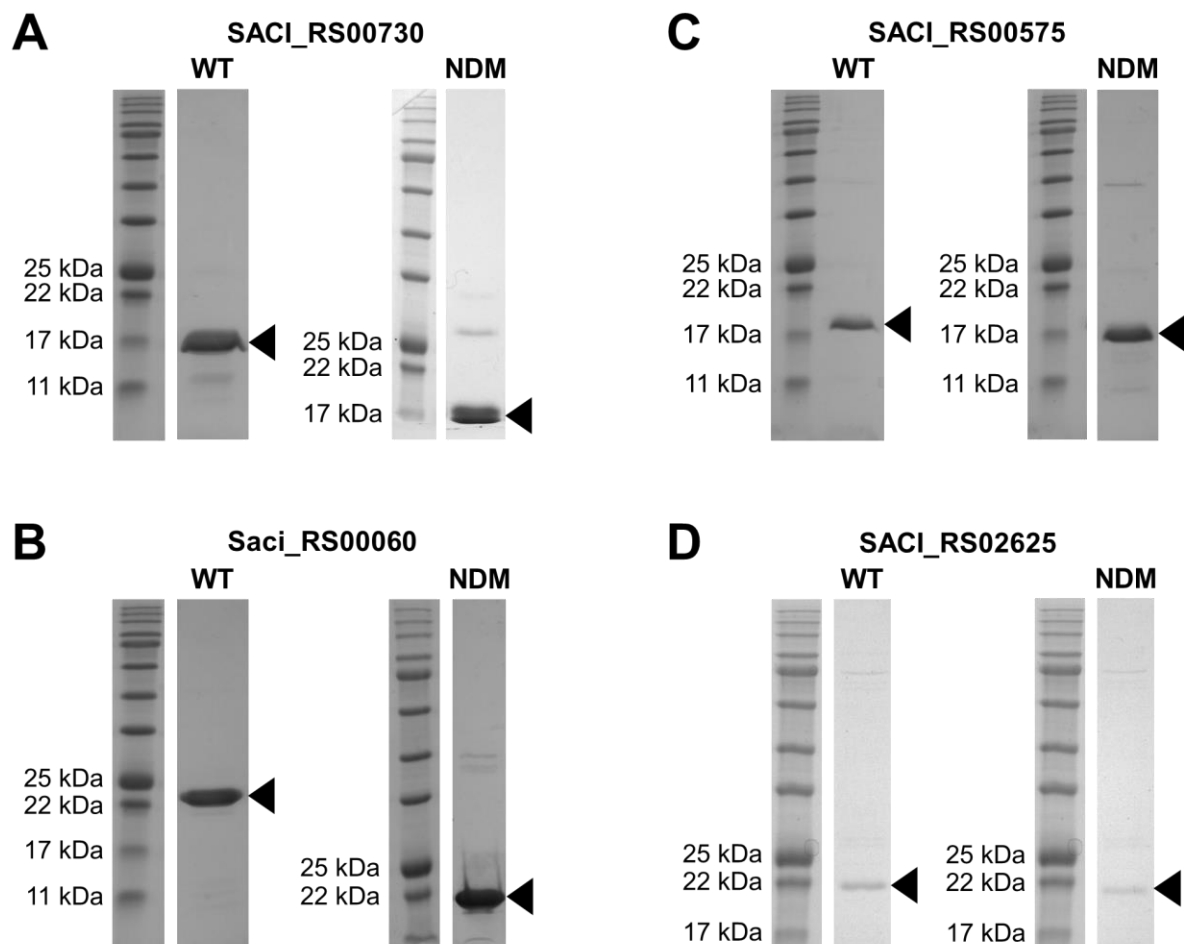


Figure 2.7: Recombinant production of the Nudix hydrolases from *S. acidocaldarius*. The proteins were recombinantly expressed in *E. coli* Rosetta 2 DE3 pLysS cells and purified via Ni-NTA chromatography. The elution fractions were analyzed via SDS-PAGE, revealing bands at A) 17 kDa for SACI_RS00730, B) 22 kDa for SACI_RS00060, C) 18 kDa for SACI_RS00575 and D) 20 kDa for SACI_RS02625. WT = wild type, NDM = Nudix domain-mutant.

2.6.2 Decapping assays

The purified archaeal Nudix hydrolases were subjected to decapping assays to investigate their potential to decap differently 5'-capped RNAs *in vitro*. SACI_RS00730, SACI_RS00060, SACI_RS02625, SACI_RS00575 and their respective Nudix domain-mutants (NDM) were incubated with a 5'-capped NAD-RNA model substrate whose sequence was comprised exclusively of G, C and U (see Table 4.14 in Materials) except for an +1A that was replaced with NAD. Reactions were performed for 5 min at 65°C to avoid degradation of the RNA substrate. NudC from *E. coli* was included as a positive control and this reaction was performed for 5 min at 37°C. All reactions were resolved on a denaturing gel containing urea, acrylamidophenyl boronic acid (APB) and polyacrylamide (PAA). The addition of APB results in a gel matrix in which nucleic acids can be separated according to their 5'-modification status due to the formation of stable complexes between the boronyl groups and the 1,2-*cis* diols from the nicotinamide riboside (Nübel et al., 2017). Consequently, RNAs carrying metabolite-caps like 5'-NAD or 5'-ADPR are retarded more strongly than 5'-ppp-RNAs or 5'-p-RNAs. Figure 2.8A shows that the integrity of the RNA substrate remains intact at 65°C (lane 1) as well as the successful decapping of NAD-RNA to 5'-p-RNA (and NMN) by NudC (lane 2). No decapping activity was observed for any of the Nudix hydrolases from *S. acidocaldarius* (Figure 2.8A lanes 3, 5, 7, 9).

Based on sequence analysis and specifically the sequence similarity of SACI_RS00060 to other ADPR hydrolases, the archaeal Nudix proteins and their mutant variants were tested with 5'-ADPR-RNA. Following the same experimental setup described above, the proteins were incubated with the same RNA model substrate, this time carrying a 5'-ADPR cap. The positive control was conducted using the human Nudix hydrolase hNudT5 which had previously been shown to hydrolyze ADPR *in vitro* (Yang et al., 2000; Zha et al., 2006). Reactions were again separated on a denaturing APB-PAA gel, showing the successful production of 5'-p-RNA from 5'-ADPR-RNA by decapping from hNudT5 and SACI_RS00060 (Figure 2.8B, lanes 2 and 3). Based on this result SACI_RS00060 was renamed to Saci_NudT5. The Nudix domain-mutant variant of Saci_NudT5 showed no decapping activity (lane 4) and thereby confirmed the essentiality of the three exchanged glutamic acid residues to this protein's activity, as well as serving as a negative control to the Saci_NudT5

ADPR-RNA decapping reaction. None of the other three Nudix hydrolases showed any activity towards 5'-APDR-RNA.

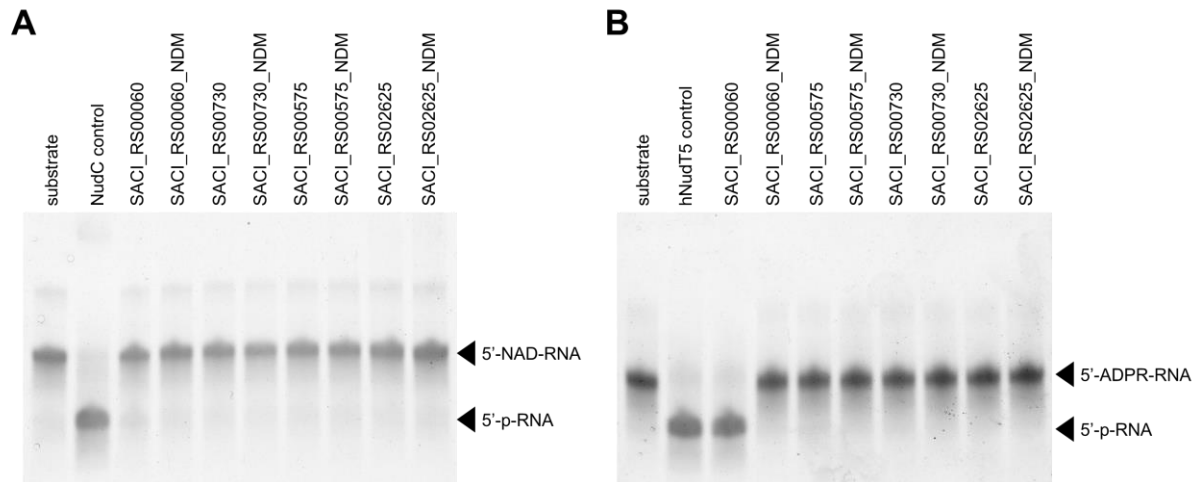


Figure 2.8: Decapping assays using the Nudix hydrolases from *S. acidocaldarius* on A) 5'-NAD-RNA and B) 5'-ADPR-RNA. Reactions with the archaeal enzymes were incubated for 5 min at 65°C and with the control enzymes (NudC for NAD-RNA and hNudT5 for ADPR-RNA) for 5 min at 37°C. Reactions were analyzed via denaturing APB-PAGE. Black arrows indicate the position of the intact NAD-RNA or ADPR-RNA substrate and the post-decapping product 5'-p-RNA in the gel. Image by José Vicente Gomes-Filho.

Furthermore, the RNA model substrate was generated carrying a 5'-Ap4A-cap to test the ability of the archaeal Nudix hydrolases, specifically SACI_RS00575, in decapping dinucleoside polyphosphate-capped RNAs. The bacterial pyrophosphohydrolase RppH from *E. coli* served as a positive control. As the reactions were resolved via standard denaturing PAGE and decapping by RppH results in 5'-p-RNA, the product is visible as a small shift in the gel, corresponding to a size difference of one nucleotide (Figure 2.9 lane 2). None of the archaeal Nudix hydrolases showed any activity on polyphosphate-capped RNA (Figure 2.9 lanes 3-10).

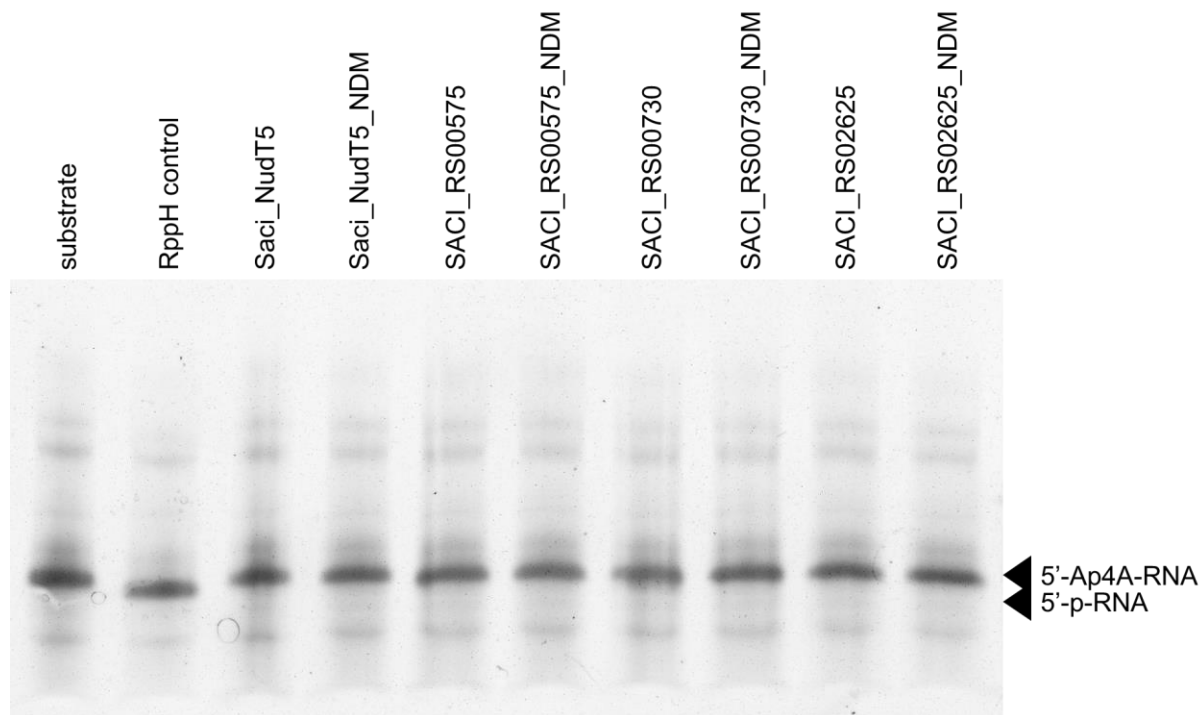


Figure 2.9: Decapping Assays using the Nudix hydrolases from *S. acidocaldarius* on 5'-Ap4A-RNA. Reactions with the archaeal enzymes were incubated for 5 min at 65°C and with the control enzyme RppH 5 min at 37°C. Reactions were analyzed via Urea-PAGE. Black arrows indicate the positions of Ap4A-RNA (pre-decapping) and 5'-p-RNA (post-decapping) in the gel. Image by José Vicente Gomes-Filho.

Additionally, an experiment was performed to test possible interactions of the archaeal Nudix hydrolases. To this end, equimolar amounts of Saci_NudT5 and another Nudix hydrolase were incubated with NAD-RNA or ADPR-RNA for 5 min at 65°C and separated via denaturing APB-PAGE. Control reactions were performed in parallel with Saci_NudT5 and NAD-RNA (no decapping, Figure 2.10A lane 2) and Saci_NudT5 or hNudT5 with ADPR-RNA (decapping, Figure 2.10A lanes 3-4). No activity or change to the RNA substrate was observed when NAD-RNA was incubated with Saci_NudT5 and another Nudix hydrolase (Figure 2.10A lanes 5-7). Similarly, incubation with SACI_RS00730 or SACI_RS00575 had no effect on the decapping of ADPR-RNA by Saci_NudT5 (Figure 2.10A lanes 8-9). However, decreased efficiency of the decapping reaction was observed in the presence of SACI_RS02625. Here, Saci_NudT5 was able to decap approx. 50% of the substrate during a 5 min reaction, as opposed to 100% in all previous reaction setups (Figure 2.10A lane 10). Following this observation, the experiment was repeated by adding increasing concentrations of SACI_RS02625 to the reaction. As shown in Figure 2.10B, increased concentrations

of SACI_RS02625 coincided with decreased amounts of the decapping product 5'-p-RNA (lanes 3-5). The same effect was observed for the Nudix domain-mutant variant of SACI_RS02625 (lanes 6-8).

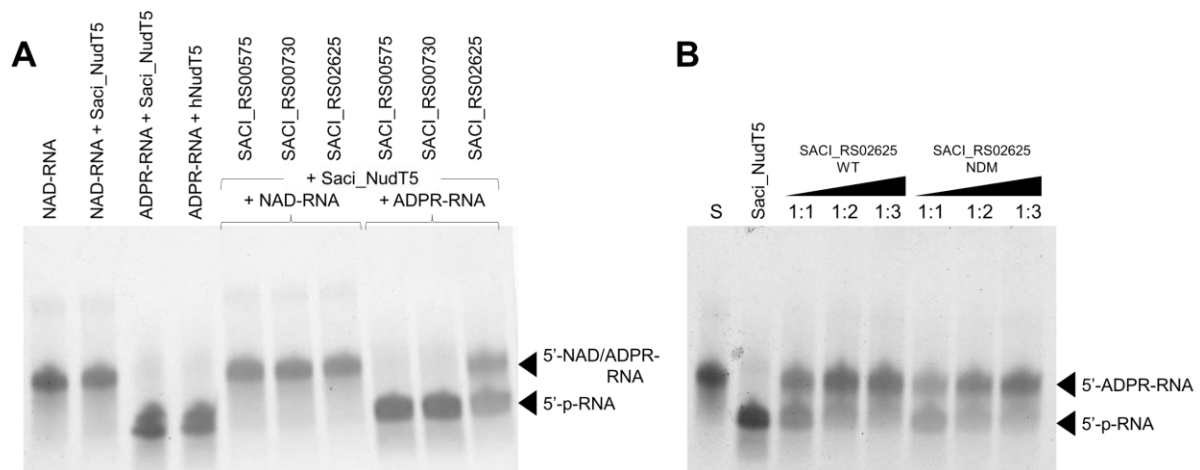


Figure 2.10: Interaction assay with the Nudix hydrolases from *S. acidocaldarius*. A) Saci_NudT5 is incubated with either NAD-RNA or ADPR-RNA and one of the other Nudix hydrolases SACI_RS00730, SACI_RS00575 or SACI_RS02625. B) Saci_NudT5 is incubated with ADPR-RNA and increasing concentrations of SACI_RS02625 wild-type protein (lanes 3-5) or Nudix domain-mutant protein (lanes 6-8). Reactions were analyzed via denaturing APB-PAGE. Black arrows indicate the positions of ADPR-RNA (pre-decapping) and 5'-p-RNA (post-decapping) in the gel. Images by José Vicente Gomes-Filho.

2.6.3 Malachite Green assays

To assess the activity of the purified recombinant Nudix hydrolases and elucidate possible substrates, the proteins and their respective Nudix domain-mutant variants were subjected to assays using Malachite Green. Briefly, this assay is based on the formation of a complex between Malachite Green, molybdate and free orthophosphate. The colorimetric product stably forms at room temperature in 30 min and absorbance at 620 nm is directly correlated to the amount of phosphate in the reaction. Due to the high affinity of Malachite Green to free phosphate, all reagents and components were tested for phosphate contamination prior to assay setup. All protein samples containing SACI_RS02526 and its mutant variant exhibited high levels of phosphate contamination and were consequently excluded from this assay. SACI_RS00730, Saci_NudT5, SACI_RS00575 and their mutant variants were tested for hydrolysis activity towards the canonical nucleotide substrates ATP, dATP and dGTP and the metabolites ADPR, NAD and Ap4A which had previously been used to 5'-cap the model RNA substrate. As the exact nature of their activity was unknown,

the Nudix hydrolases were first incubated with the substrate in so-called “uncoupled” reactions for 10 min at 65°C, followed by incubation with a “coupling” enzyme. The coupling enzyme Inorganic Pyrophosphatase from *E. coli* (“PPase”) was used for hydrolysis reactions producing pyrophosphate, while Bovine Alkaline Phosphatase (“APase”) was used for hydrolysis reactions yielding a sugar-phosphate product. All proteins were tested with all substrates both in uncoupled and coupled reactions. Phosphate release from ADPR, NAD and Ap4A was detected only in coupled reactions. The mutant proteins served as controls for their wild-type counterparts and showed no activity during the experiments.

SACI_RS00730 exhibited release of free phosphate from ATP, dATP and dGTP even without the presence of the coupling enzyme (Figure 2.11). The levels of phosphate released during coupled and uncoupled reactions are similar. For dATP with PPase, as well as dGTP with and without PPase, the amount of released phosphate exceeded the assay’s detection limit of 60 μM phosphate. In accordance with the decapping assays, SACI_RS00730 did not hydrolyze ADPR or NAD, as no free phosphate was detected after incubation with the coupling enzyme. However, a small amount of phosphate was detected from Ap4A after addition of APase (Figure 2.11).

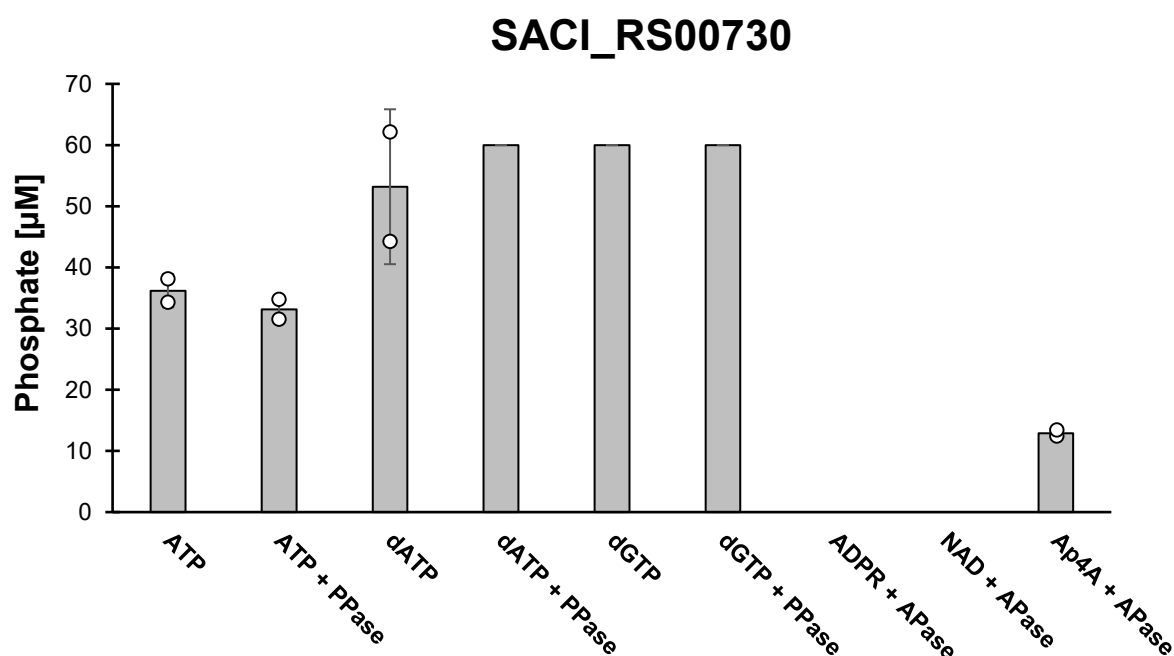


Figure 2.11: *In vitro* assay using Malachite Green to assess the activity of SACI_RS00730 towards hydrolysis of different substrates. Successful hydrolysis is indicated by the release of orthophosphate, measured in μM . Substrate + PPase indicates treatment with the coupling enzyme

Inorganic Pyrophosphatase from *E. coli* and substrate + APase indicates treatment with the coupling enzyme Bovine Alkaline Phosphatase.

Saci_NudT5 exhibited similar levels of released phosphate in uncoupled and coupled reactions for ATP, dATP and dGTP (Figure 2.12). Notably, dGTP hydrolysis produced more phosphate than that of ATP and dATP. Incubation with ADPR and APase produced a small amount of phosphate, while no phosphate was detected for NAD and Ap4A.

Incubation of SACI_RS00575 with dATP and dGTP resulted in small amounts of phosphate which increased after addition of the coupling enzyme PPase (Figure 2.13). Notably, this protein showed no activity towards ATP, ADPR, NAD or Ap4A, while the highest phosphate amount was released from dGTP.

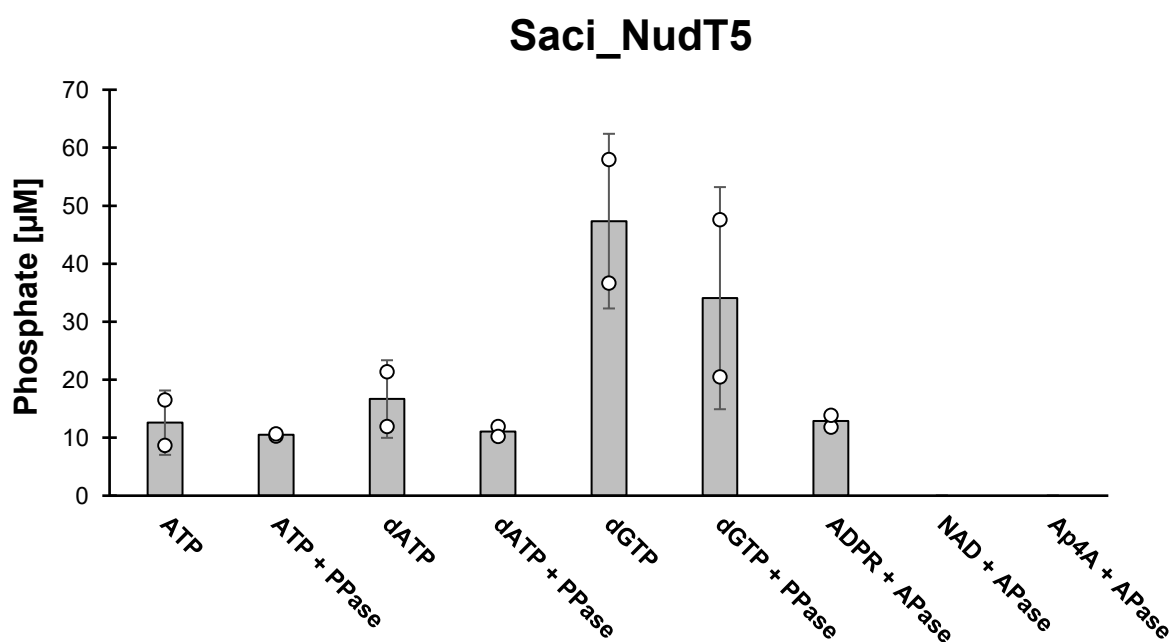


Figure 2.12: *In vitro* assay using Malachite Green to assess the activity of Saci_NudT5 towards hydrolysis of different substrates. Successful hydrolysis is indicated by the release of orthophosphate, measured in µM. Substrate + PPase indicates treatment with the coupling enzyme Inorganic Pyrophosphatase from *E. coli* and substrate + APase indicates treatment with the coupling enzyme Bovine Alkaline Phosphatase.

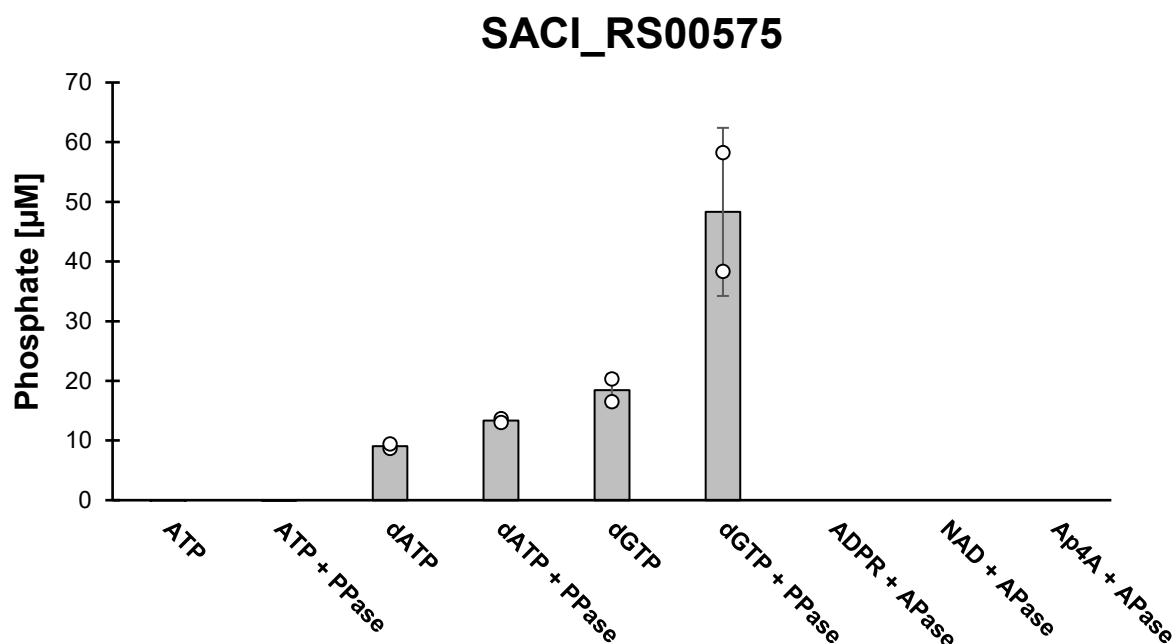


Figure 2.13: *In vitro* assay using Malachite Green to assess the activity of SACI_RS00575 towards hydrolysis of different substrates. Successful hydrolysis is indicated by the release of orthophosphate, measured in μM . Substrate + PPase indicates treatment with the coupling enzyme Inorganic Pyrophosphatase from *E. coli* and substrate + APase indicates treatment with the coupling enzyme Bovine Alkaline Phosphatase.

2.7 *In vivo* characterization

2.7.1 Generation of Nudix deletion strains

Parallel to protein purification and *in vitro* assays, the genes encoding the Nudix proteins in *S. acidocaldarius* were targeted for deletion. The generation of markerless deletion mutants was conducted in a two-step process using homologous recombination and the double marker cassette-carrying plasmid pSVA431 (Wagner et al., 2012). Here, the deletion plasmid carried a dual marker system consisting of the uracil cassette *pyrEF* and the *lacS* gene from *Sa. solfataricus* plus two multiple cloning sites. The first multiple cloning site harboured part of the GOI, while the second multiple cloning site harboured its upstream and downstream flanking regions (Figure 2.14A). The entire cassette was transformed as a linear fragment and integrated into the genome via homologous recombination induced by uracil selection. Successful integration was subsequently confirmed with Blue-White screening (Figure 2.14B). To obtain markerless deletion mutants, cells were grown on plates containing uracil and 5-FOA to induce uracil counterselection and remove the marker cassette in a second homologous recombination event (Figure 2.14C).

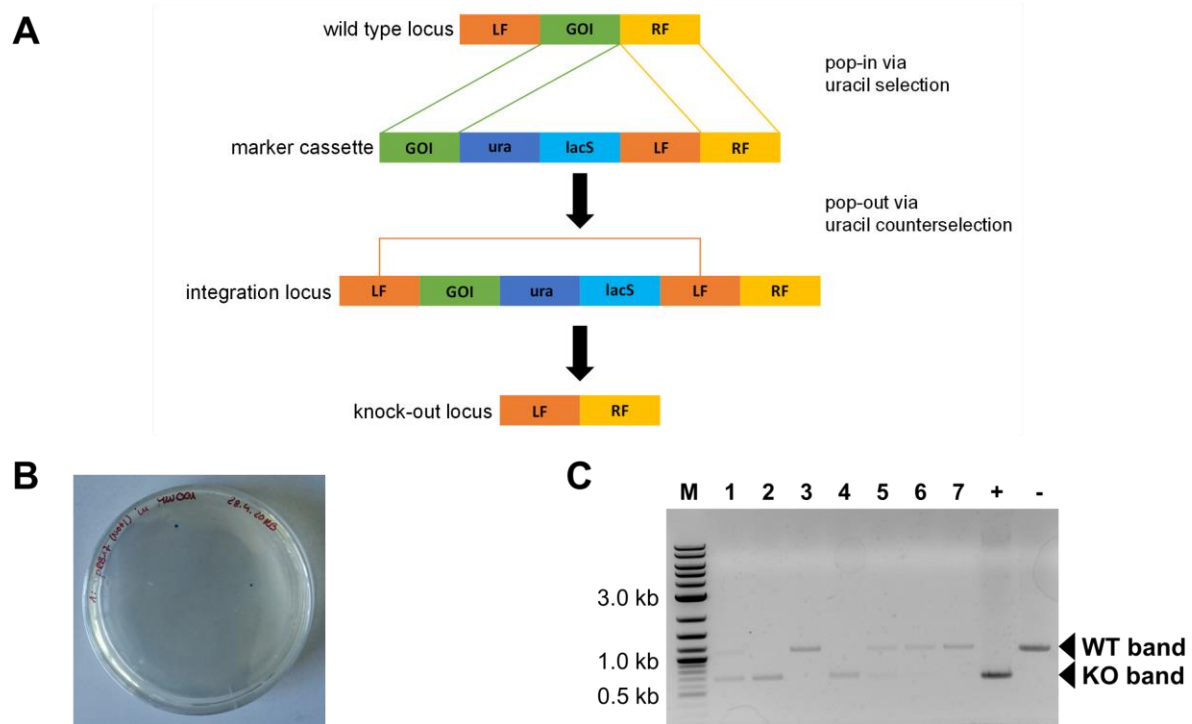


Figure 2.14: Deletion of the genes encoding the Nudix family hydrolases in *S. acidocaldarius* via homologous recombination. A) Schematic representation of the pop-in / pop-out method using a linear marker cassette fragment and indication of crossover scenarios between homologous regions. B) Confirmation of integration of the marker cassette fragment with Blue-White Screening. C) Representative PCR analysis of 7 colonies after treatment with 5-FOA to induce counterselection. The 1 kb band represents the wild-type locus and the 0.6 kb band represents the locus after deletion of the GOI. Depicted are clones from the deletion of the gene encoding SACI_RS02625. "+" = wild type, negative control = water.

With this approach, the genes encoding all four Nudix proteins SACI_RS00730, Saci_NudT5 (SACI_RS00060), SACI_RS02625 and SACI_RS00575 were individually deleted from the genome of *S. acidocaldarius* DSM639 MW001. As the Nudix genes, with the exception of SACI_RS00575, were overlapping with likely essential genes, the GOIs were removed without interrupting their neighbouring overlapping genes. To account for possible redundancy, a double deletion strain of the genes encoding the two proteins with the highest sequence similarity, SACI_RS00730 and Saci_NudT5 (SACI_RS00060), was generated. Here, electro-competent cells from the SACI_RS00060 deletion strain were transformed with the linear marker cassette targeting SACI_RS00730 and submitted to the previously described two-step selection process. The successful removal of the Nudix genes without disturbing their gene neighbourhoods was subsequently verified by RNA-sequencing (see below).

2.7.2 Phenotypical analysis

To investigate the effects of the deletion of the single Nudix genes on the *S. acidocaldarius* phenotype, the wild-type MW001 and the Nudix deletion strains were grown in standard medium, as well as under nitrogen stress and carbon stress conditions at 75°C over a period of 5 days. To track of cell growth over this extended time period and to not starve the cells, stationary phase cell culture was transferred into fresh medium and samples were taken for the measurement of the optical density (OD) every 24h. Each strain was measured in triplicates for each condition. Under standard conditions, cells showed constant growth over the first 48h, at which point they entered the early stationary phase and growth slowed down visibly before reaching a plateau shortly thereafter (Figure 2.15). Under nitrogen stress conditions cell growth was noticeably slowed down, however cells kept growing for about 72h before dying rapidly (Figure 2.16). None of the Nudix deletion strains exhibited a significant growth phenotype compared to the wild type strain under standard or nitrogen stress conditions. Under carbon stress conditions, cells grew slowly but constantly for 24h before reaching a plateau lasting another 24h and cell death setting in after a total of 48h (Figure 2.17). Surprisingly, the SACI_RS02625 deletion strain exhibited significantly increased cell growth in the first 24h compared to the wild-type strain, even though cell death occurred around the same timepoint and at the same rate. No significant difference was detected between the other Nudix deletion strains and the wild-type strain under carbon stress conditions. After 96h the reliability of the final OD measurements was affected by evaporation, as well as formation of cell aggregates in the cultures grown under nitrogen and carbon stress conditions.

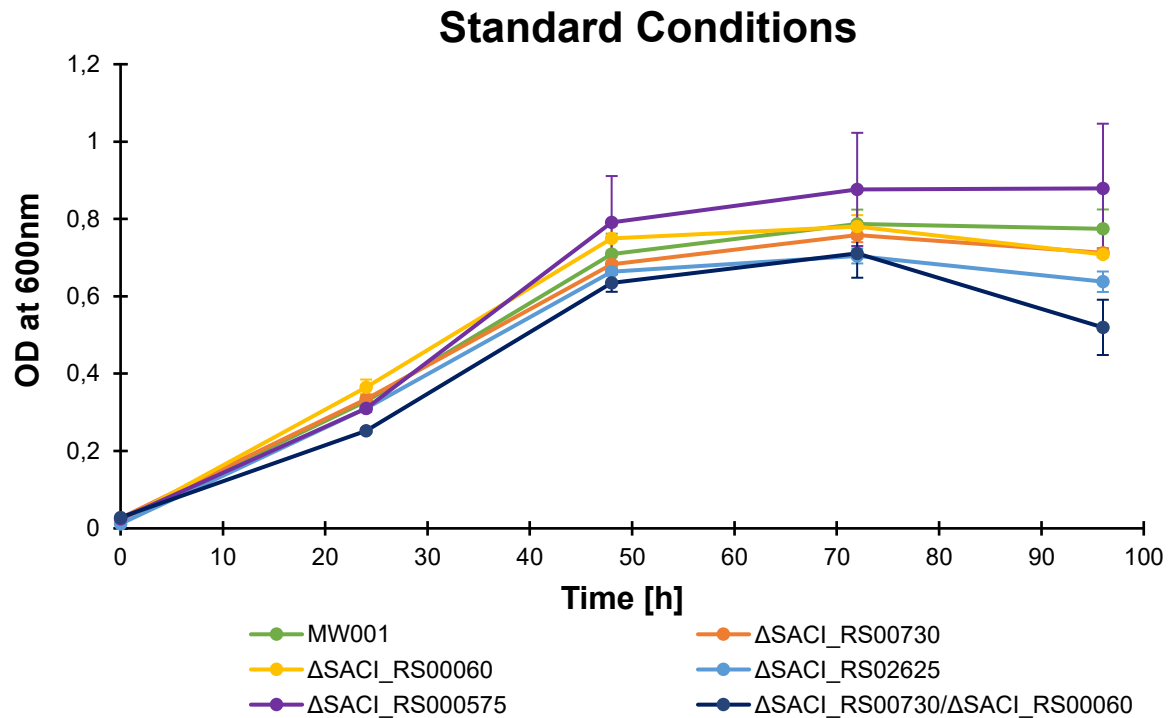


Figure 2.15: Growth curves depicting the cell growth of the *S. acidocaldarius* DSM639 MW001 wild-type and Nudix deletion strains over 5 days under standard growth conditions. All strains were grown in triplicates.

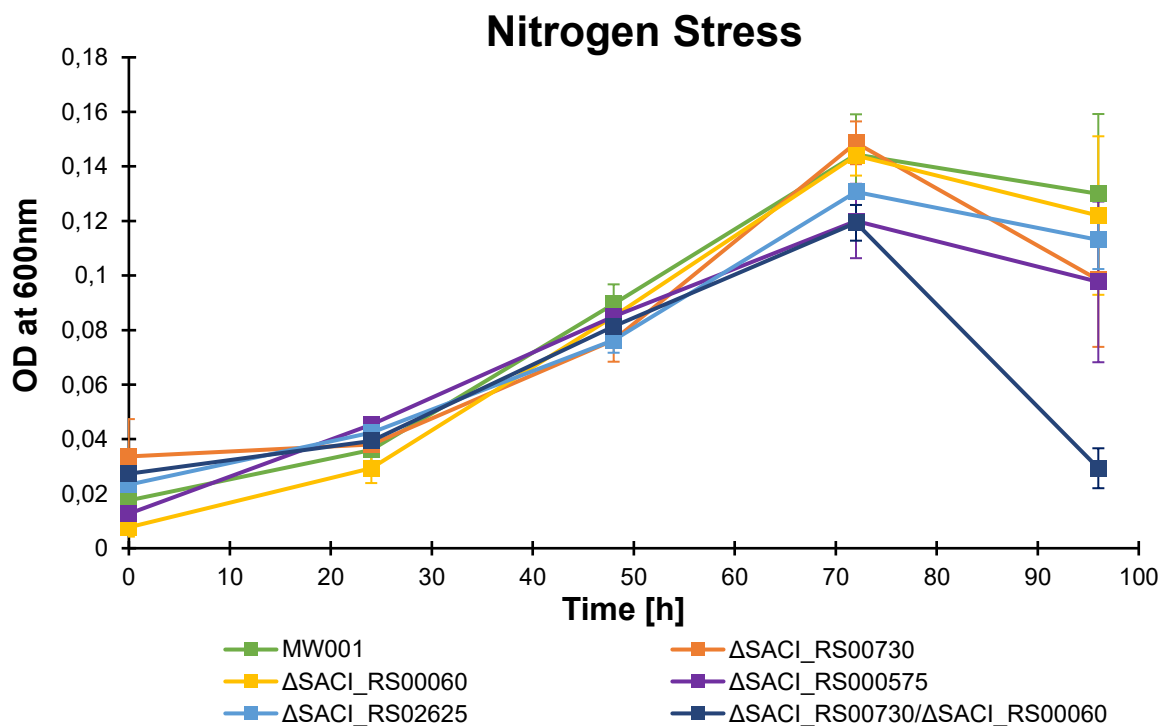


Figure 2.16: Growth curves depicting the cell growth of the *S. acidocaldarius* DSM639 MW001 wild-type and Nudix deletion strains over 5 days under nitrogen stress conditions. To induce nitrogen stress, the cells were grown in standard medium lacking NZ-Amine. All strains were grown in triplicates.

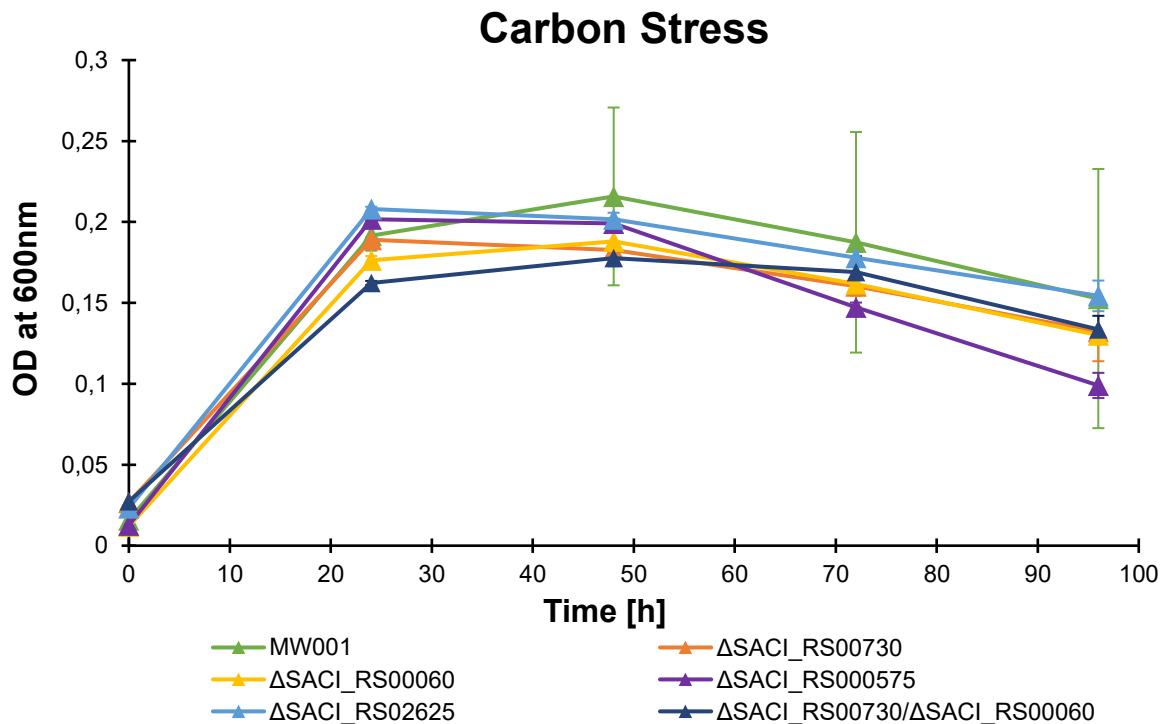


Figure 2.17: Growth curves depicting the cell growth of the *S. acidocaldarius* DSM639 MW001 wild-type and Nudix deletion strains over 5 days under carbon stress conditions. To induce carbon stress, the cells were grown in standard medium lacking dextrin. All strains were grown in triplicates.

To assess the effect of another common environmental stressor, wild-type and Nudix deletion strains were subjected to heat stress at 87°C and cells were subsequently spotted on plates (Figure 2.18). To this end, cells were grown in triplicates to the early stationary phase and 1 ml from each culture was transferred onto a thermomixer. After a short adaption period, control samples were taken and cells were submitted to heat shock at 87°C for 30 min. Afterwards, the OD for each culture was equalized to 0.1, followed by preparation of a 10⁻¹ to 10⁻⁶ dilution series and subsequent spotting of 3 μl from each dilution onto plates supplemented with NZ-Amine, dextrin and uracil. After 5 days, plates were photographed and cell viability was determined by measuring spot density from the 10⁻⁴ dilution using the oval selection and area measurement tools from Fiji (Schindelin et al., 2012).

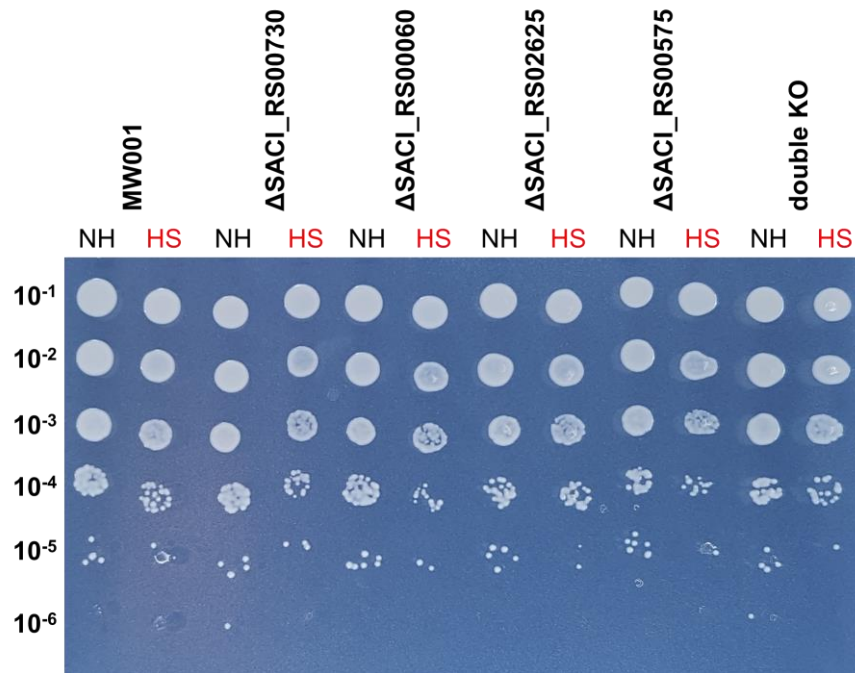


Figure 2.18: Exemplary heat shock spotting assay with *S. acidocaldarius* DSM639 MW001 wild type and Nudix deletion strains. Cells from the early stationary growth phase were heat-shocked (HS) by incubation at 87°C for 30 min in triplicates and spotted next to non-heat-shocked (NH) control samples. Plates were incubated for 5 days at 75°C. Depicted is replicate no. 3.

Regarding growth on solid medium, none of the deletion strains showed significantly reduced or increased cell growth relative to the WT (Figure 2.19), thereby corroborating the results observed for growth in liquid medium under standard conditions (Figure 2.15). Similar behavior was observed for the relative survival after heat shock exposure, where none of the deletion strains showed significantly reduced or increased survival (Figure 2.20). However, not all strains were affected by the heat shock to a similar extent. Exposure to 87°C caused significant reduction in relative cell viability compared to non-heated control samples for all strains except the Δ SACI_RS02625 strain. While heat-shocked cells showed survival rates between 33–65% compared to their control samples, in the Δ SACI_RS02625 strain 80% of cells were still viable after heat shock exposure (Figure 2.21).

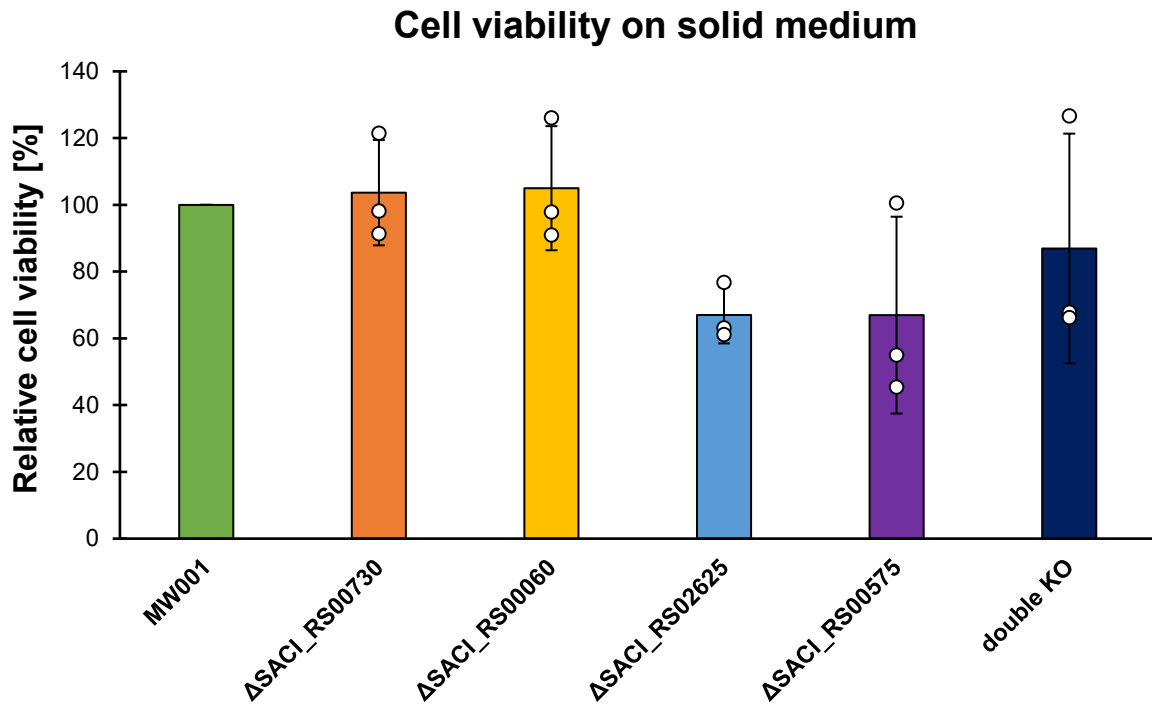


Figure 2.19: Cell viability of *S. acidocaldarius* Nudix deletion strains on solid medium under standard growth conditions. Depicted is the relative cell viability of the Nudix deletion strains grown on standard solid medium normalized against the wild type strain MW001.

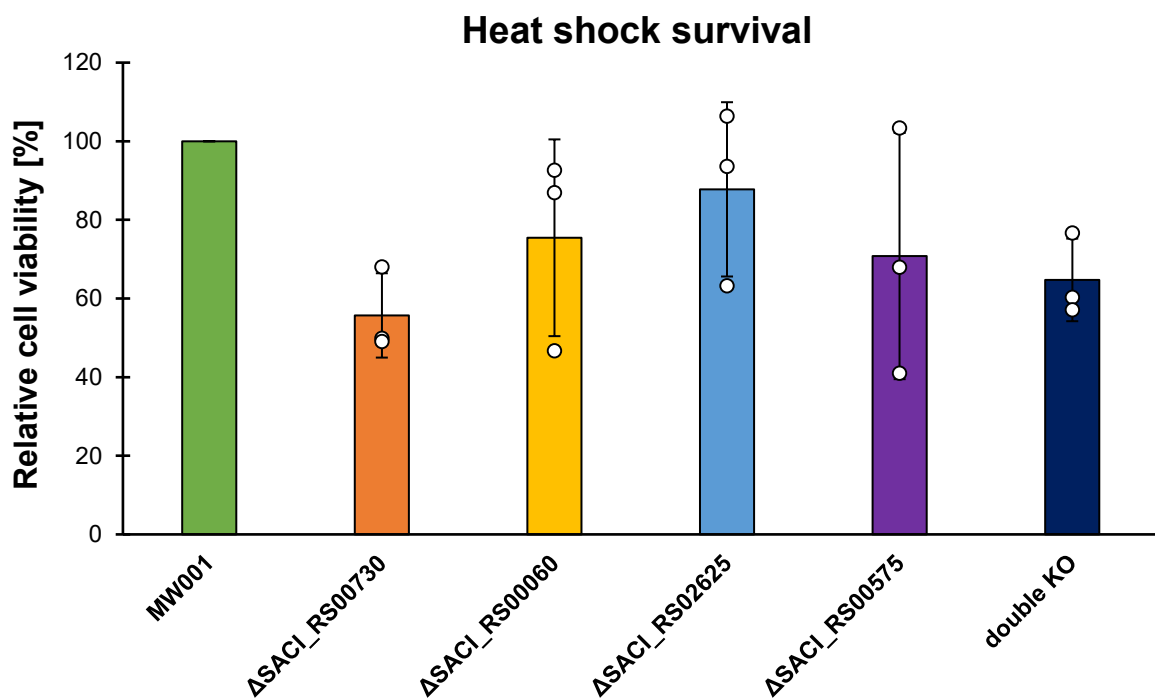


Figure 2.20: Survival after heat shock treatment of the *S. acidocaldarius* Nudix deletion strains. Cells were heat-shocked by incubation at 87°C for 30 min. Depicted is the relative cell viability after heat treatment normalized against the heat-shocked wild type strain MW001.

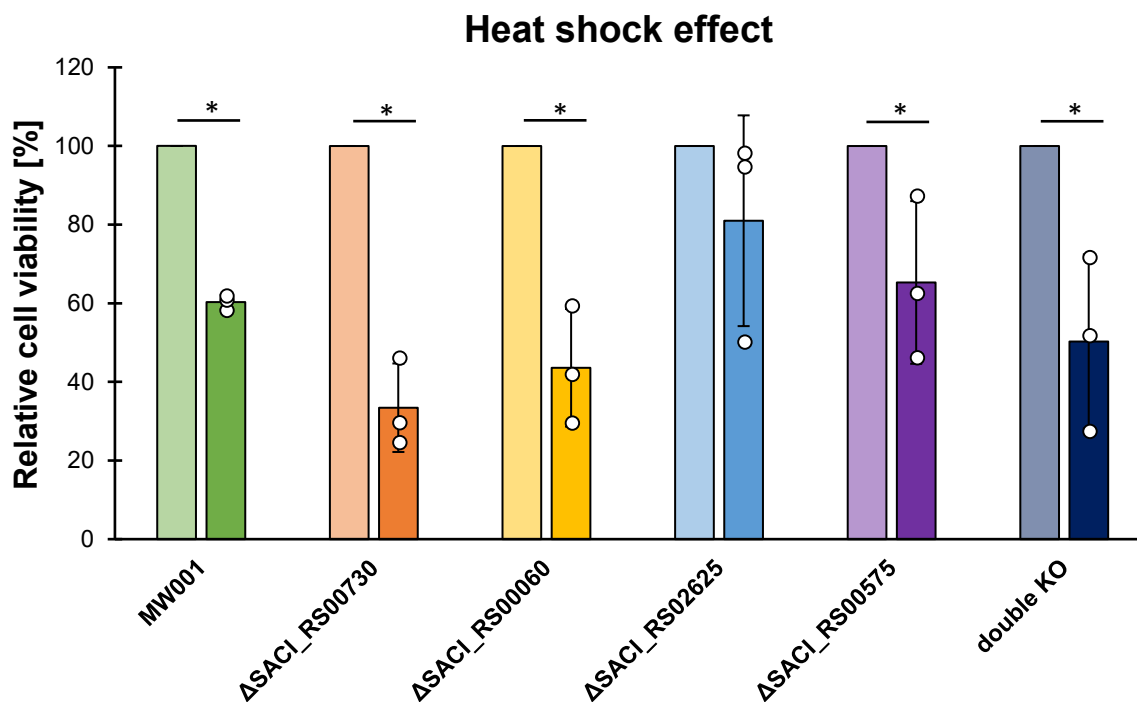


Figure 2.21: Effect of heat shock treatment on *S. acidocaldarius* DSM639 MW001 wild-type and Nudix deletion strains. Cells were heat-shocked by incubation at 87°C for 30 min. Depicted is the relative cell viability after heat treatment (solid bars) normalized by non-heat-treated control samples (opaque bars). Asterisk (*) denotes Student's t-test value <0.005.

2.8 Transcriptome Analysis

To establish their transcriptomic profiles, wild-type and Nudix deletion strains were grown in duplicates to mid-log or early stationary phase and cell pellets were collected for the respective timepoints. Total RNA extraction, rRNA depletion and library preparation were conducted as described in the Methods section and sequencing was performed on an Illumina® NextSeq550 at the Genomics Core Facility of the Philipps-Universität Marburg. The sequencing reads were aligned to the genome to corroborate the successful deletion of the Nudix genes. As depicted in Figure 2.22 panels A–D, no reads were detected for the genes encoding SACI_RS00730, Saci_NudT5 (SACI_RS00060) and SACI_RS00575 located on the reverse strand and the gene encoding SACI_RS02625 located on the forward strand. Similarly, no reads were detected for SACI_RS00730 and SACI_RS00060 in the double knock-out (KO) strain (Figure 2.23A and B). As evident from the genome annotation, three out of the four Nudix genes overlap with neighboring genes and knock-outs were created to leave overlapping genes intact (Figures 2.22 and 2.23).

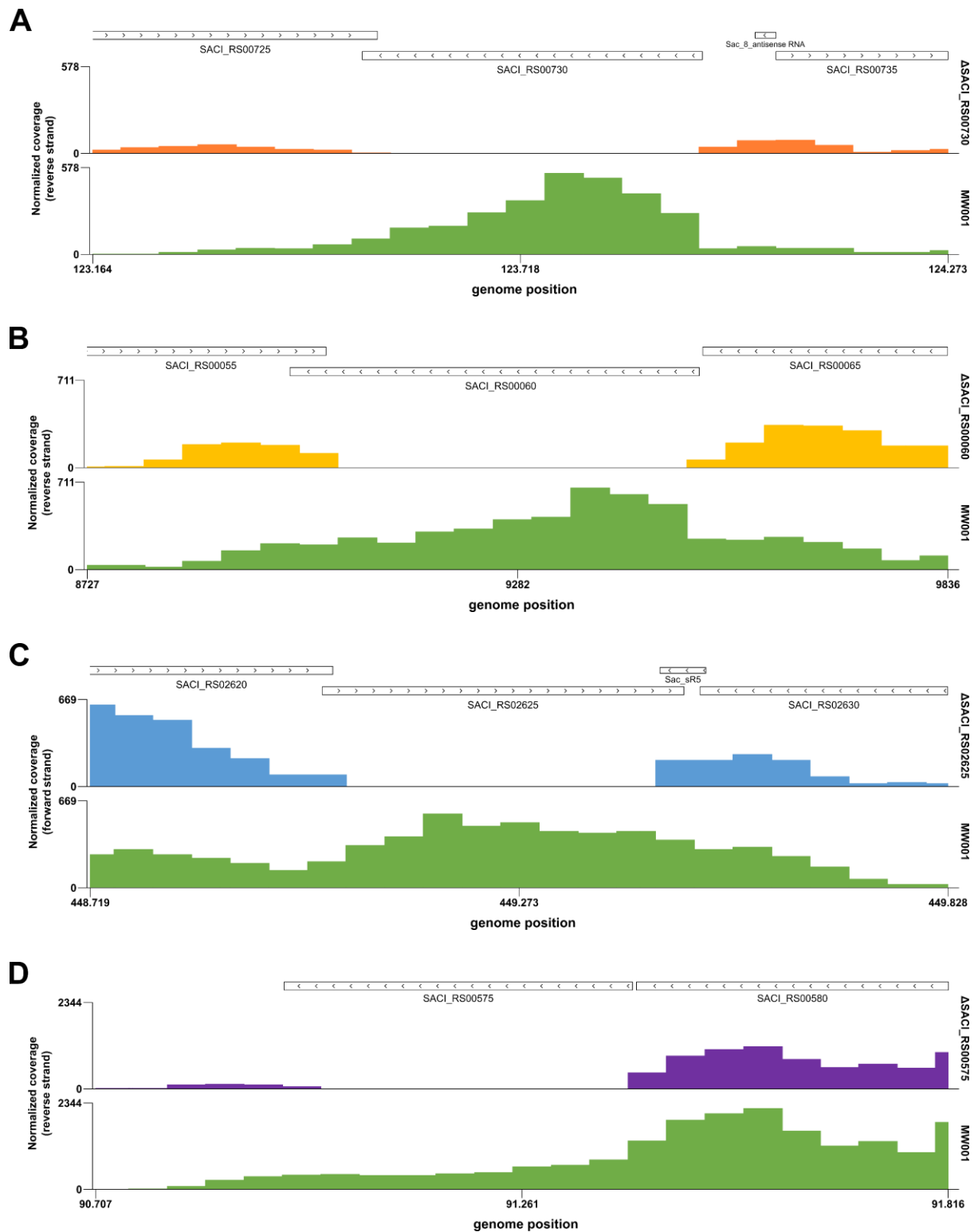


Figure 2.22: Coverage plots of the loci of the genes encoding the Nudix family hydrolases in *S. acidocaldarius* DSM639 MW001. Depicted are the loci of A) SACI_RS00730, B) SACI_RS00060, C) SACI_RS02625 and D) SACI_RS00575. For each gene knock-out, the WT locus (green) and the deletion locus (coloured) are shown. Coverage plots were visualized with the Integrative Genomics Viewer (IGV) (Robinson et al., 2011).

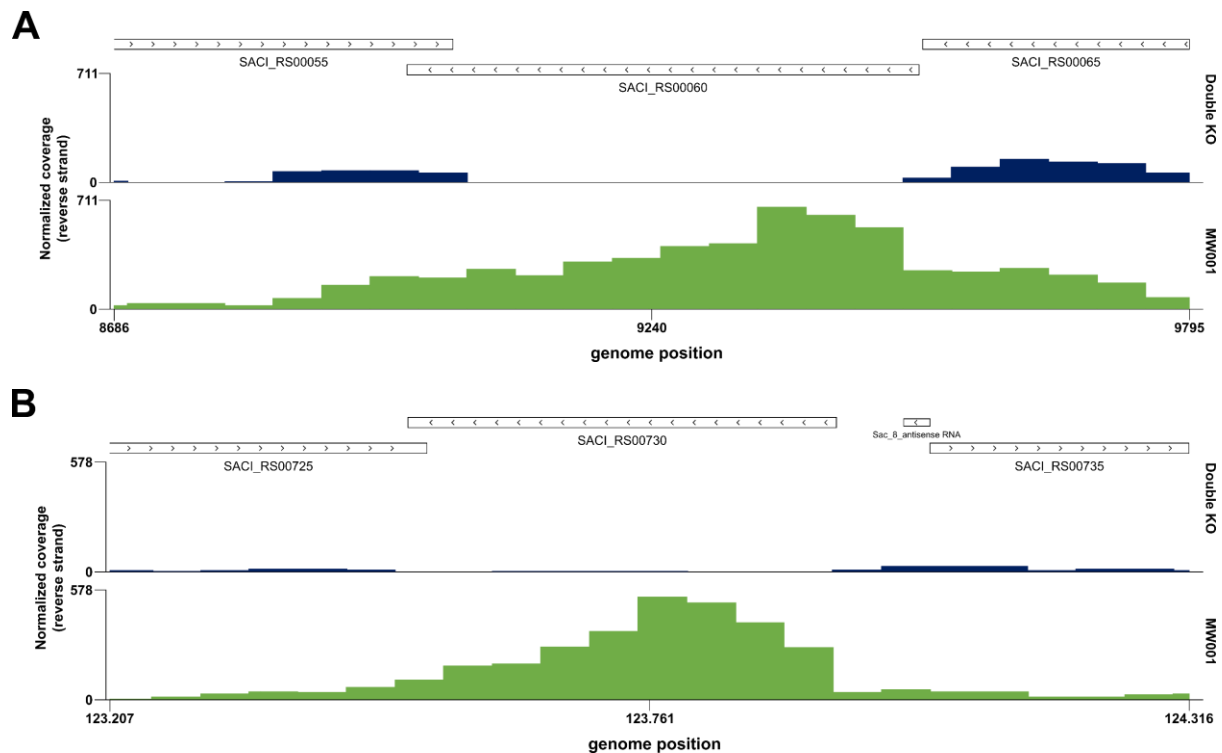


Figure 2.23: Coverage plots of the deletion loci in the Nudix double deletion strain. Depicted are the loci of A) SACI_RS000730 and B) SACI_RS00060 from the double knock-out strain (blue) in comparison to the respective WT locus (green). Coverage plots were visualized with the Integrative Genomics Viewer (IGV) (Robinson et al., 2011).

Coverage plots from the WT strain revealed similar coverage for SACI_RS00730, SACI_RS00060 and SACI_RS02625, while SACI_RS00575 exhibited approx. twice as many reads (Figure 2.22D).

To visualize the transcriptomic profiles of each strain, each dataset was normalized against the WT and assembled into a heatmap depicting the differentially regulated genes in the early stationary growth phase (Figure 2.24) and the mid-logarithmic growth phase (Supplementary Figure S4). Overall, the datasets revealed a more significant number of differentially regulated genes in the early stationary compared to the mid-log phase in all deletion strains (see Figures 2.24 and 2.25 for early stationary, Figures S4 and S5 for mid-log phase transcriptomes). Both heatmaps showed a similar clustering of the strains according to the similarity of their transcriptomic profiles with the exception of Δ SACI_RS00730 and Δ SACI_RS00575 switching their places on the opposite ends of the neighborhood tree when moving from mid-log into the early stationary phase. Nevertheless, both strains remained on opposite branches of the tree, clearly stating that these two transcriptomic profiles are most dissimilar. In

fact, almost all downregulated genes in Δ SACI_RS00575 were either unaffected or upregulated in the Δ SACI_RS00730 strain and vice versa. Notably, in the early stationary phase, the highest similarity was shared between the Δ SACI_RS00730 and Δ SACI_RS00060 strains, both of which are affected by the double KO, which in turn shows a distinct profile from the two single-deletion strains. The most significant number of differentially regulated genes is present in the double KO and the Δ SACI_RS00575 strain, thereby establishing these deletions as most impactful on the transcriptome. The smallest transcriptomic impact was caused by the individual deletions of SACI_RS00730 and SACI_RS00060 (Figure 2.24). In summary, each deletion strain revealed a distinct transcriptomic profile and clusters of similarly affected genes were rarely shared between more than two strains, giving each strain a unique profile and consequently hinting at unique roles for the enzymes encoded by the deleted genes.

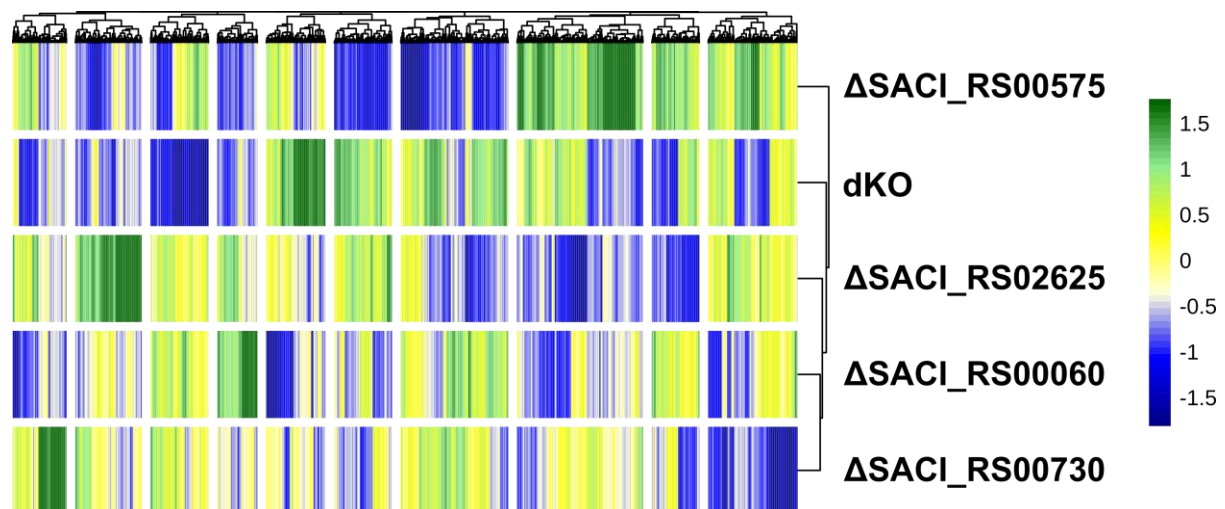


Figure 2.24: Heatmap of the \log_2 (FoldChange) of the transcriptome of the Nudix deletion strains relative to the WT strain *S. acidocaldarius* DSM639 MW001 in the early stationary growth phase. Genes were hierarchically clustered according to their expression behavior in the samples. The dendrogram represents Euclidean distances. Green: upregulated genes, blue: downregulated genes, yellow: unaffected. Heatmap generated by José Vicente Gomes-Filho.

To gain more insight into the impact of the individual Nudix deletions, the differentially regulated genes for each deletion strain in the early stationary growth phase (Figure 2.25) and the mid-logarithmic growth phase (Supplementary Figure S5) were assembled into iModulons according to the iModulonDB database (Chauhan et al., 2021; Rychel et al., 2021). By definition, an iModulon (*i*ndependently *m*odulated

signal) is a group of genes that are similarly expressed under different (growth) conditions and therefore suspected to share a common regulator. The iModulons were identified by observing patterns in transcriptomic datasets using unsupervised machine learning and independent component analysis (ICA) (Rychel et al., 2021). To date, the genes encoding the four Nudix family hydrolases are not assigned to any iModulons.

Deletion of SACI_RS00060 exhibited minimal impact on the transcriptome regarding the number of the differentially regulated genes in the mid-logarithmic phase (Supplementary Figure S5A) and only slightly more so in the early stationary phase (Figure 2.25A). Overall, this deletion strain exhibited upregulation of genes implicated with heat and cold stress response, amino acid metabolism (specifically an upregulation of glutamine, serine and threonine, contrasted by downregulation of lysine biosynthesis), genes controlled by the XylR-SoxM transcriptional regulators and a large number of upregulated genes implicated in translational regulation, the largest group in the database, represented by three different iModulons (Figure 2.25A).

Similarly, deletion of SACI_RS00730 caused upregulation of genes implicated in cold stress, UV stress and translational regulation in mid-log phase cells (Supplementary Figure S5B). Purine metabolism experienced some downregulation while the iModulon controlled by XylR-SoxM was generally upregulated. In the early stationary phase, the transcriptome was characterized by upregulation of genes involved in sulfur assimilation, cold/heat/UV stress, translational regulation and the XylR-SoxM-controlled iModulon, while lysine biosynthesis exhibited downregulation (Figure 2.25B).

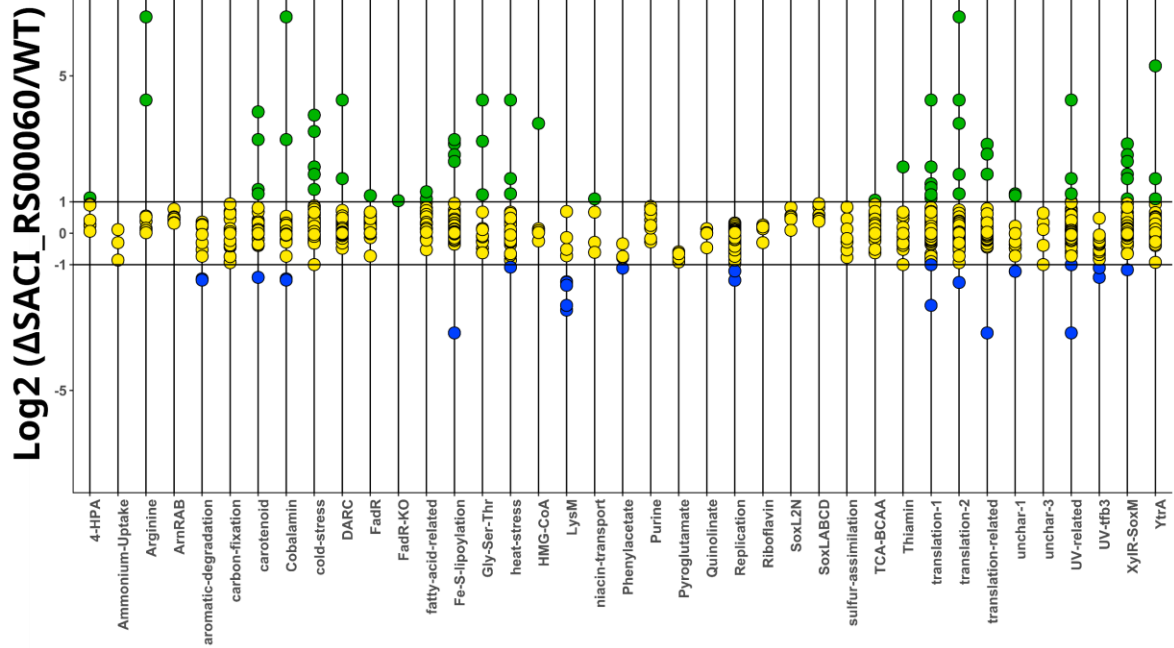
Deletion of SACI_RS02625 predominantly triggered upregulation of genes controlled by XylR-SoxM and YtrA, as well as genes involved in translational regulation, cold and UV stress and the carotenoid iModulon in mid-log phase cells (Supplementary Figure S5C). In early stationary phase cells, the impact of the deletion was notably increased and many iModulons were affected by upregulation of the genes assembled therein, such as the iModulons associated with fatty acid metabolism, transcriptional and translational regulation, cobalamin (vitamin B) metabolism and heat/cold/UV stress (Figure 2.25C). Significant downregulation was exhibited by genes attributed to the iModulon associated with replication and cell division. Furthermore, this deletion strain showed upregulation of *nadA* and *nadB*, two genes whose products presumably

catalyze the first two steps of the *de novo* NAD biosynthesis pathway. Notably, *nadB* (locus tag SACI_RS02620) is located upstream of SACI_RS02625.

Deletion of SACI_RS00575 affected transcriptional and translational regulation-associated iModulons in the mid-log phase and elicited upregulation of several UV stress-related genes (Supplementary Figure S5D). A more pronounced effect on the transcriptome was observed in the early stationary phase by upregulation of genes from a large variety of iModulons, such as transcriptional and translational regulation, heat/cold/UV stress, fatty acid, amino acid, carotenoid and nucleotide (specifically purine) metabolism (Figure 2.25D). Notably, the iModulons for lysine biosynthesis (LysM) and archaellum formation (ArnRAB) experienced downregulation. In the early stationary phase, this deletion strain also exhibited upregulation of two thermosome subunits and two genes from the CcdA and VapC families of Type II toxin-antitoxin systems.

Deletion of SACI_RS00730 and SACI_RS00060 in the double KO strain caused upregulation of purine and quinolinate biosynthesis (specifically the genes *nadA* and *nadB* in the *de novo* NAD biosynthesis pathway) in mid-log phase cells, as well as predominant but not exclusive upregulation of genes associated with transcriptional and translational regulation (Supplementary Figure S5E). Downregulation of a few genes associated with amino acid and fatty acid metabolism, as well heat stress was also observed. In the early stationary phase, a large variety of iModulons was affected, often experiencing up- and downregulation of several genes attributed to the same operon, such as in the iModulons for transcriptional and translational regulation, heat stress and UV stress (Figure 2.25E). Predominantly upregulated iModulons encompassed carotenoid metabolism, cold stress, fatty acid metabolism and purine biosynthesis. Differentially upregulated genes also included two thermosome subunits and two genes from the CcdA and VapC families of Type II toxin-antitoxin systems. Notably, downregulation of almost the entire archaellum formation and lysine biosynthesis iModulons was observed.

A



B

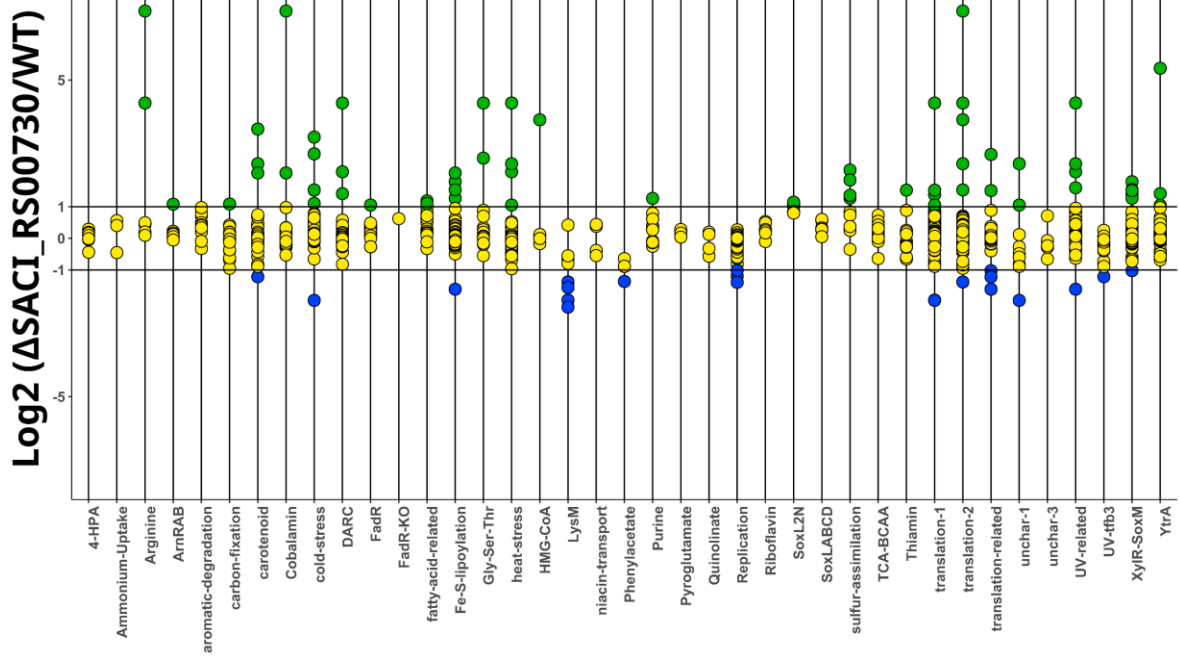
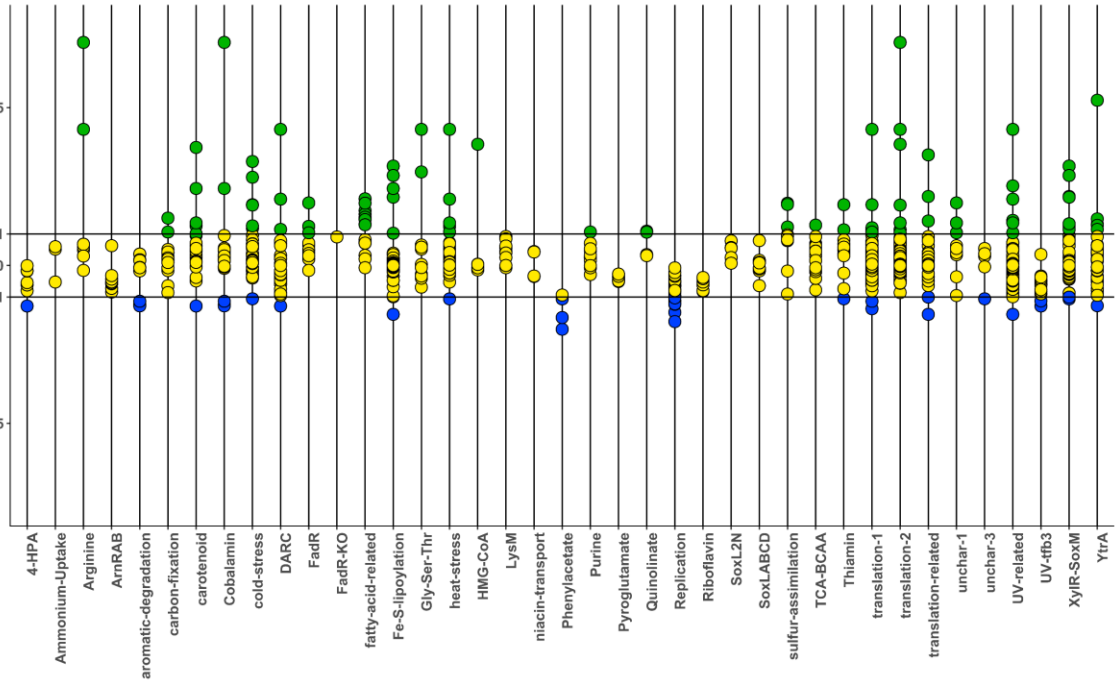


Figure continued on the next page

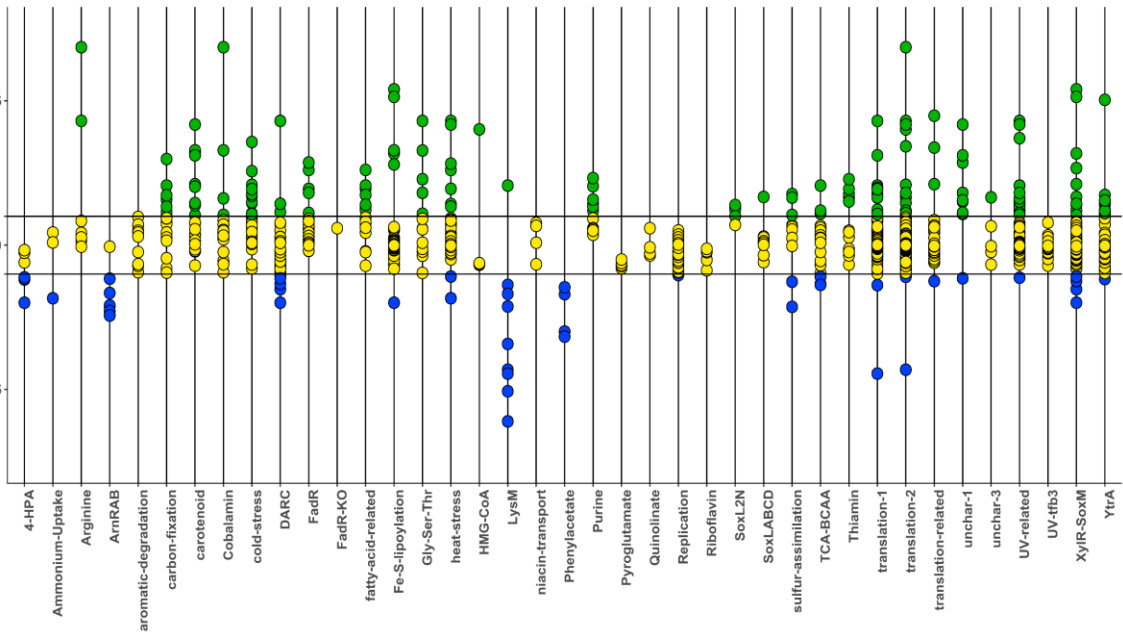
C

Log2 (Δ SACI_RS02625/WT)



D

Log2 (Δ SACI_RS00575/WT)



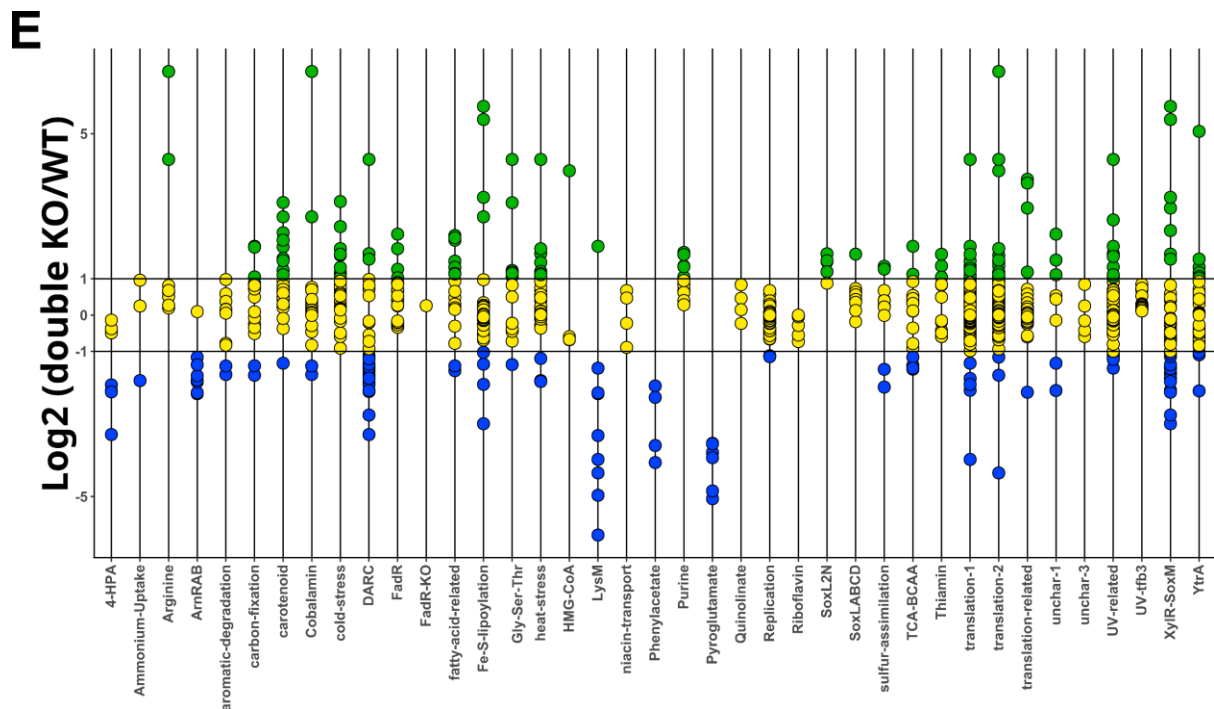


Figure 2.25: Dot Plots of differentially regulated genes in the Nudix deletion strains in the early stationary growth phase. Log₂ (FoldChange) in relation to the WT strain *S. acidocaldarius* DSM639 MW001 for A) Δ SACI_RS00730, B) Δ SACI_RS00060, C) Δ SACI_RS02625, D) Δ SACI_RS00575 and E) the double KO strain. Green: upregulated genes, blue: downregulated genes, yellow: unaffected. Genes were assembled into clusters of similarly expressed genes based on the iModulonDB database (Chauhan et al., 2021; Rychel et al., 2021). Dot Plots generated by José Vicente Gomes-Filho.

Between the five Nudix deletion strains, 25 genes were identified to be differentially upregulated in all strains in the early stationary phase (Table 2.1). No common genes were identified for the mid-log phase or differentially downregulated genes. Approx. half of these genes encode hypothetical proteins or proteins with domains of unknown function (DUF) (Table 2.1). Furthermore, several transcriptional regulators were affected in all deletion strains. Sulfite exporter, thioredoxin and FAD-dependent oxidoreductase encoding genes were also upregulated among all strains. Most of these genes are attributed to the iModulons of translational regulation and transcriptional regulation by XylR-SoxM or YtrA, as well as cold stress response (Supplementary Table S1). Lastly, a correlation between the 5'-NAD-capped RNAs identified in *S. acidocaldarius* and the deletion of any of the Nudix family hydrolases was not observed.

Table 2.1: Differentially upregulated genes in all Nudix deletion strains relative to the wild-type strain *S. acidocaldarius* DSM639 MW001. Genes are displayed with new and old locus tags, as well as annotated iModulons and functions according to the archaeal cluster of orthologous genes (arCOG) database (Chauhan et al., 2021; Makarova et al., 2015; Rychel et al., 2021; Tatusov et al., 2000).

New locus tag	Old locus tag	iModulon	arCOG	function
SACI_RS00295	Saci_0065	-	R	Predicted transcriptional regulator
SACI_RS01470	Saci_0301	Arginine, Translation-2, Cobalamin	S	Uncharacterized membrane protein, DUF981 family
SACI_RS01585	Saci_0324	Fe-S-liposylation, XylR-SoxM	P	Sulfite exporter, TauE/SafE family
SACI_RS01880	Saci_0384	HMG-CoA, Translation-2	S	Uncharacterized protein, contains N-terminal coiled-coil domain, DUF2203 family
SACI_RS04775	Saci_1000	-	-	tRNA
SACI_RS04790	Saci_1003	-	G	MFS family permease
SACI_RS05570	Saci_1169	Fe-S-liposylation, XylR-SoxM	O	FAD-dependent Thioredoxin reductase
SACI_RS05830	Saci_1223	Heat Stress, UV-related, DARC	K	MarR family transcriptional regulator, contains HTH domain
SACI_RS06205	Saci_1298	Translation-1	R	Predicted Rossmann fold nucleotide-binding protein
SACI_RS08205	n.a.	-	-	hypothetical protein
SACI_RS08380	Saci_1753	Heat Stress, Translation-1, Arginine, Translation-2, UV-related, DARC, Gly-Ser-Thr	X	Uncharacterized membrane protein, virus associated, DUF5658 family
SACI_RS08740	Saci_1823	Fe-S-liposylation, XylR-SoxM	O	Thiol-disulfide isomerase or thioredoxin
SACI_RS08850	Saci_1845	Carotenoid	S	Uncharacterized protein
SACI_RS09990	Saci_2066	Cold Stress	S	Uncharacterized protein
SACI_RS09995	Saci_2067	Cold Stress, Translation-2	S	Hemerythrin HHE cation binding domain containing protein
SACI_RS10000	Saci_2068	Cold Stress	S	Cupin domain fused to uncharacterized domain of COG4309, DUF488 family
SACI_RS10005	Saci_2069	Cold Stress, Translation-1, Thiamin	O	Metal-sulfur cluster biosynthetic enzyme
SACI_RS10475	Saci_2166	Gly-Ser-Thr	S	Uncharacterized protein, DUF488 family

Table continued on the next page

SACI_RS10515	Saci_2175	XylR-SoxM, YtrA, DARC	S	Uncharacterized membrane protein
SACI_RS10550	Saci_2183	-	K	Transcriptional regulator, contains HTH domain
SACI_RS10555	Saci_2184	-	S	Uncharacterized protein, DUF488 family
SACI_RS10705	Saci_2214	Fatty-acid- related, YtrA	S	Uncharacterized membrane protein
SACI_RS10825	Saci_2239	-	P	Predicted divalent heavy-metal cations transporter
SACI_RS11045	Saci_2283	-	H	Thiaminase, TenA family transcriptional regulator
SACI_RS11050	Saci_2284	YtrA	K	Acetyltransferase (GNAT) family

n.a.: not available, G: Carbohydrate Metabolism and Transport, H: Coenzyme Metabolism and Transport, K: Transcription, O: Post-Translational Modification, Protein Turnover, Chaperones, P: Inorganic Ion Transport and Metabolism, R: General Functional Prediction Only, S: Function Unknown, X: Mobilome: Prophages, Transposons

3 Discussion

3.1 Designing a circular SRP RNA for *S. acidocaldarius*

The SRP RNA is an essential non-protein-coding small RNA present in organisms from all three domains of life. Hence it was initially surprising to discover archaeal organisms, like the hyperthermophile *Thermoproteus tenax*, which did not seem to possess an SRP RNA (Siebers et al., 2011). Further investigation revealed that *T. tenax* indeed possesses an SRP RNA gene, which had escaped discovery thus far due to its permutation, i.e. positioning of the 3' half upstream of the 5' half (Plagens et al., 2015). As the new termini are present in a functionally important region, functionality of the SRP RNA can only be restored by its circularization which is conducted by the tRNA splicing machinery via its recognition feature, the bulge-helix-bulge (BHB) motif (Plagens et al., 2015). This represents a remarkable deviation from an otherwise highly conserved molecule and raises questions as to its evolution and possible fitness benefits. To this end, *S. acidocaldarius* provides an ideal model, as it is a closely related hyperthermophilic archaeon living under similar environmental conditions, while possessing a canonical, linear SRP RNA molecule (Batey et al., 2000). Furthermore, as *S. acidocaldarius* exhibits 21 intron-containing tRNAs (listed in the genomic tRNA database GtRNAdb (Chan & Lowe, 2009)), it must consequently possess the machinery to process them into mature tRNAs, consisting of a tRNA splicing endonuclease and a tRNA ligase (Kaine, 1987). Accordingly, the *S. acidocaldarius* SRP RNA gene was modified to contain the distinct features of the *T. tenax* SRP RNA gene and introduced into the organism, yielding a strain carrying both the original and the modified SRP RNA gene variants in the genome and on a plasmid, respectively.

Identification of the circular SRP RNA variant, marked by its unique identifier in the functional loop of helix 8b, via inverse reverse transcription PCR was unsuccessful. When changing the detection strategy to RNA-seq, the presence of the circular SRP RNA molecule was finally confirmed and the reason for lack of discovery with the previous method became apparent. Compared to the wild-type SRP RNA, the coverage of the circular variant was decreased by about 100-fold, suggesting low expression of this RNA molecule. For initial investigation, the permuted gene including its native promoter had been cloned into an *E. coli/S. acidocaldarius* shuttle vector. As this expression plasmid already contained a promoter (the arabinose-inducible

promoter *saci_2122*), the latter was removed from the plasmid to prevent any interference regarding transcription from the native SRP RNA promoter. One half of this plasmid, relevant for propagation in *E. coli*, originates from the cloning vector pBR322, while the other half, relevant for cloning in *Sulfolobus*, is derived from the plasmid pRN1 which was originally isolated from *S. islandicus* and exhibits a copy number of 2-8 (Berkner et al., 2007). Additionally, circular molecules are notably less susceptible to adapter ligation and it is possible that this bias was created during the process of cDNA library preparation. Other studies on circular RNAs in Archaea have also reported a decreased number of reads from circular RNA molecules compared to linear reads (Danan et al., 2012; Plagens et al., 2015; Schwarz et al., 2020). To this end, sequencing targeted at circular RNA molecules should emphasize the enrichment step, e.g. by treatment with the 3'→5' exonuclease RNase R which digests linear but not circular molecules, as well as the fragmentation step, usually conducted in the form of chemical fragmentation using incubation in presence of divalent cations with variable temperatures and times, or physical fragmentation using acoustic shearing. Nevertheless, reads likely stemming from precursor molecules were identified among the transcriptome, encompassing part of the SRP RNA gene and the respective up- and downstream intron and plasmid sequences, clearly confirming the plasmid-origin. In further corroboration, reads starting exactly one nucleotide after the 3' splicing site were identified, hence providing strong evidence towards processing by the tRNA splicing machinery.

In *T. tenax*, splicing of non-tRNA BHB motifs is possible due to the heteromeric nature of its splicing endonuclease. This type of endonuclease, which possesses two different subunits and has been shown to recognize a broad range of noncanonical BHB motifs, is present in all Crenarchaeota, including *S. acidocaldarius* (Calvin et al., 2005; Plagens et al., 2015; Randau, Calvin, et al., 2005; Tocchini-Valentini et al., 2005a, 2005b; Yoshinari et al., 2005, 2009). To verify that the *S. acidocaldarius* tRNA splicing endonuclease can indeed be induced to cleave the BHB motif of a non-tRNA molecule, *in vitro* splicing assays were conducted with recombinantly produced tRNA splicing endonuclease from *S. acidocaldarius* and an artificial RNA substrate which folds into a BHB structure upon self-hybridization. The sequence of the assay substrate faithfully represents the 5' and 3' terminal sequences of the synthetic SRP RNA precursor. As expected due to its phylogeny-based classification as a heteromeric splicing

endonuclease, the *S. acidocaldarius* tRNA splicing endonuclease cleaved the BHB substrate, presumably at the intended positions.

To date, four different structures have been reported for archaeal tRNA splicing endonucleases: I) an α_4 homotetramer as in *Methanocaldococcus jannaschii*, II) an α_2 homodimer as in *Archaeoglobus fulgidus*, III) a heterotetramer ($\alpha\beta$)₂ as in *Nanoarchaeum equitans* and IIII) an irregular hexamer ϵ_2 as in *Candidatus Microarchaeum acidiphilum* (Fujishima et al., 2011; Li et al., 1998; Li & Abelson, 2000; Lykke-Andersen & Garrett, 1997; Mitchell et al., 2009). The highest substrate specificity is exhibited by the homotetrameric enzymes which cleave only canonical BHB motifs, contrasted by the heterotetrameric enzymes which also accept a broad range of non-canonical BHB motifs, bulge-helix-loop (BHL) or BHL-like structures (Tocchini-Valentini et al., 2005a). The substrate range of the irregularly hexameric enzyme is comparable to heterotetrameric enzymes (Fujishima et al., 2011). Recently, a study in *H. volcanii* identified one mRNA and several rRNAs (e.g. the 16S rRNA precursor) as substrates for the tRNA splicing endonuclease, even though this organism possesses an α_2 homodimeric tRNA splicing endonuclease with comparably stricter substrate recognition requirements (Schwarz et al., 2020; Thompson & Daniels, 1990). Processing of rRNAs by the tRNA splicing endonuclease has also been reported in *Sa. solfataricus* and *Methanlobus psychrophilus* (Ciammaruconi & Londei, 2001; Qi et al., 2020). Additionally, an mRNA intron predicted to form a structure similar to the BHB was identified in *Aeropyrum pernix*, *Sa. solfataricus* and *S. tokodaii* (Watanabe et al., 2002).

The occurrence of heterotetrameric splicing endonucleases coincides with the presence of a high number of non-canonically positioned tRNA introns (Marck & Grosjean, 2003). The broad substrate range of heterotetrameric splicing endonucleases in Crenarchaea has been traced back to a structure called the Crenarchaea specific loop (CSL) and insertion of the CSL into the homodimeric splicing endonuclease from *Archaeoglobus fulgidus* enabled this enzyme to cleave non-canonical substrates (Hirata et al., 2011; Yoshinari et al., 2009). It is hypothesized that the homotetramer α_4 presents the ancestral form of the splicing endonuclease and that two independent gene duplication events led to the emergence of the other two classes: A) the homodimeric form via one gene encoding two fused subunits in a common ancestor of Archaeoglobales, Halobacteriales and Methanosarcinales and

B) the heterotetrameric form via subfunctionalization in the common ancestor of Crenarchaeota and Nanoarchaeota (Tocchini-Valentini et al., 2005b). The most recently discovered three-unit structure is proposed to have evolved following both a gene duplication and fusion event (Fujishima et al., 2011). The general consensus agrees on an evolution towards a more relaxed substrate specificity favouring a larger substrate range.

Processing of a synthetic BHB motif attached to an SRP RNA precursor is only the beginning of substrate characterization for the *S. acidocaldarius* splicing endonuclease. The structure is expected to resemble the splicing endonuclease of *Sa. solfataricus* which is a heterotetramer with a broad substrate range (Calvin et al., 2005). On the other hand, it remains to be determined whether the circular SRP RNA can be bound by SRP19, SRP54 and L7Ae to form a functional SRP in *S. acidocaldarius*. In summary, these results clearly prove that the activity of the tRNA splicing endonuclease extends far beyond the processing of tRNAs. What might have arisen out of necessity in thermophilic archaea, offers exciting opportunities regarding a reliable, protein-based mechanism for the circularization of RNA molecules. For example, RNA-based sensors used for the fluorescent imaging of small molecules could benefit from circularization and broaden the application spectrum to include hyperthermophilic organisms (Litke & Jaffrey, 2019). It might also provide a basis for high-yield *in vitro* protein synthesis, based on recent efforts to improve protein production from circular RNAs in Eukaryotes (R. Chen et al., 2022).

3.2 Evolutionary implications of a permuted SRP RNA gene

As the permuted SRP RNA gene had successfully been processed into a mature, circular SRP RNA in *S. acidocaldarius*, the following experiment focused on the replacement of the original with the permuted SRP RNA gene variant in the genome. To this end, the permuted gene was first integrated into the genome using homologous recombination based on the “pSVA431 method” described by Wagner et al., (2012). This step was successful and clones carrying the marker cassette fragment with the permuted SRP RNA gene variant were identified by Blue-White-Screening and confirmed by Sanger sequencing. This first integration step was followed by a second crossover event to remove the original gene by homologous recombination between the two left flanks. However, as the modification of the SRP RNA gene mainly entails

switching of the gene halves, the overall sequence is still highly similar to the original SRP RNA gene. Consequently, three different recombination scenarios are theoretically possible, that is recombination between the left flank, the 5' gene half and 3' gene half, all of which are present twice in the locus. While recombination between the left flanks would result in the intended gene exchange, recombination between either of the gene halves would significantly alter the gene, likely to the point of loss-of-function and was therefore not expected to occur. Indeed, screening of clones following uracil counterselection did not yield a clone in which the intended exchange was successful. Instead, the marker cassette fragment was either lost in its entirety and the locus returned to its wild-type state, or it was maintained with the locus consequently encompassing both SRP RNA gene variants, separated by the *pyrEF* and *lacS_{SSO}* marker cassettes. Several counterselection attempts led to either one of the two scenarios and due to the essentiality of the SRP RNA gene, as well as the high sequence similarity between the two gene variants, further attempts are not expected to result in the intended exchange.

As circular RNA molecules exhibit higher thermal stability than linear RNAs, the circularization of the SRP RNA is presumably beneficial to thermophilic organisms. This idea is reinforced by the lack of helix 1 in the SRP RNA from *T. tenax*, which is believed to prevent the thermal unfolding of linear SRP RNAs (Plagens et al., 2015; Zwieb et al., 2005). Furthermore, thermophilic archaea have been shown to possess circular pre-rRNAs with BHB motifs in their processing stems, which were shown to be indispensable for subsequent rRNA maturation *in vivo* (Birkedal et al., 2020; Danan et al., 2012; Jüttner et al., 2020; Tang et al., 2002). While the improved thermal stability of a circular molecule undoubtedly provides a downstream advantage, the initial circularization event itself is likely caused by the need for restoration of a permuted (or otherwise fragmented) essential gene. In this regard, gene fragmentation is argued to confer an evolutionary advantage by preventing the integration of mobile genetic elements into highly conserved genomic regions, e.g. tRNA genes (Randau & Söll, 2008). As the SRP RNA is an essential and highly conserved RNA molecule, it too presents an ideal target for viral integration which could be counteracted by permutation (Plagens et al., 2015). Hydrothermal environments are by no means devoid of viruses and specifically the hot springs of Yellowstone National Park and its local *Sulfolobus* communities harbour diverse viral particles (Rachel et al., 2002; Rice

et al., 2001). It has been proposed that acquisition (instead of loss) of introns in tRNA genes poses the later evolutionary event and the high variability of intron locations in tRNA genes (anticodon stem, acceptor stem, D-loop, t-loop, variable region) is listed as proof (Marck & Grosjean, 2003; Randau & Söll, 2008). The same scenario can therefore be applied to intron acquisition in the SRP RNA gene. In the case of *T. tenax*, it has been proposed that the permuted SRP RNA gene evolved from an intron-containing ancestor gene via genome rearrangement (Gomes-Filho et al., 2018). Notably, a gene encoding a C/D box sRNA, which tend to occur next to split genes, is located near its 5' terminus (Plagens et al., 2015; Randau, 2012). Despite the need of a processing step to yield the functional RNA molecule, the downstream advantages, such as improved thermal stability, possibly predominated and consequently resulted in the maintenance of the permuted gene.

3.3 Experimental analysis of the archaeal Nudix family hydrolases

Parallel to the investigation of the SRP RNA circularization, it was the objective of this study to follow up on the discovery of archaeal NAD-capped RNAs by discovering enzymes which are involved in regulating these RNAs. BLAST analyses and multiple sequence alignments revealed the existence of four Nudix domain-containing proteins in *Sulfolobus acidocaldarius* (Figure 2.6). The presence of the complete Nudix box with all conserved residues strengthened the idea of their putative ability to perform RNA-decapping. *S. acidocaldarius* might likely possess more than one decapping enzyme, as e.g. mammalian cells possess more than 20 decapping enzymes, each regulating specific subsets of capped RNA (Li et al., 2011; McLennan, 2006; Song et al., 2010). Currently, *E. coli* lists 13 genes encoding Nudix family hydrolases, *Saccharomyces cerevisiae* 4, *Caenorhabditis elegans* 14, *Drosophila melanogaster* 20 and *Arabidopsis thaliana* 25-28 (Bessman, 2019; McLennan, 2006). In the archaeal domain, *Haloferax volcanii* exhibits 12 genes encoding Nudix domain-containing proteins, while *Methanococcus jannaschii*, *M. maripaludis* and *Thermococcus kodakarensis* each possess a single Nudix domain protein. Among the other Sulfolobales/Saccharolobales, *Sa. solfataricus* possesses 3, *S. tokodaii* 4 and *S. islandicus* 4 genes encoding Nudix domain-containing proteins. In the organisms where only one gene is present, it is annotated as a putative ADPR hydrolase (microbesonline.org, Alm et al., (2005)). It has been reported that the number of Nudix

family members in bacteria, eukaryotic microorganisms and fungi is linearly correlated with genome size (McLennan, 2006).

To start the experimental investigation, the Nudix hydrolases from *S. acidocaldarius* were recombinantly produced in *E. coli*. Expression and purification of the His-tagged proteins was successful for SACI_RS00730, Saci_NudT5 and SACI_RS00575 (Figure 2.7). Strikingly, the gene encoding SACI_RS02625 was not maintained on its plasmid following transformation into several *E. coli* cloning and expression strains. Due to this singular behaviour, likely caused by toxicity of the gene product, SACI_RS02625 was produced by *in vitro* cell-free protein synthesis which proved generally successful, albeit protein quantity was comparably low and the production method proved problematic for a downstream assay (see below).

Following their production, all *S. acidocaldarius* Nudix proteins were tested in *in vitro* decapping assays. Under the tested reaction conditions, none of the Nudix hydrolases showed activity towards 5'-NAD-RNA, as opposed to the control enzyme NudC from *E. coli* (Figure 2.8A). Notably, the activity of Nudix proteins relies on the presence of divalent cations presently provided in the form of magnesium ions (Frick & Bessman, 1995). However, some Nudix proteins like *B. subtilis* BsRppH exhibit higher decapping activity in the presence of manganese ions (Frindert et al., 2018). To account for this possibility, a reaction buffer containing manganese was prepared but did not reveal decapping activity stimulation.

To allow for the possibility of target molecules other than NAD, especially regarding the large substrate range of the Nudix family hydrolases, RNA substrates carrying other metabolites at their 5' end were prepared and tested. Here, particular interest was placed on ADP-ribose (ADPR), as NAD thermally degrades into ADPR and nicotinamide at temperatures equivalent to those in *Sulfolobus* habitats (Hachisuka et al., 2017). When incubated with 5'-ADPR-RNA, Saci_NudT5 showed decapping activity. This is in agreement with the computational prediction as an ADPR pyrophosphatase and sequence similarity to other known ADPR hydrolases (Dunn et al., 1999). Furthermore, it was confirmed that, regardless of substrate specificity, activity depends on the three conserved glutamic acid residues in the Nudix motif, as the triple exchange mutant did not show any decapping activity (Figure 2.8B). Past studies on the decapping enzymes *E. coli* NudC, mammalian Nudt12 and *B. subtilis*

BsRppH agreed that substitution of either one of the first two glutamic acid residues in the REX₂EE sequence of the Nudix motif renders the protein inactive (Frindert et al., 2018; Grudzien-Nogalska et al., 2019; Höfer et al., 2016; Song et al., 2013). These residues were exchanged in the motifs of other Nudix proteins and rendered the respective protein inactive (Cahová et al., 2015; Duong-Ly et al., 2011).

Saci_NudT5 was correctly predicted as an ADPR pyrophosphatase based on the indicator residue at position 16 after the G of the Nudix motif (a proline). SACI_RS00575 was predicted as a dinucleoside polyphosphatase by a tyrosine residue at this position (Dunn et al., 1999). To this end, RNA carrying 5'-Ap4A was prepared, however no protein activity could be detected other than that of the control enzyme RppH from *E. coli* (Figure 2.9). This result reinforces the need for experimental validation of computational predictions and the following Malachite Green assays shed some light on the inability of SACI_RS00575 to act on this substrate. In a final decapping assay, the active ADPR-decapping enzyme Saci_NudT5 was incubated with one of the other Nudix hydrolases each to investigate possible interactions between the proteins. For 5'-NAD-RNA, still no activity was detected (Figure 2.10A). In the presence of SACI_RS00730 and SACI_RS00575, ADPR-RNA was completely decapped by Saci_NudT5 as seen in previous reactions. Surprisingly, incomplete decapping was observed in presence of SACI_RS02625, hinting at a possible inhibition of the reaction on account of SACI_RS02625. The decrease of decapped RNA with an increase in SACI_RS02625 concentration further reinforced this observation (Figure 2.10B). This effect was also observed when the triple exchange-mutant of SACI_RS02625 was added to the reaction. As the exchange concerns catalytically active residues, substrate binding should not be affected in the mutant (Zhang et al., 2016). Whether the inhibition of the decapping reaction was caused by binding of SACI_RS02625 to the ADPR-RNA or Saci_NudT5 remains to be determined. Though SACI_RS02625 did not show any activity towards ADPR-RNA in terms of decapping, electrophoretic mobility shift assays (EMSA) will reveal a possible interaction between this protein and 5'-ADPR-RNA.

Considering the results from the decapping assays, it became apparent that the activity of some of the Nudix family hydrolases from *S. acidocaldarius* might not be related to RNA. To this end, and to provide a different direction towards their functional characterization, Malachite Green assays were performed. Briefly, Malachite Green

serves towards the detection of orthophosphate, as both components bind to form a stable, dark green colorimetric product. This assay can therefore be used to visualize and measure enzymatic reactions that produce free phosphate. Notably, the high sensitivity of the Malachite Green reagent towards free phosphate created unexpected challenges in finding sufficiently pure substrates. To date, the canonical nucleotides ATP, dATP and dGTP were tested, as well as the metabolites NAD, ADPR and Ap4A which had previously been used to cap the model RNA substrate. Among the Nudix hydrolases, the recombinantly produced proteins SACI_RS00730, Saci_NudT5 and SACI_RS00575 exhibited sufficient purity to be tested in the Malachite Green assay. Unfortunately, this was not the case for the *in vitro* produced SACI_RS02625. The protein sample contained high amounts of phosphate, leading within minutes to considerable amounts of precipitate when mixed with the reagent and was therefore unsuitable for this assay. As the reagent binds orthophosphate and some reactions were expected to produce pyrophosphate or sugar-phosphate products, all reactions were tested with and without the presence of a coupling enzyme. This coupling enzyme releases the phosphate from the product of the Nudix reaction, while not hydrolysing the substrate itself. For pyrophosphate-producing reactions *E. coli* pyrophosphatase was employed; for sugar-phosphate-producing reactions it was Bovine Alkaline Phosphatase (Baykov et al., 1988; Carter et al., 2015).

SACI_RS00730 exhibited phosphate release from ATP, dATP, dGTP and Ap4A. As phosphate was released from ATP, dATP and dGTP without the addition of the pyrophosphatase coupling enzyme, and equal levels of released phosphate were displayed for ATP with and without coupling enzyme, the product of the hydrolysis reaction of the canonical nucleotide substrates appears to be orthophosphate and not pyrophosphate (Figure 2.11). Notably, SACI_RS00730 released considerably more phosphate from the deoxynucleotide substrates, exceeding the detection limit of the experiment, compared to ATP. Furthermore, SACI_RS00730 released a small amount of phosphate from Ap4A. Due to its dinucleoside structure, detection of this activity required addition of the coupling enzyme. The Ap4A hydrolysis activity is surprising, on the other hand SACI_RS00730 could not be initially classified, as its amino acid sequence does not exhibit any of the currently known motifs characterising the Nudix hydrolase subfamilies. Dinucleoside polyphosphates, and in particular Ap4A, are synthesized in prokaryotic and eukaryotic cells in response to various environmental

or physiological stresses. Several studies have raised implications in DNA replication, DNA damage repair and mRNA regulation, hinting at regulation of cellular stress responses via Ap4A as a signalling molecule, however, the exact mechanisms remain elusive (Ferguson et al., 2020). It is unclear whether the hydrolysis of Ap4A by SACI_RS00730 has any biological relevance or is simply a secondary activity. It should be noted, that SACI_RS00730 did not hydrolyse NAD or ADPR, thereby clearly exhibiting the ability to distinguish between adenine-based substrates.

Similar to SACI_RS00730, Saci_NudT5 released similar amounts of phosphate from ATP, dATP and dGTP with and without coupling enzyme, establishing orthophosphate instead of pyrophosphate as the reaction product. Notably, phosphate release from dGTP far exceeded levels of phosphate released from ATP or dATP. Nevertheless, hydrolysis of free ADPR was confirmed as suggested based on the results of the ADPR-RNA decapping assays, albeit in much lower quantity than expected (Figure 2.12). Despite the somewhat similar structures of NAD and ADPR, Saci_NudT5 was unable to hydrolyse NAD (or Ap4A). Hence in agreement with SACI_RS00730, this enzyme shows specificity among adenine-based substrates. While Saci_NudT5 has thus been confirmed as an ADPR hydrolase with the ability of decapping 5'-ADPR-RNA, it remains to be determined whether the decapping reaction involves interacting with the RNA molecule or if ADPR is hydrolysed regardless of the RNA body. On the same note, 5'-capped ADPR-RNAs have not been identified in Archaea yet. However, ADPR-capped mRNAs were recently identified in human cells (Weixler et al., 2022). The essential cofactor NAD degrades into nicotinamide and ADPR at high temperatures, with ADPR posing toxicity by spontaneously linking to proteins in a process called ADP-ribosylation (Anderson & Anderson, 1963; Cervantes-Laurean et al., 1996; Jacobson et al., 1994; Kaplan et al., 1951). Consequently, hyperthermophilic organisms especially would be expected to have mechanisms for removing toxic by-products of thermal degradation. Indeed, such proteins were discovered in *Thermococcus kodakarensis* and *Methanococcus jannaschii* in the form of ADP-ribose pyrophosphatases (Hachisuka et al., 2017; Sheikh et al., 1998). In both organisms, this protein is the only representative of the Nudix family. Our results suggest that this role could be executed by Saci_NudT5 in *S. acidocaldarius*. The biological relevance of its *in vitro* decapping activity remains to be uncovered.

For SACI_RS00575, small amounts of phosphate were released from dATP and dGTP, with numbers notably increasing after the addition of the coupling enzyme (Figure 2.13). This reveals a mixture of orthophosphate and pyrophosphate as products from the SACI_RS00575 hydrolysis reaction and suggests that this enzyme might cleave the phosphate linkages randomly. As considerably more phosphate was released from dGTP over dATP – and none from ATP – this protein clearly shows a preference for guanosine-based substrates and thereby separates itself from SACI_RS00730 and Saci_NudT5. In agreement with this assumption, no activity was detected for SACI_RS00575 following incubation with NAD, ADPR or Ap4A.

Over the course of conducting the Malachite Green assays, the disadvantages of this method reinforced themselves. Notably, the phosphate levels determined in the Malachite Green assays do not represent absolute numbers and should be interpreted carefully, as some protein samples (especially the coupling enzyme Alkaline Phosphatase) exhibited higher blank absorbance values than others. On this note, this assay may undoubtedly be used for initial substrate screening, as it is suited to determine whether or not an enzyme can hydrolyse a specific compound. Positive results however, should be independently corroborated by different methods. Other experiments, varying in time and complexity, are available for substrate characterization for Nudix family hydrolases, such as the P_i sensor kinetic assay which employs a fluorescently labelled phosphate binding protein for phosphate detection (Xu et al., 2013). Enzymatic production of several compounds (e.g. AMP, ADP) can be measured using commercially available kits and product formation during hydrolysis reactions can be monitored by high-pressure liquid chromatography (HPLC).

Currently it is not assumed that canonical nucleotides represent biologically relevant substrates for any of the Nudix hydrolases from *S. acidocaldarius*. The Nudix family is known for displaying a large substrate range, especially under *in vitro* conditions, encompassing canonical and oxidized nucleotides, nucleotide sugars, dinucleotide coenzymes, diadenosine polyphosphates and recently capped RNAs, as well as non-nucleotide substrates such as inositol pyrophosphates (McLennan, 2013; Srouji et al., 2017). For example, mammalian NudT5 has shown activity not only towards ADPR but also 8-oxo-GDP (Arimori et al., 2011; Ishibashi et al., 2003; Ito et al., 2011). This agrees with the observed phosphate release from dGTP by Saci_Nudt5 which is

noticeably higher than for dATP or ATP (Figure 2.12). Though a biological function for the 8-oxo-GDP-hydrolysis activity cannot be excluded, current research points towards ADPR hydrolysis as the more important physiological activity (Ito et al., 2011). Hence, hydrolysis activity towards a certain substrate in the context of Malachite Green or another *in vitro* assay does not automatically establish biological relevance. To this end, the genes encoding the Nudix family hydrolases in *S. acidocaldarius* were individually deleted from the genome. Nevertheless, the degree of substrate specificity exhibited in the *in vitro* assays hints at each protein fulfilling a distinct role in the metabolism of *S. acidocaldarius*.

3.4 *In vivo* characterization and transcriptome analysis

Parallel to the *in vitro* investigation of the putative decapping enzymes, the genes encoding the Nudix hydrolases were individually deleted from the genome of *S. acidocaldarius* DSM639 MW001. Using the approach based on homologous recombination described by Wager et al. (2012), the genes were successfully deleted in all four cases, thereby proving their non-essentiality to the organism. The deletion strains were grown in parallel to the wild-type strain DSM639 MW001 under standard, nitrogen stress and carbon stress conditions. Under the tested conditions, all strains showed similar growth behaviour and no significant deviation from the wild-type strain was detected (Figures 2.15-2.17). Similarly, no significant deviation was observed between the wild type and the mutant strains after submission to heat shock and cell growth was significantly reduced in all strains except for Δ SACI_RS02625 (Figure 2.21). It is apparent that the effect of the deletion does not manifest itself in a phenotype which can be observed under the tested environmental conditions. The Nudix proteins were initially characterized as “housecleaning enzymes” that cleanse the cell of potentially toxic metabolites (Bessman et al., 1996). While this remains true, it has since been revealed that their biological roles can be even more diverse. For example, the *E. coli* Nudix hydrolase NudB hydrolyses 8-oxo-dADP, 8-oxo-dGDP and 2-oxo-dADP and was thus awarded antimutator activity (Hori et al., 2005). However, subsequent studies revealed dihydroneopterin triphosphate (DHNTTP), which is structurally similar to GTP, to be the preferred substrate (Gabelli et al., 2007). This result was corroborated by *in vivo* studies where a Δ *nudB* deletion strain exhibited

impaired folate synthesis, as DHNTP poses an intermediate in this pathway (Gabelli et al., 2007).

On the transcriptomic level, the highest impact is caused by the deletion of SACI_RS00575 as well as the double deletions of SACI_RS00730 and SACI_RS00060 (encodes Saci_NudT5). The least impact is observed for the single deletion of SACI_RS00060. Interestingly, both heatmaps (Figure 2.24 and Supplementary Figure S4) reveal distinct transcriptomic profiles for each deletion strain. It was initially believed that some of the Nudix proteins could exhibit redundant activities, specifically SACI_RS00730 and Saci_NudT5 as they were most similar in sequence. However, during the decapping assays and the Malachite Green assays, it became apparent that both proteins exhibit quite specific activities and cannot hydrolyse the same metabolite substrates. This observation is strengthened further by their transcriptomic profiles, where some gene clusters are oppositely regulated. In fact, all five deletion strains exhibit distinct transcriptomic profiles when comparing clusters of up- or downregulated or unaffected genes. This suggests a distinct role for each protein in the metabolism of *S. acidocaldarius*, in agreement with the presence of (only) four Nudix hydrolase genes, as the likelihood for redundancies between Nudix proteins is expected to increase with the number of Nudix genes.

To visualize the impact of the Nudix gene deletions for each strain, the differentially regulated genes were assembled into iModulons based on the iModulon database (Figure 2.25 and Supplementary Figure S5) (Rychel et al., 2021). iModulons are proposed to be the data-driven analogues of regulons, in which the regulation of a group of genes depends on the gene location or the binding site location of the regulator. Instead, independently modulated groups of genes are identified across the entire genome (Rychel et al., 2021). Notably, genes can be assigned to more than one iModulon and each iModulon may encompass more genes than are currently displayed as our knowledge of the regulatory network keeps expanding. Nevertheless, the classification of differentially regulated genes into iModulons provides an excellent overview of the impact created by the individual Nudix gene deletions in *S. acidocaldarius*. Presumably, the iModulons are modulated by a common regulator which must not necessarily be part of its iModulon and for many iModulons in *S. acidocaldarius* a common regulator has not yet been identified. For the *S. acidocaldarius* Modulome, 95 RNA-seq datasets from 6 studies were examined by

Independent Component Analysis (ICA) to generate 45 iModulons which explained 72% of the variance in the joined datasets (Chauhan et al., 2021). 37 iModulons correspond to specific biological functions (see Supplementary Table S1) and five correspond to the previously known regulators ArnRAB, FadR, YtrA, UV-*tfb3* and LysM. One iModulon was termed DARC for Discovered signal with Absent Regulatory Components. The DARC iModulon which consists predominantly of poorly or completely characterized genes, explains the highest variance in the dataset. Notably, this iModulon contains two transcription factors, one of which (SACI_RS05830 / Saci_1223) is differentially upregulated in all Nudix deletion strains. The authors propose a relation of this iModulon to the cell membrane, however the large number of uncharacterized genes impedes further predictions (Chauhan et al., 2021).

FadR is a transcriptional regulator from the TetR family and regulates genes involved in lipid and fatty acid metabolism in *S. acidocaldarius*. It was suggested that acyl-CoA acts as an inducer to this repressor and intracellular acyl-CoA levels consequently influence the transcriptional expression of the FadR-regulated gene cluster (Wang et al., 2019). The FadR iModulon was shown to be activated under nutrient-limited conditions (Chauhan et al., 2021). The UV-*tfb3* iModulon comprises genes implicated in the early UV stress response in *S. acidocaldarius*. TFB3 expression is induced by UV irradiation and activates the expression of genes involved in e.g. Ups pili formation (for the formation of aggregates) and the Ced DNA importer (for DNA exchange between aggregated cells) (Schult et al., 2018). The LysM iModulon represents lysine biosynthesis in *S. acidocaldarius* and contains specifically (though not exclusively) the genes of the *lysWXJK* operon (Chauhan et al., 2021). This operon encodes bi-functional enzymes involved in lysine and arginine biosynthesis and is activated by LysM. In turn, LysM is inactivated by lysine and excess amounts of lysine were shown to inactivate the expression of the operon, leading to a shutdown of arginine synthesis (Brinkman et al., 2002; Ouchi et al., 2013). The lysine biosynthesis is downregulated in the early stationary phase in the Δ SACI_RS00575 strain and the double KO strain, however it is questionable whether a Nudix hydrolase might be involved with the negative autoregulation of lysine biosynthesis and the LysM-controlled operon, as downregulation of this operon was also overserved under nutrient limitation (Bischof et al., 2019). Notably, the lysine biosynthesis operon is downregulated in the double KO strain but not in the respective single deletion strains Δ SACI_RS00730 and

Δ SACI_RS00060. Another iModulon predominantly upregulated in all strains assembles genes regulated by XylR and SoxM. XylR is a transcriptional activator regulating genes involved in xylose/arabinose uptake and the respective degradation pathway in *S. acidocaldarius*, while SoxM constitutes a terminal oxidase complex (Komorowski et al., 2002; van der Kolk et al., 2020). The respective iModulon was activated under nutrient-limited conditions, suggesting it contains genes related to cell growth and starvation (Bischof et al., 2019; Chauhan et al., 2021). Upregulation of numerous genes responsive to nutrient limitation and environmental stress might explain why the Nudix deletion strains did not exhibit a distinct phenotype under carbon, nitrogen or heat stress conditions compared to the WT. Overall, the deletion of the genes encoding the Nudix family hydrolases, especially SACI_RS00730, Saci_NudT5 and SACI_RS02625, appears to affect many aspects of the organisms' metabolism, as judged by the transcriptome. Indeed, it elicits a response highly similar to environmental stressors, such as heat stress, cold stress or UV stress. Accordingly, genes attributed to several of these iModulons are significantly affected in all Nudix deletion strains, mostly by upregulation. Going forward, further information will be provided by metabolomic profiling of the Nudix deletion strains with special focus on metabolites such as NAD, ADPR and Ap4A which have stood out thus far.

All Nudix deletion strains exhibit a number of predominantly upregulated transcriptional regulators (Δ SACI_RS00730 and Δ SACI_RS00060: 4, Δ SACI_RS02625 and Δ SACI_RS00575: 5, double KO: 6), four of which are present in all strains. The number of affected transcriptional regulators, most of which are attributed to the MarR family, presents another explanation for the large variety of affected iModulons, considering the elevated number of differentially regulated genes in the early stationary compared to the log phase. The MarR family belongs to the super-group of transcriptional regulators present in Bacteria and Archaea which predates the divergence of the domains (Pérez-Rueda & Collado-Vides, 2001). They can act as repressors or activators and their targets comprise genes involved in diverse cellular processes, such as antibiotic resistance, stress response, virulence and catabolism of aromatic compounds (Contursi et al., 2013; Perera & Grove, 2010). Possibly, some genes are not directly but indirectly affected by the Nudix gene deletion, by way of their transcriptional regulator. In accordance with this observation, the number of differentially affected genes correlates with the number of differentially

affected transcriptional regulators. On the same note, the number of differentially regulated genes also correlates with the number of differentially upregulated thermosome subunits and Type II toxin-antitoxin system genes: zero in Δ SACI_RS00730 and Δ SACI_RS00060, one thermosome subunit gene in Δ SACI_RS02625, and 2 thermosome subunits + 2 toxin-antitoxin system genes in Δ SACI_RS00575 and the double KO. In *Sa. solfataricus*, the toxin VapC6 is a heat-dependent ribonuclease that is inactivated by VapB6 binding. The ribonucleolytic activity is suggested to aid in the repression of protein synthesis during heat shock response (Maezato et al., 2011). On a related note, another study in *Sa. solfataricus* found *vapBC* locus expression to be heat-induced, however some *vapBC* loci were also expressed under normal growth conditions, suggesting roles beyond heat stress response for this system (Tachdjian & Kelly, 2006). The upregulation of a putative *vapBC* locus (encoded by SACI_RS10050 / *saci_2079* and SACI_RS10055 / *saci_2080*) in two of the Nudix deletion strains corroborates this idea. Interestingly, the same study not only found a large number of MarR family transcriptional regulators upregulated in the heat-shocked *Sa. solfataricus* samples, but also upregulation of *sso_3167* which encodes a Nudix family hydrolase (Tachdjian & Kelly, 2006). The homolog of *sso_3167* in *S. acidocaldarius* is SACI_RS02625, whose deletion strain was the only one to not be significantly affected by the 87°C heat shock (Figure 2.21). Another study on heat shock response in *S. acidocaldarius* revealed high upregulation of the repressor YtrA (encoded by SACI_RS08880 / *saci_1851*) upon heat stress (Baes et al., 2020). Though YtrA itself is not differentially affected in the Nudix deletion strains, its iModulon is predominantly upregulated in Δ SACI_RS02625, Δ SACI_RS00575 and the double KO strain, despite their growth at normal temperatures. Notably, YtrA does not regulate known heat shock proteins but two putative membrane proteins of unknown function and its connection to thermal stress remains unclear (Lemmens et al., 2019). While the exact nature of the connection between Nudix hydrolases, specifically SACI_RS02625, and heat stress response remains unclear, our results suggest it to be more than coincidental. Notably, a definite transcription factor regulating heat shock response in the Sulfolobales remains to be identified.

In *S. acidocaldarius*, the archaellum formation operon is controlled by the inducers ArnR and ArnR1 and the repressors ArnA and ArnB (Lassak et al., 2013; Reimann et

al., 2012). ArnR (SACI_RS05625 / *saci_1180*) and the archaellum formation operon are downregulated in Δ SACI_RS00575, in contrast to upregulation of ArnR1 (SACI_RS05580 / *saci_1171*) and the archaellum formation operon in Δ SACI_RS00730. The archaellum repressors ArnA and ArnB are not affected in any of the Nudix deletion strains. ArnR was observed to be induced under tryptone starvation conditions and is suggested to be controlled by a still unidentified superior transcription factor. Perplexingly, ArnR1 is upregulated in the double KO while the archaellum formation operon itself is downregulated. However, ArnR and ArnR1 both promote motility but not to the same extent, as deletion mutants of *arnR* and *arnR1* exhibited a strongly and mildly diminished motility phenotype, respectively (Lassak et al., 2013). Several studies in different archaeal organisms report archaellum formation to be either repressed or stimulated under different nutrient limitation conditions (Hendrickson et al., 2008; Mukhopadhyay et al., 2000; Szabó et al., 2007; Xia et al., 2009). External nutrient limitation on account of growth conditions can be excluded for the Nudix deletions strains. It is therefore plausible that intracellular nutrient limitations in Δ SACI_RS00575 and the double KO strain cause the cells to shut down the energy-consuming archaellum production. To date it is unclear whether a Nudix deletion directly or indirectly affects the regulation of the archaellum formation operon. Nevertheless, the state of the archaellum formation operon and specifically its downregulation may be indicative of the cell's energy state in consequence of the Nudix gene deletion(s).

Furthermore, Δ SACI_RS02625 and the double KO strain exhibited differential upregulation of *nadA* (a putative quinolinate synthase) and *nadB* (a putative L-aspartate oxidase). In the genome, *nadB* is located directly upstream of SACI_RS02625, however its upregulation in the double KO strain refutes a locational effect. Both gene products presumably catalyse the initial two steps in the NAD *de novo* biosynthesis pathway, as inferred from homology to *Thermococcus kodakarensis*. Upregulation of the *de novo* synthesis pathway is possibly elicited by a disturbance in the NAD salvage pathway, which involves the recycling of NAD from nicotinamide and ADPR following its thermal degradation (Hachisuka et al., 2018). However, none of the other genes involved in these pathways were detected among the datasets in both strains. In Bacteria, a family of Nudix-related transcriptional regulators (NrtR) was discovered to regulate NAD metabolism and interact with ADPR

as their effector molecule. These proteins exhibit an N-terminal Nudix-like domain homologous to ADPR pyrophosphatases and a C-terminal helix-turn-helix(HTH)-like DNA-binding domain (Rodionov et al., 2008). However, an HTH-domain is not predicted for any of the Nudix family hydrolases from *S. acidocaldarius*.

3.5 Conclusion and Outlook

The permuted SRP RNA gene was introduced into *S. acidocaldarius* to accelerate evolution in this organism regarding increased stability of an essential RNA molecule. Even though the permuted gene was processed into a circular SRP RNA by the native tRNA splicing machinery, not all final questions regarding its functionality have been answered. Whether this synthetic variant can be bound by the proteins SRP19 and SRP54 to form a functional signal recognition particle can be assumed but remains to be proven experimentally. Only then can it be claimed that this synthetic, circular variant poses an equally viable alternative to the wild-type, linear SRP RNA. Nevertheless, this approach opens up possibilities towards the circularization of RNA molecules. The final component in this scenario, the protein responsible for ligating spliced tRNAs, was identified as the tRNA ligase RtcB which is conserved in all known archaea, most eukaryotes and a variety of bacterial species (Englert et al., 2011). Similarly, the deciding feature which enables the promiscuity of the crenarchaeal tRNA splicing endonucleases has been identified and can be transferred to other splicing endonucleases.

The Nudix family hydrolases from *S. acidocaldarius* showed distinct substrate specificities *in vitro* and the protein Saci_NudT5 was identified to be decapping 5'-ADPR-RNA *in vitro*. Whether this constitutes a biologically relevant activity and whether ADPR-RNA or free ADPR are preferentially degraded, remains to be determined. Due to the lack of dedicated domains for the binding of proteins or nucleic acids, especially DNA, the Nudix hydrolases are at this point not suggested to influence transcription in *S. acidocaldarius* directly. Nevertheless, the transcriptome is highly affected in the Nudix deletion strains, especially regarding iModulons which assemble genes responsive to nutrient limitation and heat stress. Considering the high number of affected transcriptional regulators, the Nudix hydrolases might be involved in the pathways of metabolites that act as effector molecules to the transcriptional regulators, leading to an altered transcriptomic state as a consequence of altered

metabolite composition. Indeed, the transcriptomes of the Nudix deletion strains exhibit remarkable similarity to the transcriptome in response to nutrient limitation stress (Bischof et al., 2019). Especially for SACI_RS02625, the results from this work strongly suggest a connection to heat stress response. Furthermore, SACI_RS02625 could not be recombinantly expressed by *E. coli* cells. While the results from this work provide a clear direction for the subsequent characterization of the Nudix hydrolases from *S. acidocaldarius*, further information should be gained from the metabolomic profiling of the Nudix deletion strains.

4 Material and Methods

4.1 Materials, instruments and consumables

4.1.1 Chemicals, kits and enzymes

The chemicals, kits, enzymes and consumables used in this work were obtained from the companies and / or suppliers listed in Table 4.1. Unlisted chemicals were supplied either by Carl Roth GmbH + Co. KG (Karlsruhe) or Sigma-Aldrich Chemie GmbH (Taufkirchen).

Table 4.1: List of chemicals, kits, enzymes and other consumables used in this work

Chemicals	Supplied by
2'-Desoxyadenosine-5'-triphosphate sodium salt solution (dATP), PCR Grade	Roche über Merck KGaA, Darmstadt
2'-Desoxyguanosine 5'-triphosphate sodium salt solution (dGTP), PCR Grade	Roche über Merck KGaA, Darmstadt
2-Log DNA Ladder (0.1-10.0 kb)	New England Biolabs GmbH, Frankfurt am Main
2X DreamTaq Green PCR Master Mix	Thermo Fisher Scientific GmbH, Dreieich
2X Gibson Assembly® Master Mix	New England Biolabs GmbH, Frankfurt am Main
3-(Acrylamido)phenylboronic acid (APB)	Sigma-Aldrich Chemie GmbH, Taufkirchen
5-Fluorotic acid (5-FOA)	Carl Roth GmbH + Co. KG, Karlsruhe
6X Purple Gel Loading Dye (no SDS)	New England Biolabs GmbH, Frankfurt am Main
Adenosine-5'-diphosphoribose sodium salt (ADPR)	Sigma-Aldrich Chemie GmbH, Taufkirchen
Adenosine-5'-triphosphate disodium salt hydrate (ATP), BioXtra	Sigma-Aldrich Chemie GmbH, Taufkirchen
Alkalische Phosphatase (AP), grade I, from calf intestine	Sigma-Aldrich Chemie GmbH, Taufkirchen
Ammonium Persulfate (APS)	Carl Roth GmbH + Co. KG, Karlsruhe
AMPure XP (SPRI beads)	Beckman Coulter GmbH, Krefeld
Antarctic Phosphatase	New England Biolabs GmbH, Frankfurt am Main
Antibiotics (Ampicillin, Kanamycin, Chloramphenicol)	Carl Roth GmbH + Co. KG, Karlsruhe; Sigma-Aldrich Chemie GmbH, Taufkirchen
β-Mercaptoethanol	Sigma-Aldrich Chemie GmbH, Taufkirchen
β-Nicotine amide adenine dinucleotide (NAD⁺)	Carl Roth GmbH + Co. KG, Karlsruhe
Bioanalyzer High Sensitivity DNA Kit	Agilent, Santa Clara, CA, USA
Bioanalyzer RNA 6000 Pico Kit	Agilent, Santa Clara, CA, USA
Breathe-Easy sealing film	Diversified Biotech, Dedham, MA, USA
Color Prestained Protein Standard, Broad Range (11-245 kDa)	New England Biolabs GmbH, Frankfurt am Main
Diethylpyrocarbonate (DEPC)	Carl Roth GmbH + Co. KG, Karlsruhe
Dimethyl Sulfoxide (DMSO)	New England Biolabs GmbH, Frankfurt am Main
DNA Oligonucleotides	Eurofins MWG Operon, Ebersberg
DNase I (RNase-free)	New England Biolabs GmbH, Frankfurt am Main
dNTP Mix (dATP, dGTP, dCTP, dTTP)	New England Biolabs GmbH, Frankfurt am Main
Gelrite	Carl Roth GmbH + Co. KG, Karlsruhe
Gene Pulser® Cuvette, 0.1cm gap	Bio-Rad Laboratories GmbH, Feldkirchen
Invitrogen™ TOPO™ TA Cloning™ Kit, Dual Promoter	Thermo Fisher Scientific GmbH, Dreieich

Invitrogen™ mirVana™ miRNA Isolation Kit	Thermo Fisher Scientific GmbH, Dreieich
Invitrogen™ SuperScript™ IV Reverse Transkriptase	Thermo Fisher Scientific GmbH, Dreieich
Invitrogen™ SYBR™ Gold Nukleinsäuregel-Färbemittel (10.000x Konzentrat in DMSO)	Thermo Fisher Scientific GmbH, Dreieich
Isopropyl-β-D-1-thiogalactopyranosid (IPTG)	Carl Roth GmbH + Co. KG, Karlsruhe
LB Broth (Luria/Miller)	Carl Roth GmbH + Co. KG, Karlsruhe
LE Agarose	Biozym Scientific GmbH, Hessisch Oldendorf
Lysozyme from chicken eggwhite	Sigma-Aldrich Chemie GmbH, Taufkirchen
Malachite Green Phosphate Assay Kit	Sigma-Aldrich Chemie GmbH, Taufkirchen
MF-Millipore mixed cellulose esters (MCE) membrane, 0.22 µm	Merck KGaA, Darmstadt
Midori Green Advance	NIPPON Genetics EUROPE GmbH, Düren
Millipore Steritop™, 0.22 µm pore size	Merck KGaA, Darmstadt
Monarch® PCR & DNA Cleanup Kit (5 µg)	New England Biolabs GmbH, Frankfurt am Main
Monarch® RNA Cleanup Kit (10 µg)	New England Biolabs GmbH, Frankfurt am Main
Monarch® RNA Cleanup Kit (50 µg)	New England Biolabs GmbH, Frankfurt am Main
NEBExpress® Cell-free <i>E. coli</i> Protein Synthesis System	New England Biolabs GmbH, Frankfurt am Main
NEBExpress® Ni Spin Columns	New England Biolabs GmbH, Frankfurt am Main
NEBNext® Multiplex Oligos for Illumina® (Index Primers Set 1-3)	New England Biolabs GmbH, Frankfurt am Main
NEBNext® Ultra II Directional RNA Library Prep Kit for Illumina	New England Biolabs GmbH, Frankfurt am Main
NEBuffer™ r3.1	New England Biolabs GmbH, Frankfurt am Main
NTPs (ATP, GTP, CTP, UTP)	Jena Bioscience, GmbH, Jena
NucleoSpin® Gel and PCR Clean-up, Mini kit for gel extraction and PCR clean up	MACHEREY-NAGEL GmbH & Co. KG, Düren
NucleoSpin® Plasmid (NoLid), Mini kit for plasmid DNA purification	MACHEREY-NAGEL GmbH & Co. KG, Düren
NucleoSpin® Tissue, Mini kit for DNA from cells and tissue	MACHEREY-NAGEL GmbH & Co. KG, Düren
NudC from <i>Escherichia coli</i>	New England Biolabs GmbH, Frankfurt am Main
P1-(5'-Adenosyl) P4-(5'-adenosyl) tetraphosphate sodium salt (Ap4A)	Jena Bioscience, GmbH, Jena
Pan-Archaea riboPOOL Probes	siTOOLS Biotech GmbH, Planegg-Martinsried
peqGREEN	VWR International GmbH, Darmstadt
Phusion High-Fidelity DNA Polymerase	New England Biolabs GmbH, Frankfurt am Main
Pyrophosphatase, Inorganic (<i>E. coli</i>)	New England Biolabs GmbH, Frankfurt am Main
Qubit dsDNA HS Assay Kit	Thermo Fisher Scientific GmbH, Dreieich
Qubit Protein Assay Kit	Thermo Fisher Scientific GmbH, Dreieich
Qubit RNA HS Assay Kit	Thermo Fisher Scientific GmbH, Dreieich
Random Hexamers (50 µM)	Applied Biosystems™, Thermo Fisher Scientific GmbH, Dreieich
READYBLUE™ PROTEIN GEL STAIN	Sigma-Aldrich Chemie GmbH, Taufkirchen
Restriction Endonucleases	New England Biolabs GmbH, Frankfurt am Main
RNA 5' Pyrophosphohydrolase (RppH)	New England Biolabs GmbH, Frankfurt am Main
RNA Oligonucleotide	Merck KGaA, Darmstadt
RNase Exitus Plus™	Applichem GmbH, Darmstadt
RNase Inhibitor Murine	New England Biolabs GmbH, Frankfurt am Main
ROTIPHORESE®Gel 30 (37,5:1)	Carl Roth GmbH + Co. KG, Karlsruhe
ROTIPHORESE®Gel 40 (29:1)	Carl Roth GmbH + Co. KG, Karlsruhe

ROTIPHORESE®Sequenziergel Puffer-Konzentrat (10x TBE mit 50 % Harnstoff (8,3 M))	Carl Roth GmbH + Co. KG, Karlsruhe
ROTIPHORESE®Sequenziergel-Konzentrat (25%ige Acrylamid-Bisacrylamid-Stammlösung im Verhältnis 19:1, mit 50% Harnstoff (8,3 M))	Carl Roth GmbH + Co. KG, Karlsruhe
ROTIPHORESE®Sequenziergel-Verdünner (50% (g/v; 8,3 M) Lösung von Harnstoff in Wasser)	Carl Roth GmbH + Co. KG, Karlsruhe
SDS	Carl Roth GmbH + Co. KG, Karlsruhe
Streptavidin-coated magnetic beads	siTOOLS Biotech GmbH, Planegg-Martinsried
Syringe filter ROTILABO® PVDF, 0.22 µm and 0.45 µm	Carl Roth GmbH + Co. KG, Karlsruhe
T7 RNA Polymerase	New England Biolabs GmbH, Frankfurt am Main
Terminator™ 5'-Phosphate-Dependent Exonuclease	Lucigen Corporation, Middleton, WI, USA
Tetramethylethyldiamine (TEMED)	Sigma-Aldrich Chemie GmbH, Taufkirchen

4.1.2 Instruments

Table 4.2: Instruments used in this work

Instruments	Model and Company
Agarose gel electrophoresis	Chambers and casting trays were produced by a company technician of the Philipps-University Marburg; Power Supplies Consort E835, MS Laborgeräte, Dielheim
Aqua bidest, water system	Milli-Q® Direct Wasseraufbereitungssystem, Merck KGaA, Darmstadt
Autoclave	Systec VX-95, Systec GmbH, Linden
Balance	Analysenwaage ADJ 200-4, KERN & SOHN GmbH, Balingen-Frommern; Fisherbrand™ Precision Series Balance, Fisher Scientific GmbH, Schwerte
Bioanalyzer	Agilent 2100 Bioanalyzer, Agilent, Santa Clara, CA, USA
Cell Density Meter	Amersham Biosciences Ultrospec® 10, GE Healthcare, Amersham, UK
Centrifuges	Centrifuge 5424, Eppendorf SE, Hamburg; Heraeus Fresco21, Thermo Fisher Scientific Inc., Waltham, MA, USA; Sigma 3-30K, Sigma Laborzentrifugen GmbH, Osterode am Harz; Sorvall Lynx 4000 with Fiberlite Lex F10 and F21 rotors, Fisher Scientific GmbH, Schwerte
Chromatography System	ÄKTApurifier™ 10, GE Healthcare Bio-Sciences AB, Uppsala, Sweden

Digital Pocket Thermometer, K-type probe	Traceable® Products, Webster, TX, USA
Electroporation device	Gene Pulser® II Electroporation System, Pulser Controller Plus, Capacitance Extender Plus, Bio-Rad Laboratories GmbH, Feldkirchen
Fluorometer	Qubit® 2.0, Thermo Fisher Scientific GmbH, Dreieich
Incubators	Binder™ BD56, Fa. BINDER GmbH, Tuttlingen; HeraTherm™ IGS400, Thermo Fisher Scientific Inc., Waltham, MA, USA
Magnetic Separation Rack	MagRack 6, Jena Bioscience GmbH, Jena
Magnetic Stirrer	IKA® RCT Standard, IKA®-Werke GmbH & CO. KG, Staufen
Nanophotometer	NanoPhotometer® NP80, Implen GmbH, München
Ni-NTA chromatography column	HisTrap HP column, GE Healthcare GmbH, Solingen
pH-Meter	FiveEasy™ pH meter F20, Mettler-Toledo GmbH, Gießen
Plate Reader	CLARIOstar® <i>Plus</i> Plate Reader, BMG LABTECH GmbH, Ortenberg
Polyacrylamide gel electrophoresis	Mini-PROTEAN Tetra Cell, Bio-Rad Laboratories GmbH, Feldkirchen Power Supply PowerPac Basic, Bio-Rad Laboratories GmbH, Feldkirchen
Refrigerated circulator	Julabo Kälteumwälzthermostat, JULABO GmbH, Seelbach
Rocker	Stuart Gyrorocker SSL3, Cole-Parmer Ltd., Stone, UK
Scanner	Typhoon Trio Variable Mode Imager, Amersham Biosciences, Amersham, UK
Sequencing	Illumina® MiniSeq Sequencing System, Illumina Inc., San Diego, CA, USA
Size exclusion chromatography column	Superose™ 6 Increase 30/100 GL, GE Healthcare GmbH, Solingen
Sonicator	Branson Sonifier 250, Branson Ultrasonics, Brookfield, CT, USA
Thermocycler	C1000 Touch, Bio-Rad Laboratories GmbH, Feldkirchen
Thermomixer	Thermomixer Comfort 5350 and Compact, Eppendorf SE, Hamburg; Thermoschüttler-Mixer HC, STARLAB INTERNATIONAL GmbH, Hamburg
Thermoshaker	HT Thermotron, Infors AG, Bottmingen, Switzerland; Innova S44i, Eppendorf SE, Hamburg
UV-Transilluminator	GEL Stick “Touch”, INTAS Science Imaging Instruments GmbH, Göttingen
Vacuum pump	LABOPORT® N 86 KT.18, KNF DAC GmbH, Hamburg
Vortex Mixer	Vortex Genie 2, Scientific Industries Inc., Bohemia, NY, USA

4.1.3 Buffers and Solutions

All buffers, media and other solutions are mentioned in the respective method section. If applicable, buffers, media and solution were autoclaved for 20 min at 121°C prior to use. Heat-labile solutions were filtered using a sterile filter unit.

4.2 Strains and Culture Conditions

4.2.1 Strains

Table 4.3: Archaeal and bacterial strains used in this work

Strain	Relevant genotype	Reference
<i>Escherichia coli</i> K12 DH5 α	F ⁻ Φ 80/ <i>lacZ</i> Δ M15 Δ (<i>lacZ</i> YA-argF) U169 <i>recA1 endA1 hsdR17</i> (r _K ⁻ , m _K ⁺) <i>phoA supE44</i> λ - <i>thi-1 gyrA96 relA1</i>	Hanahan (1983)
<i>Escherichia coli</i> Rosetta 2 (DE3) pLysS	F ⁻ <i>ompT hsdS_B</i> (r _B ⁻ m _B ⁻) <i>gal dcm</i> (DE3) pLysSRARE2 (Cam ^R)	Novagen, Darmstadt
<i>Escherichia coli</i> BL21 DE3 pLysS	F ⁻ <i>ompT hsdS_B</i> (r _B ⁻ m _B ⁻) <i>gal dcm</i> (DE3) pLysS (SpecR ^R)	Novagen, Darmstadt
<i>Escherichia coli</i> K12 ER1821 carrying plasmid pM.EsaBC4I	F ⁻ <i>glnV44 e14</i> (McrA ⁻) <i>rfbD1? relA1? endA1 spoT1? thi-1</i> Δ (<i>mcrC-mrr</i>)114::IS10 (K12 ER1821)	New England Biolabs GmbH, Frankfurt am Main; Wagner et al., (2012)
<i>Sulfolobus acidocaldarius</i> DSM639 MW001	DSM639 Δ <i>pyrE</i> (SACI_1597; Δ 91–412bp)	Wagner et al., (2012)
<i>Sulfolobus acidocaldarius</i> DSM639 MW001 Δ SACI_RS00730	DSM639 Δ <i>pyrE</i> (SACI_1597; Δ 91–412bp) Δ SACI_RS00730	This work
<i>Sulfolobus acidocaldarius</i> DSM639 MW001 Δ SACI_RS00060	DSM639 Δ <i>pyrE</i> (SACI_1597; Δ 91–412bp) Δ SACI_RS00060	This work
<i>Sulfolobus acidocaldarius</i> DSM639 MW001 Δ SACI_RS02625	DSM639 Δ <i>pyrE</i> (SACI_1597; Δ 91–412bp) Δ SACI_RS02625	This work
<i>Sulfolobus acidocaldarius</i> DSM639 MW001 Δ SACI_RS00575	DSM639 Δ <i>pyrE</i> (SACI_1597; Δ 91–412bp) Δ SACI_RS00575	This work
<i>Sulfolobus acidocaldarius</i> DSM639 MW001 Δ SACI_RS00730/ Δ SACI_RS00060	DSM639 Δ <i>pyrE</i> (SACI_1597; Δ 91–412bp) Δ SACI_RS00730 Δ SACI_RS00060	This work

4.2.2 Culture conditions for *Escherichia coli*

E. coli cell cultures (5-1000 ml) were cultivated in culture flasks by shaking in a shaking incubator at 180 rpm, 37°C in LB (lysogeny broth) medium (0.5% (w/v) yeast extract, 1% (w/v) tryptone, 1% (w/v) NaCl) supplied with the appropriate antibiotics (ampicillin 100 μ g/ml, chloramphenicol 34 μ g/ml, kanamycin 50 μ g/ml). Solid medium plates (LB medium containing 1.5% (w/v) agar-agar and the appropriate, plasmid-encoded

antibiotic) were incubated at 37°C. Cell growth was measured photometrically at OD₆₀₀ using a cell density meter and the corresponding culture medium as a reference. Culture stocks were generated by addition of 40% (v/v) glycerol and storage at -80°C.

The strain *E. coli* K12 DH5α was used for cloning, preparation and storage of plasmids. The strain *E. coli* K12 ER1821 pM.EsaBC4I was used for the methylation of plasmids prior to transformation into *S. acidocaldarius* DSM638 MW001. This step is required to circumvent cleavage of plasmid DNA by the restriction endonuclease *SuaI* (Berkner et al., 2007; Grogan, 2003). The strain *E. coli* Rosetta 2 (DE3) pLysS was used for heterologous protein expression and handled as described in sections 4.6.1. and 4.6.2.

4.2.3 Culture conditions for *Sulfolobus acidocaldarius*

This work used the uracil auxotrophic strain *Sulfolobus acidocaldarius* DSM639 MW001. Cultures were grown aerobically at 120 rpm and 75°C in Brock media (Brock et al., 1972). The media were supplied with 0.1% (w/v) NZ-amine and 0.2% (w/v) dextrin for normal growth. The pH was adjusted to 3.5 using sulfuric acid. Growing strains without a plasmid required addition of 10 µg/ml uracil to the medium. Cell growth was determined by measuring the optical density (OD) at 600 nm with a cell density meter. For solid medium plates, two times concentrated Brock medium was prepared and supplemented with 6 mM CaCl₂ and 20 mM MgCl₂. For first selection plates, 0.2% (w/v) NZ-Amine and 0.4% (w/v) dextrin was added. For second selection plates, 0.2% (w/v) NZ-Amine, 0.4% (w/v) dextrin, 200 µg/ml 5-FOA and 20 µg/ml uracil was added. The media components solution was pre-warmed to 75°C and mixed with an equal volume of boiling 1.2% (w/v) Gelrite solution.

4.2.4 Growth Curves for *S. acidocaldarius*

S. acidocaldarius DSM639 MW001 wild type and Nudix deletion strains (Table 4.3) were grown as pre-cultures in 25 ml Brock media supplied with 0.1% (w/v) NZ-Amine, 0.2% (w/v) dextrin and 10 µg/ml uracil at 75°C, 120 rpm. Upon reaching stationary phase, a calculated volume of each strain was transferred into 50 ml fresh medium corresponding to a starting OD₆₀₀ = 0.01. Each strain was grown in triplicates in three different media: Brock + NZ-Amine + Dextrin + Uracil (= "full Brock"), Brock + NZ-Amine + Uracil (= "-Dex"), Brock + Dex + Ura (= "-NZA"). 200 µl starting culture from each flask were transferred into a 96 well plate and OD₆₀₀ was measured in a plate reader to verify starting OD values. Cultures were subsequently incubated at 75°C,

120 rpm, over a period of five days, taking samples every 24h. Sample taking included transferring 200 μ l culture into a 96 well plate to measure OD₆₀₀, as well as transferring 2 ml culture into an aliquot, harvesting cells for 5 min at max. speed, RT, in a tabletop centrifuge and storing pellets at -80°C until further use.

4.2.5 Heat shock spotting assay for *S. acidocaldarius*

S. acidocaldarius DSM639 MW001 wild type and Nudix deletion strains were grown as pre-cultures in 25 ml Brock media supplied with 0.1% (w/v) NZ-Amine, 0.2% (w/v) dextrin and 10 μ g/ml uracil at 75°C, 120 rpm. Upon reaching stationary phase, a calculated volume of each strain was transferred into 40 ml fresh medium in triplicates corresponding to a starting OD₆₀₀ = 0.01 and cultures were incubated at 75°C, 120 rpm. After 48h, 1 ml from each culture was transferred into a pre-warmed aliquot without cap and incubated at 75°C, 300 rpm, on a Thermomixer. During an adaptation period of 15 min, OD₆₀₀ of each culture was determined using a plate reader. After the adaptation period, 200 μ l of each culture were transferred into a 0.2 ml aliquot as control samples and temperature on the Thermomixer was increased to 85°C. A digital pocket thermometer with a K-type probe placed inside an aliquot filled with 1 ml H₂O was used to monitor the temperature of the liquid and aliquots were covered with a gas-permeable sealing membrane to minimize evaporation. After reaching the target temperature of 85°C on the thermometer, cultures were incubated at 85°C, 300 rpm, for 30 min (= "heat shock"). Afterwards, 200 μ l culture were transferred into 0.2 ml aliquots. Heat shock as well as control samples were diluted down to a calculated OD₆₀₀=0.1 and a 10⁻¹ to 10⁻⁶ dilution series in Brock Recovery medium (Brock medium supplied with 0.1% (w/v) NZ-Amine, no pH adjustment) was prepared. 3 μ l of each dilution for heat shock and control samples of each culture were spotted onto a solid Brock Gelrite plate supplied with 0.1% (w/v) NZ-Amine, 0.2% (w/v) dextrin and 10 μ g/ml uracil using a Multichannel pipet. Plates were incubated upside down in a plastic box lined with wet paper towels at 75°C for 5-6 days.

4.3 Plasmids and oligonucleotides

4.3.1 Progenitor plasmid and constructed recombinant vectors

Table 4.4: Progenitor plasmids used in this work

Vector	Features	Application	Reference
pRSFDuet-1	Kan ^R , IPTG-inducible T7 promoter, N-terminal His _{6x} -Tag	Heterologous gene expression in <i>E. coli</i>	Novagen, Darmstadt
pSVA431	Amp ^R , <i>pyrEF</i> , <i>lacS</i> from <i>Sa. solfataricus</i>	Generation of markerless deletion mutants in <i>S. acidocaldarius</i>	Gift of Prof. Dr. Sonja-Verena Albers (Albert-Ludwigs-Universität Freiburg), Wagner et al., 2012
pSVAaraFX-Stop	Amp ^R , <i>pyrEF</i> , arabinose-inducible promoter <i>SACI_2122</i>	Expression of permuted SRP RNA gene	Gift of Prof. Dr. Sonja-Verena Albers (Albert-Ludwigs-Universität Freiburg)

Table 4.5: Recombinant plasmids for the overproduction of recombinant proteins from *S. acidocaldarius* in *E. coli* Rosetta.

Plasmid + Insert	Description of insert
pRSF + SACI_RS00730	N-terminally His _{6x} -tagged SACI_RS00730 gene, restriction sites BamHI, HindIII; this work
pRSF + SACI_RS00060	N-terminally His _{6x} -tagged SACI_RS00060 gene, restriction sites BamHI, HindIII; this work
pRSF + SACI_RS02625	N-terminally His _{6x} -tagged SACI_RS02625 gene, restriction sites BamHI, HindIII; this work ¹
pRSF + SACI_RS00575	N-terminally His _{6x} -tagged SACI_RS00575 gene, restriction sites BamHI, HindIII; this work
pRSF + SACI_RS00575_E48A_E51A_E52A	N-terminally His _{6x} -tagged SACI_RS00575_a143c_a152c_a155c gene, restriction sites BamHI, HindIII; this work
pRSF + SACI_RS00730_E52A_E55A_E56A	N-terminally His _{6x} -tagged SACI_RS00730_a155c_a164c_a167c gene, restriction sites BamHI, HindIII; this work
pRSF + SACI_RS00060_E81A_E84A_E85A	N-terminally His _{6x} -tagged SACI_RS00060_a242c_a251c_a254c gene, restriction sites BamHI, HindIII; this work
pRSF + SACI_RS02625_E55A_E58A_E59A	N-terminally His _{6x} -tagged SACI_RS02625_a164c_a173c_a176c gene, restriction sites BamHI, HindIII; this work ¹
pRSF + SACI_RS04105 + SACI_RS03165	N-terminally His _{6x} -tagged SACI_RS04105, restriction sites BamHI, HindIII and N-terminally His _{6x} -tagged SACI_RS03165, restriction sites NdeI, XhoI; this work

¹ Gene synthesis and subcloning by Genscript Inc., Piscataway, NJ, USA

pET28a + hNudT5	C-terminally His _{6x} -tagged human NudT5, restriction sites NcoI, XhoI; gift of Dr. Katharina Höfer (MPI Marburg)
------------------------	---

Table 4.6: Recombinant plasmids for the generation of Nudix deletion strains in *S. acidocaldarius* DSM639 MW001.

Plasmid + Insert	Description of insert
pSVA431 + part of <i>SACI_RS00730</i>	<i>SACI_RS00730</i> position 1 – 400 of coding sequence, restriction site SacII; this work
pSVA431 + part of <i>SACI_RS00730</i> + del 00730 donor DNA	<i>SACI_RS00730</i> position 1 – 400 of coding sequence, restriction site SacII; donor DNA fragment comprises deletion of <i>SACI_RS00730</i> position 1 – 421 of coding sequence with each 500 bp left flank and right flank, restriction site BamHI; this work
pSVA431 + part of <i>SACI_RS00060</i>	<i>SACI_RS00060</i> position 1 – 450 of coding sequence, restriction site SacII; this work
pSVA431 + part of <i>SACI_RS00060</i> + del 00060 donor DNA	<i>SACI_RS00060</i> position 1 – 450 of coding sequence, restriction site SacII; donor DNA fragment comprises deletion of <i>SACI_RS00060</i> position 1 – 481 of coding sequence with each 600 bp left flank and right flank, restriction site BamHI; this work
pSVA431 + part of <i>SACI_RS02625</i>	<i>SACI_RS02625</i> position 41 – 440 of coding sequence, restriction site SacII; this work
pSVA431 + part of <i>SACI_RS02625</i> + del 02625 donor DNA	<i>SACI_RS02625</i> position 41 – 440 of coding sequence, restriction site SacII; donor DNA fragment comprises deletion of <i>SACI_RS02625</i> position 15 – 440 of coding sequence with each 500 bp left flank and right flank, restriction site BamHI; this work
pSVA431 + part of <i>SACI_RS00575</i>	<i>SACI_RS00575</i> position 1 – 425 of coding sequence, restriction site SacII; this work
pSVA431 + part of <i>SACI_RS00575</i> + del 00575 donor DNA	<i>SACI_RS00575</i> position 1 – 425 of coding sequence, restriction site SacII; donor DNA fragment comprises deletion of <i>SACI_RS00575</i> position 1 – 453 of coding sequence with each 500 bp left flank and right flank, restriction site BamHI; this work

Table 4.7: Recombinant plasmids for the expression of the permuted SRP RNA gene variant in *S. acidocaldarius*, as well as for the exchange of the permuted and the original gene variant in the genome

Plasmid + Insert	Description of the insert
pUC57 + <i>SACI_RS00445</i>_{perm}	permuted SRP RNA gene with native promoter, restriction sites NcoI, NdeI; this work ²
pSVAaraFX-Stop + <i>SACI_RS00445</i>_{perm}	permuted SRP RNA gene with native promoter, restriction sites NcoI, BamHI, removal of the promoter <i>SACI_2122</i> ; this work
pSVAaraFX-Stop + <i>SACI_RS00445</i>_{perm}a388g	permuted SRP RNA gene with nucleotide exchange and native promoter, restriction sites NcoI, BamHI, removal of the promoter <i>SACI_2122</i> ; this work

² Gene synthesis and subcloning by Genscript Inc., Piscataway, NJ, USA

pSVA431 + SACI_RS00445	SACI_RS00445 (SRP RNA gene) position 1 – 307 of coding sequence, restriction site SacII; this work
pSVA431 + SACI_RS00445 + SACI_RS00445 _{perm_a388g} donor DNA	SACI_RS00445 (SRP RNA gene) position 1 – 307 of coding sequence, restriction site SacII; 500 bp left flank including native promoter and 722 bp right flank including SACI_RS00445 _{perm_a388g} , restriction site BamHI; this work ²

4.3.2 Oligonucleotides

Genomic DNA of *S. acidocaldarius* DSM639 MW001 was used as the PCR template for the oligonucleotides listed below.

Table 4.8: Oligonucleotides used for the production of recombinant plasmids for the overproduction of proteins from *S. acidocaldarius* in *E. coli* Rosetta listed in Table 4.5.

Name	Sequence 5' → 3'	Remarks
SACI_RS00730 for	TTTGGATCCCATGGAACGACCTTTAGTTGC	Forward primer for SACI_RS00730, BamHI
SACI_RS00730 rev	TTTAAGCTTCTACTTGGAGGTTGAGTGA	Reverse primer for SACI_RS00730, HindIII
SACI_RS00060 for	TTTGGATCCCATGAGAATATATTCGTCTAA	Forward primer for SACI_RS00060, BamHI
SACI_RS00060 rev	TTTAAGCTTCTATCCTTGTAGGAGAGATC	Reverse primer for SACI_RS00060, HindIII
SACI_RS00575 for	TTTGGATCCCATGGAGACATGTTTAGGAGT	Forward primer for SACI_RS00575, BamHI
SACI_RS00575 rev	TTTAAGCTTCTAGGTAAATTCGGTTAAAC	Reverse primer for SACI_RS00575, HindIII
SACI_RS04105 for	TTTGGATCCCATGATCCAAGGGGAAATATT	Forward primer for SACI_RS04105, BamHI
SACI_RS04105 rev	AAAAAGCTTTTATAATTTCAACCATTTAA	Reverse primer for SACI_RS04105, HindIII
SACI_RS03165 for	TTTCATATGCATCACCATCATCACCACATGACTGAAAGTACAAATAT	Forward primer for SACI_RS03165, NdeI, N-term. His _{6x} -Tag
SACI_RS03165 rev	AAACTCGAGTCATTTTTTATTTAGCCTTA	Reverse primer for SACI_RS03165, XhoI

The oligonucleotides listed below were used to generate Nudix domain-mutant proteins by triple nucleotide exchange via site-directed mutagenesis. The respective plasmids listed in Table 4.5 carrying the wild type protein sequence were used as PCR templates.

Table 4.9: Oligonucleotides used for the production of recombinant plasmids for the overproduction of Nudix domain mutant proteins from *S. acidocaldarius* in *E. coli* Rosetta listed in Table 4.5.

Name	Sequence 5' → 3'	Remarks
SACI_RS00730_a155c_a164c_a167c for	AGATGCTGTAAAAAGAGCAATGAAGGCG GCAACTGCCCTAGACGTGG	Forward primer for <u>triple nucleotide exchange</u> in SACI_RS00730
SACI_RS00730_a155c_a164c_a167c rev	CCACGTCTAGGGCAGTTGCCGCCTTCAT TGCTCTTTTTACAGCATCT	Reverse primer for <u>triple nucleotide exchange</u> in SACI_RS00730
SACI_RS00060_a242c_a251c_a254c for	GATCTAACTGCAAGAAGAGCGTTAGAGG CGGCAATAGTTATGTTCCCCTT	Forward primer for <u>triple nucleotide exchange</u> in SACI_RS00060
SACI_RS00060_a242c_a251c_a254c rev	AAGGGGAACATAACCTATTGCCGCCTCTA ACGCTCTTCTTGACGTTAGATC	Reverse primer for <u>triple nucleotide exchange</u> in SACI_RS00060
SACI_RS00575_a143c_a152c_a155c for	GAATGCGTCGAAAAGAGCACTTTACGCGG CGTTGGGGATCAGAGTC	Forward primer for <u>triple nucleotide exchange</u> in SACI_RS00575
SACI_RS00575_a143c_a152c_a155c rev	GACTCTGATCCCCAACGCCGCGTAAAGT GCTCTTTCGACGCATTC	Reverse primer for <u>triple nucleotide exchange</u> in SACI_RS00575

Genomic DNA of *S. acidocaldarius* DSM639 MW001 was used as the PCR template for the oligonucleotides listed below. Plasmids were constructed via two separate Gibson Assemblies, firstly to introduce part of the gene of interest into MCSI and secondly to introduce the donor DNA fragment comprised of the respective left and right flanks into the MCSII of the vector pSVA431.

Table 4.10: Oligonucleotides used for the production of plasmids for the generation of Nudix deletion strains in *S. acidocaldarius* DSM639 MW001 listed in Table 4.6.

Name	Sequence 5' → 3'	Remarks
part SACI_RS00730 for	CCGGCCGCCATGGCGGCCGCGGAGGGAGT TTTTCTCCGTTAAAG	Forward primer for 400 bp fragment of SACI_RS00730
part SACI_RS00730 rev	AGGTACCATCGAATTCCCGCGGATGGAACG ACCTTTAGTTG	Reverse primer for 400 bp fragment of SACI_RS00730
part SACI_RS00060 for	CCGGCCGCCATGGCGGCCGCGGTATTTTTTC CTTCATCTATCATTTTAATTG	Forward primer for 450 bp fragment of SACI_RS00060
part SACI_RS00060 rev	AGGTACCATCGAATTCCCGCGGATGAGAAT ATATTCGTCTAAGAAATTTG	Reverse primer for 450 bp fragment of SACI_RS00060
part SACI_RS02625 for	CCGGCCGCCATGGCGGCCGCGGAGGTAGG AAAAATTCTAATAATAAAG	Forward primer for 400 bp fragment of SACI_RS02625

part SACI_RS02625 rev	AGGTACCATCGAATTCCC CGGACTGTGTAT AATTTCTTTTGAATTATATC	Reverse primer for 400 bp <u>fragment of</u> <u>SACI_RS02625</u>
part SACI_RS00575 for	CCGGCCGCATGGCGGCGCGG TCTCCTC CAAAGAATTCTTTC	Forward primer for 425 bp <u>fragment of</u> <u>SACI_RS00575</u>
part SACI_RS00575 rev	AGGTACCATCGAATTCCC CGGATGGAGAC ATGTTTAGGAG	Reverse primer for 425 bp <u>fragment of</u> <u>SACI_RS00575</u>
SACI_RS00730 LF for	ACTGCTCAAACCTAGGTCAGGATCC AGTGA GCAAACCTTAGAG	<u>Left flank forward primer</u> for <u>SACI_RS00730</u>
SACI_RS00730 LF rev	TAATTTTAT TCACTCAAACCTCCAAGTAG	<u>Left flank reverse primer</u> for <u>SACI_RS00730</u>
SACI_RS00730 RF for	GGTTTGAGTGAATAAAATTAACATAGGATAA AAGTTAATATATAG	<u>Right flank forward</u> primer for <u>SACI_RS00730</u>
SACI_RS00730 RF rev	GTGATCCGATACGCGTACTGGATCC ATATTC TGGTTCATTAACTTAAATG	<u>Right flank reverse</u> primer for <u>SACI_RS00730</u>
SACI_RS00060 LF for	ACTGCTCAAACCTAGGTCAGGATCC AAACAA GAAGGAATATATTAATAGAAATAG	<u>Left flank forward primer</u> for <u>SACI_RS00060</u>
SACI_RS00060 LF rev	TTTTAGTCCTC ATTCAAGAAAATATCAAGAG ATC	<u>Left flank reverse primer</u> for <u>SACI_RS00060</u>
SACI_RS00060 RF for	TCTTGAAATGAGGACTAAAAATTAATCCAAT GATATTTTTG	<u>Right flank forward</u> primer for <u>SACI_RS00060</u>
SACI_RS00060 RF rev	GTGATCCGATACGCGTACTGGATCCATAATT ATCTATTAGAGGCAATAATAATATTC	<u>Right flank reverse</u> primer for <u>SACI_RS00060</u>
SACI_RS02625 LF for	ACTGCTCAAACCTAGGTCAGGATCC GGTGG TTTACGTGTTAAC	<u>Left flank forward primer</u> for <u>SACI_RS02625</u>
SACI_RS02625 LF rev	TGCCGACTGACAATTACAATCTTCCATACT CTTTATTGCT	<u>Left flank reverse primer</u> for <u>SACI_RS02625</u>
SACI_RS02625 RF for	AGCAATAAAGAGTATGGAAGATTGTAATTGT CAGTCCGGCA	<u>Right flank forward</u> primer for <u>SACI_RS02625</u>
SACI_RS02625 RF rev	GTGATCCGATACGCGTACTGGATCC GCTCG ATATAGAAGCGTTCTC	<u>Right flank reverse</u> primer for <u>SACI_RS02625</u>
SACI_RS00575 LF for	ACTGCTCAAACCTAGGTCAGGATCC ATAGAT GTAGGGAATAAGGATG	<u>Left flank forward primer</u> for <u>SACI_RS00575</u>
SACI_RS00575 LF rev	AGTGAGATTCAACGTATTTTACTGTGAGC	<u>Left flank reverse primer</u> for <u>SACI_RS00575</u>
SACI_RS00575 RF for	AAAATACGTTGAATCTCACTTGGCACTAAAT C	<u>Right flank forward</u> primer for <u>SACI_RS00575</u>
SACI_RS00575 RF rev	GTGATCCGATACGCGTACTGGATCC ACAGG GTTTAATGAAATAGATTTAC	<u>Right flank reverse</u> primer for <u>SACI_RS00575</u>

The oligos listed below were used in different combinations to identify the circular SRP RNA via inverse reverse transcription PCR (iRT-PCR). The template was cDNA which was reverse transcribed from total RNA from *S. acidocaldarius* DSM639 MW001 carrying the plasmid pSVAaraFX-Stop + SACI_RS00445_{perma}388g.

Table 4.11: Oligonucleotides used for inverse Reverse Transcription-PCR

Name	Sequence 5' → 3'	Remarks
iRT-PCR for 1.1	CGCCCGACGGGGCGAGATAG	Forward primer, binds in 5'-half
iRT-PCR for 1.2	TTGACCGGGGAACCGGCCA	Forward primer, binds in 5'-half
iRT-PCR for 1.3	TTCCCTTTCTGGAGGGAGAG	Forward primer, binds in 5'-half
iRT-PCR for 1.4	TTCGTCGGTCTCCGATAGGA	Forward primer, binds in 5'-half
iRT-PCR rev 2.1	CCGCTCCCCTATGCCATAAC	Reverse primer, binds in 3'-half
iRT-PCR rev 2.2	AGTTACTGGTGCCACGTTG	Reverse primer, binds in 3'-half
iRT-PCR rev 2.3	AGCAGGTATTATAGCATAGG	Reverse primer, binds in 3'-half

The first pair of oligonucleotides listed below was used to perform a single nucleotide exchange in the sequence of the permuted SRP RNA gene variant using site-directed mutagenesis on the plasmid pSVAaraFX-Stop + SACI_RS00445_{perm}. The second pair of oligonucleotides listed below was used for the production of the plasmid pSVA431 + SACI_RS00445 listed in Table 4.7 via Gibson Assembly. As PCR template genomic DNA from *S. acidocaldarius* DSM639 MW001 was used.

Table 4.12: Oligonucleotides used for the production of the plasmids listed in Table 4.7.

Name	Sequence 5' → 3'	Remarks
SACI_RS00445 _{perm} _a388g for	GGCCAGGCCCGGGAGAGCCAATCCA	Forward primer for nucleotide exchange in SACI_RS00445 _{perm}
SACI_RS00445 _{perm} _a388g rev	TGGATTGGCTCTCCGGGCCTGGCC	Reverse primer for nucleotide exchange in SACI_RS00445 _{perm}
SACI_RS00445 for	CCGGCCGCCATGGCGGCCGCGGTGGTCAG GTAGGGTGGAG	Forward primer for SACI_RS00445
SACI_RS00445 rev	AGGTACCATCGAATTCCCGCGGTGGTCAGC TCCCCTATGC	Reverse primer for SACI_RS00445

The RNA oligonucleotide listed below was used for the splicing assays described in section 4.6.7.

Table 4.13: RNA oligonucleotide used for *in vitro* splicing assays

Name	Sequence 5' → 3'	Remarks
BHB model from SACI_RS00445_{perm}	GAUUGGCUCCGAAGGAGCAGUAGUGCUC GGGAGAGCCAAUC	5' modification: 6-FAM®, this work ³

The DNA oligos listed below were hybridized and used as a template in *in vitro* transcription reactions for the production of 5'-capped NAD-RNA, ADPR-RNA and Ap4A-RNA.

Table 4.14: DNA oligonucleotide template for the production of differently 5'-capped RNA

Name	Sequence 5' → 3'	Remarks
Model-NAD-RNA-sense	GATCACTAATACGACTCACTATTACTGTGTC GTCGTCTGCTGTCTCTCTCTCGCGGGC	IVT template with <u>Class II T7 RNAP promoter</u>
Model-NAD-RNA-antisense	GCCC GCGAGAGAGAGACAGCAGACGACGA CGACACAGTAATAGTGAGTCGTATTAGTGAT C	IVT template with <u>Class II T7 RNAP promoter</u>
Model-RNA-substrate	ACUGUGUCGUCGUCGUCGUCUCUCUCU CUCGCGGGC	RNA substrate for decapping assays

Table 4.15: Oligonucleotides used for the sequencing of plasmids constructed or used in this work

Name	Sequence 5' → 3'	Remarks
Duet UP1	TCTCGACGCTCTCCCTTATG	Forward primer for pRSFDuet MCSI
Duet DOWN 1	GATTATGCGGCCGTGTACAA	Reverse primer for pRSFDuet MCSI
Duet UP 2	TTGTACACGGCCGCATAATC	Forward primer for pRSFDuet MCSII
Duet DOWN 2	GCTAGTTATTGCTCAGCGG	Reverse primer for pRSFDuet MCSII
M13 reverse	CAGGAAACAGCTATGAC	Forward primer for pCRII-TOPO, reverse primer for pSVA431 MCSII
M13 forward	GTAAAACGACGGCCAG	Reverse primer for pCRII-TOPO
T7 promoter	TAATACGACTCACTATAGGG	Forward primer for pSVA431 MCSI

³ Synthesis by Sigma, Merck KGaA, Darmstadt

pSVA431 MCSI rev	TCGAGGTACCATCGAATTCC	Reverse primer for pSVA431 MCSI
pSVA431 MCSII for	GTCGCTTGACTTGACCAGAG	Forward primer for pSVA431 MCSII
pSVAaraFX-Stop for	GCGAGTCAGTGAGCGAGGAA	Forward primer for pSVAaraFX-Stop
pSVAaraFX-Stop rev	TTGTATGGTCTACCCATTTGTGGATCAAAA	Reverse primer for pSVAara-FX-Stop

Table 4.16: Oligonucleotides used for the sequencing of loci in the genome of *S. acidocaldarius* to verify gene deletions and/or insertions via PCR

Name	Sequence 5' → 3'	Remarks
Locus SACI_RS00730 for	AAATATATATGAAATTGCTA	Binds 300 bp upstream of goi
Locus SACI_RS00730 rev	TATGTTTAGCTTATTTACAA	Binds 300 bp downstream of goi
Locus SACI_RS00060 for	ACCTTATATTGGTGGTTCAG	Binds 300 bp upstream of goi
Locus SACI_RS00060 rev	ATTCATCCTTTCTGTAATTC	Binds 300 bp downstream of goi
Locus SACI_RS02625 for	CAAGCATCTGGTGGGATAAC	Binds 300 bp upstream of goi
Locus SACI_RS02625 rev	TTATTCAGACCAGACCATAC	Binds 300 bp downstream of goi
Locus SACI_RS00575 for	ATATACAAACCGTGTGGTTC	Binds 300 bp upstream of goi
Locus SACI_RS00575 rev	TGTAGTTACACAACTAGGT	Binds 300 bp downstream of goi
Locus SACI_RS00445 (SRP RNA gene) for	AAAGCCCTTGATAGACTTGG	Forward primer, binds upstream of WT left flank
Locus SACI_RS00445 (SRP RNA gene) rev	CCGGCGCCATGAATATTATC	Reverse primer, binds inside right flank

4.4 Molecular working with DNA

4.4.1 DNA isolation

4.4.1.1 Genomic DNA isolation from *S. acidocaldarius*

Cell cultures of *S. acidocaldarius* were grown to the late logarithmic phase and 2 ml cultures were harvested by centrifugation for 5 min at max. speed (13.000 rpm) and RT. Genomic DNA isolation was performed using the NucleoSpin® Tissue Kit (Macherey-Nagel), following the standard protocol for cultured cells according to the manufacturer's instructions.

4.4.1.2 Isolation of plasmid DNA from *E. coli*

Plasmid DNA was prepared from *E. coli* overnight cultures (5 ml culture volume) using the NucleoSpin® Plasmid (NoLid) Mini kit (Macherey-Nagel) according to the manufacturer's instructions.

4.4.2 DNA quantitation

4.4.2.1 Spectrophotometric DNA quantitation and quality control

The concentration of DNA in aqueous solutions was determined spectrophotometrically at a wavelength of $\lambda = 260$ nm. At this wavelength, an extinction value of 1 correlates to 50 μg dsDNA/ml (Sambrook et al., 1989). To determine DNA sample quality, the photometer determines absorption at $\lambda = 280$ nm, the absorption wavelength of proteins. An A260/A280 ratio between 1.8 – 2.0 indicates sufficiently pure DNA samples, whereas lower values indicate protein contamination in the sample.

4.4.2.2 Fluorometric quantitation

High-sensitivity quantification of low-yield DNA samples (e.g. cDNA libraries) was performed using a Qubit® 2.0 fluorometer. Sample concentration is determined using a fluorescent dye which emits a signal only when bound to its specific target. Quantitation of dsDNA samples was performed using the Qubit™ dsDNA High Sensitivity Assay kit and measurements and calibrations were conducted according to the manufacturer's protocol.

4.4.3 Polymerase chain reaction (PCR)

4.4.3.1 Amplification of genomic and plasmid DNA

In vitro amplification of genomic and plasmid DNA was performed using the polymerase chain reaction (PCR) technique (Mullis et al., 1986; Saiki et al., 1988). Here, the sequence of interest is flanked by two sequence-specific DNA oligonucleotides ("primers") which hybridize to the 3' end of the sense and the 5' end of the antisense strands. The heat-stable and proof-reading Phusion DNA Polymerase then elongates the oligonucleotides in 5'→3' direction.

The PCR reaction consists of three steps: i) denaturation, ii) annealing and iii) elongation. First, the dsDNA is melted into two ssDNA strands by denaturation at 98°C. During the annealing step, the primers hybridize to the ssDNA strands and are subsequently extended in 5' → 3' direction via nucleotide incorporation by the DNA polymerase during the elongation step. Repetition of these three steps leads to

exponential amplification of the target DNA. A crucial factor is the annealing temperature, which corresponds to the melting temperature of the primers and was determined using the NEB T_m calculator online tool (<https://tmcalculator.neb.com>).

PCR reactions were set up using 50 ng template DNA (genomic or plasmid origin), each 10 pmol forward and reverse primer, 10 nM of each dNTP, 5X Phusion HF buffer and 1 U Phusion Polymerase. Standard PCR cycling parameters were programmed according to Table 4.17.

Table 4.17: Standard PCR program using Phusion polymerase

Step	Temperature	Time	Cycle
Initial Denaturation	98°C	30 sec	1
Denaturation	98°C	10 sec	
Annealing	42 – 65°C	30 sec	2 – 30
Elongation	72°C	30 sec/kb	
Final Elongation	72°C	5 min	31
Cooling	14°C	∞	∞

4.4.3.2 Colony PCR

To investigate the presence of plasmids and integration or recombination events in the genome, single colonies were analyzed using Colony PCR. Reactions were set up using the 2X DreamTaq Green PCR Master Mix according to the manufacturer's instructions but scaling all reactions down to half the total volume. For analysis of *E. coli* colonies, single colonies were picked and transferred directly into the tube containing the PCR components. For analysis of *S. acidocaldarius*, single colonies were lysed in 20 μ l 0.2 M NaOH for 5 min at RT. Afterwards, the suspension was neutralized by addition of 80 μ l 0.2 M Tris-HCl pH 6.5 and 2 μ l were used in the PCR reaction. Alternatively, 20 μ l of a *S. acidocaldarius* cell culture was lysed in 20 μ l 0.2 M NaOH for 5 min at RT, neutralized by addition of 80 μ l 0.2 M Tris-HCl and 5 μ l suspension were used in the reaction.

4.4.3.3 Site-directed mutagenesis PCR

Introduction of insertion, deletions or nucleotide exchanges in plasmid sequences was performed using site-directed mutagenesis (Ho et al., 1989). The forward and reverse primers were designed using the QuikChange Primer Design online tool from Agilent (<https://www.agilent.com/store/primerDesignProgram.jsp>). PCR reactions and program were set up according to Wang & Malcolm (1999), an adaptation of Stratagene's QuikChange Site-Directed Mutagenesis Kit manual (catalog no.

200518), with the exception of using Phusion DNA polymerase. Briefly, two single-primer extension reactions are set up and run for 10 cycles. Equal volumes of both reactions are then mixed, added with fresh Phusion polymerase and run for another 20 cycles. Lastly, the reactions are treated with DpnI to degrade the template plasmid and transformed into chemically-competent *E. coli* cells.

4.4.4 DNA electrophoresis

Differently sized DNA fragments were separated in an electric field using agarose gel electrophoresis. Gels were cast with 1% (w/v) agarose in 1X TAE buffer (40 mM Tris-Acetate, 1 mM EDTA, 20 mM acetic acid pH 8.0) and 0.04% (v/v) of the nucleic acid stains Midori Green Advance or peqGREEN. DNA samples were mixed with either 6X Purple Gel Loading Dye (no SDS) or self-made 6X loading dye (40% (v/v) sucrose, 0.25% (w/v) bromophenol blue, 0.25% (w/v) xylene cyanol) and run next to the 2-Log DNA Ladder serving as a size standard. Gel Electrophoresis was performed at 120 V for 20 – 30 min in 1X TAE running buffer and bands were visualized under UV light (254 nm) using a gel documentation system).

4.4.5 DNA purification

4.4.5.1 Purification of PCR reactions

PCR reactions yielding the DNA fragment of interest were directly purified using the NEB Monarch® PCR & DNA Cleanup Kit (5 µg) according to the manufacturer's instructions.

4.4.5.2 Gel extraction from agarose gels

DNA fragments after agarose gel electrophoresis were purified from the gel using the NucleoSpin® Gel and PCR Clean-up kit according to the manufacturer's instructions.

4.4.6 Hybridization of DNA oligonucleotides

To prepare the dsDNA template for *in vitro* transcription, each 50 µM of the complementary DNA oligonucleotides were mixed and then hybridized by incubation for 5 min at 95°C in a thermomixer, followed by cooling down to 4°C with a ramp rate of 0.2°C/sec.

4.4.7 Enzymatic modification of DNA

4.4.7.1 Restriction

A standard DNA restriction reaction was performed using 1 µg template DNA and 10-20 U restriction enzyme with its recommended buffer. When applicable, restrictions

were incubated at 37°C for 1-2h or overnight, according to the manufacturer's instructions.

4.4.7.2 Dephosphorylation

To avoid self-ligation, the 5' ends of digested plasmids were dephosphorylated. A standard dephosphorylation reaction consisted of 1 µg template DNA and 5-10 U Antarctic Phosphatase with its recommended buffer. Incubation for 1h at 37°C was followed by heat inactivation for 15 min at 65°C, according to the manufacturer's instructions.

4.4.7.3 Ligation

Ligation reactions were performed by mixing linearized vector and restricted insert fragments in a 1:5 molar ratio in the presence of 400 U T4 DNA Ligase, 10X T4 DNA Ligase Buffer and 10 mM ATP. Reactions were incubated at room temperature for 20 minutes and subsequently transformed into *E. coli* cells.

4.4.8 TOPO-Cloning

The method of ligase-independent TOPO cloning was employed to identify products with unknown sequences from the iRT-PCR (section 11) by incorporation into the linearized pCR®II TOPO® vector following the instructions of the TOPO™ TA Cloning™ Kit, Dual Promoter. Briefly, the gel purified products were treated with *Taq* DNA Polymerase for the post-amplification addition of a single deoxyadenosine (A) to their 3' end and subsequently ligated with the TOPO vector in the presence of salt solution. During this reaction, the Topoisomerase I of the TOPO vector establishes a covalent bond between the complementary residues of vector and insert. Afterwards, the reaction was directly used for transformation into chemically competent *E. coli* DH5α cells which were plated on LB plates supplied with 100 µg/ml ampicillin, 40 µl 100 mM IPTG and 40 µl X-Gal (40 mg/ml) for Blue-White screening. Subsequently, white colonies were analyzed by Colony PCR (section 4.4.3.2.), plasmids were isolated (section 4.4.1.2.) and insert sequences were identified via Sanger Sequencing (section 4.4.12.) using the M13 forward and reverse primers (Table 4.15).

4.4.9 Gibson Assembly

Gibson Assembly allows for the "scar-less" assembly of multiple DNA fragments and was employed to clone the plasmids for the generation of markerless deletion mutants in *S. acidocaldarius* (listed in Table 4.6), as well as cloning the SRP RNA gene from *S. acidocaldarius* (*SACI_RS00445*) into the vector pSVA431 (see Table 4.7). Briefly,

Gibson Assembly constitutes a single-tube isothermal reaction where multiple overlapping DNA fragments are joined by the activities of three different enzymes: a T5 exonuclease digests the PCR products in 5' → 3' direction creating single-stranded 3' overhangs with complementarity to their neighboring fragments, a DNA polymerase fills in the gaps by nucleotide addition and finally a DNA ligase repairs the nicks in the assembled DNA fragments (Gibson et al., 2009). Primers were designed using the NEBuilder® Assembly Tool (<https://nebuilder.neb.com>) and gel purified fragments of linearized vector and insert DNA were assembled using the 2X Gibson Assembly® Master Mix according to the manufacturer's instructions. Colonies were analyzed via Colony PCR (section 4.4.3.2.) and insert sequence verified via Sanger sequencing (section 4.4.12.).

4.4.10 Transformation

4.4.10.1 Preparation of chemically competent *E. coli* cells

Chemically competent *E. coli* cells were generated by treatment with RbCl (rubidium chloride) and CaCl₂ (Inoue et al., 1990). To this end, 100 ml LB medium supplied with 10 mM MgCl₂ and 10 mM MgSO₄ were inoculated with 2 ml of an *E. coli* overnight culture and subsequently grown at 37°C, 200 rpm, until OD₆₀₀=0.6. Cells were cooled on ice for 30 min and subsequently harvested by centrifugation for 10 min at 3,000×g and 4°C. The cell pellet was resuspended in 33 ml cold RF1 solution (30 mM potassium acetate pH 5.8, 100 mM RbCl, 50 mM MnCl₂, 10 mM CaCl₂, 15 % (v/v) glycerol) and incubated on ice for another 30 min. Afterwards, cells were again centrifuged for 10 min at 3,000×g and 4°C and the pellet resuspended in 5 ml cold solution RF2 solution (10 mM RbCl, 10 mM MOPS pH 5.8, 75 mM CaCl₂, 15 % (v/v) glycerol). After another final incubation for 30 min on ice, 100 µl aliquots were prepared and stored at -80°C until further use.

4.4.10.2 Transformation of *E. coli*

100 µl of competent *E. coli* cells were mixed with either 2 µl plasmid DNA or 5 µl ligation reaction and incubated on ice for 30 min. Subsequently, cells were heat-shocked for 45 sec at 42°C, immediately returned on ice and incubated for another 5 min. Afterwards, 900 µl LB medium was added to the cells and recovery was performed for 30 min at 37°C, 300 rpm, in a thermomixer. Finally, 100 µl cell solution was plated on an LB plate containing the appropriate antibiotics and the remaining cells were harvested by centrifugation for 2 min at 6000 rpm, RT, resuspended in 100 µl LB and plated on another LB plate supplied with the appropriate antibiotics. Plates

were incubated over night at 37°C and colonies were analyzed the following day via Colony PCR (section 4.4.3.2.).

4.4.10.3 Preparation of electrocompetent *S. acidocaldarius* cells

S. acidocaldarius DSM639 MW001 cells were grown in 50 ml Brock medium supplied with 0.1% (w/v) NZ-Amine, 0.2% (w/v) dextrin and 10 µg/ml uracil, pH 3.5, at 75°C and 120rpm to OD₆₀₀=0.3-0.7. A calculated amount of culture was subsequently transferred into 50ml fresh medium, use the following formulas:

$$\left(\frac{OD_{wanted}}{2^{division\ rate}}\right) * \frac{volume}{OD_{measured}} \text{ and } Division\ rate = \frac{time\ until\ harvest\ [h]}{doubling\ rate\ [h]}$$

The fresh culture was grown at 75°C and 120rpm to OD₆₀₀=0.2–0.3 overnight and afterwards incubated on ice for 10-15 min. Cells were harvested by centrifugation for 15-20 min at 2500×g and 4°C and the pellet was subsequently washed three times with each 30ml of ice-cold 20mM sucrose. Afterwards, the pellet was resuspended in 1ml of ice-cold 20mM sucrose, transferred to a 1.5 ml aliquot and centrifuged for another 5 min at 2500×g, 4°C. Finally, the pellet was resuspended in 20mM ice-cold sucrose to a theoretical OD₆₀₀=20 and 50 µl aliquots were stored at -80°C until further use.

4.4.10.4 Transformation of *S. acidocaldarius*

Prior to transformation into *S. acidocaldarius*, all plasmids or linearized DNA fragments must be methylated to circumvent the activity of the restriction endonuclease Sual (Berkner et al., 2007). To this end, plasmids are transformed into and subsequently prepared from the strain *E. coli* ER1821 carrying the plasmid pM.ESABC4I. This strain methylates the N4-position of the inner cytosine residues of GGCC, which is the recognition sequence of Sual (Grogan, 2003). Successful methylation can be tested by digestion with HaeIII for 1-4 h at 37°C in 10X CutSmart buffer. 300–500 ng of methylated DNA were mixed with 50 µl competent *S. acidocaldarius* cells and transferred into pre-cooled 1 mm electroporation cuvettes. Electroporation was performed in a constant time protocol using the parameters 1.5 kV, 25 µF, 600 Ω, followed by the quick addition of 350µl Brock Recovery Medium (Brock medium supplied with 0,1% (w/v) NZ-Amine, no pH adjustment) and transfer into a pre-warmed aliquot. Recovery was conducted for 30 min at 75°C, 300 rpm, followed by plating 150 µl cells on a pre-warmed first selection plate (section 4.2.3.). Plates were incubated upside down in a plastic box lined with wet paper towels at 75°C for 5-7 days. For

plasmids and DNA fragments containing the *lacS* cassette from *Sa. solfataricus*, successful transformation was verified via Blue-White Screening. To this end, plates with visible colonies were sprayed with freshly prepared 5 mg/ml X-gal in 20% (w/v) dextrin and incubated for 30 – 60 min at 75°C.

4.4.11 Gene deletion and gene exchange in *S. acidocaldarius*

The generation of markerless Nudix deletion strains was performed using the plasmid pSVA431, as described in Wagner et al., 2012. Briefly, this plasmid contains the two marker cassettes *pyrEF*_{SSO} and *lacS*_{SSO} as well as two multiple cloning sites. The first multiple cloning site harbors up to 500 bp of the gene of interest, while the second multiple cloning site harbors the upstream and downstream regions of the gene of interest, omitting the sequence about to be deleted. After methylation, the plasmid was digested with NotI to yield the marker cassette as a linear fragment and transformed into *S. acidocaldarius* via electroporation (section 4.4.10.4.). Cells were plated on uracil-lacking first selection plates to induce the first crossover event and integrate the marker cassette into the genome. Successful integration was confirmed with Blue-White Screening. Blue colonies were grown as liquid cultures and subsequently plated on second selection plates containing uracil as well as 5-fluorotic acid (5-FOA). As 5-FOA is metabolized into the toxic product fluorodeoxyuridin by cells with an active uracil cassette, they are induced to perform a second crossover event, looping out both marker cassettes, as well as the gene of interest, thereby yielding markerless deletion mutants. All deletion mutants were verified by sequencing of PCR products of the deletion locus, as well as confirmed by RNA-sequencing later on. The double deletion strain was generated by making electro-competent cells from strains *S. acidocaldarius* DSM639 MW001 Δ *SACI_RS00730* and *S. acidocaldarius* DSM639 MW001 Δ *SACI_RS00060* and transforming them with the marker cassette for the deletion of *SACI_RS00060* and *SACI_RS00730*, respectively.

The same approach was used to replace the original SRP RNA gene with its permuted variant. Here, the multiple cloning site harbored the original SRP RNA gene (*SACI_RS00445*) and the second multiple cloning site harbored the upstream flanking region including the native promoter at its 3'-end, followed by the downstream flanking region including the sequence of the permuted SRP RNA gene variant at its 5'-end. Transformation and selection procedure were performed as described above.

4.4.12 Sequencing

The sequencing of constructed recombinant plasmids or PCR products was performed via Sanger sequencing at Microsynth SeqLab GmbH, Göttingen.

4.5 Molecular working with RNA

4.5.1 Treatment of solutions, glassware and other equipment

Solutions were treated with 0.1% (w/v) Diethyl pyrocarbonate (DEPC) by overnight incubation at RT and 400 rpm and subsequent autoclaving. Plastic consumables were purchased in RNase-free conditions and autoclaved prior to use. Glassware was sterilized either by autoclaving or sterilization at 200°C for >4h. Heat-labile equipment was treated with RNase Exitus Plus™ prior to use.

4.5.2 Isolation of total RNA from *S. acidocaldarius*

Total RNA from *S. acidocaldarius* was extracted using the *mirVana*™ miRNA Isolation Kit according to the manufacturer's instructions. Briefly, the sample was lysed in a denaturing lysis solution which stabilizes RNA while simultaneously inactivating RNases. RNA was subsequently extracted from the lysate via organic extraction using Acid-Phenol:Chloroform. Further purification was achieved by immobilizing the RNA to a glass-fiber filter followed by several washing steps. Finally, the RNA was eluted with a low ionic-strength solution (DEPC-treated water). Subsequently, total RNA extractions were digested with 1 U DNaseI/μg RNA (max. 5 μl DNaseI) in the presence of MnCl₂ for 2h at 37°C to remove residual DNA contaminations. Reactions were then cleaned using the Monarch® RNA Cleanup Kit (50 μg) and RNA samples were stored at -80°C until further use.

4.5.3 RNA quantitation

4.5.3.1 Spectrophotometric RNA quantitation and quality control

For quantitation and quality control of RNA samples, a spectrophotometer was employed as described previously (section 4.4.2.1.).

4.5.3.2 Fluorometric quantitation

High-sensitivity quantification of RNA samples was performed using the Qubit® 2.0 fluorometer. Sample concentration is determined using a fluorescent dye which emits a signal only when bound to its specific target. Quantitation of RNA samples was performed using the Qubit™ RNA High Sensitivity Assay kit and measurements and calibrations were conducted according to the manufacturer's protocol.

4.5.4 Inverse reverse transcription PCR

Inverse reverse transcription PCR (iRT-PCR) was performed to detect the permuted SRP RNA gene in total RNA extracted from *S. acidocaldarius* DSM639 MW001 carrying the plasmid pSVAaraFX-Stop + SACI_RS00445_{perma}388g. To this end, total RNA extractions were prepared from this strain as described previously (section 4.5.2.). Afterwards, reverse transcription was performed using Superscript IV Reverse Transcriptase according to the manufacturer's instructions, using Random Hexamers and elevated temperatures for account for the source organism cultivation temperatures. Briefly, the Random Hexamers were annealed to the RNA for 5 min at 100°C, then snap-cooled on ice and subsequently incubated with the Superscript IV Reverse Transcriptase and RNase Inhibitor Murine for 10 min at 65°C for reverse transcription, followed by inactivation for 10 min at 80°C. This reaction then served as template for a standard PCR using Phusion DNA Polymerase (section 4.4.3.1.) and inversely oriented primers binding to unique regions of the permuted SRP RNA gene variant (Table 4.11). PCR products were run on and subsequently purified from a 1% (w/v) agarose gel (section 4.4.4.), cloned into a TOPO vector (section 4.4.8.) and analyzed via Sanger sequencing (section 4.4.12.) to identify the sequence of the products of the iRT-PCR.

4.5.5 *In vitro* transcription of differently 5'-capped RNA

Each *in vitro* transcription (IVT) reaction contained 1 µg dsDNA template (see Table 4.14), 1 mM of each UTP/CTP/GTP and 4 mM NAD (for NAD-RNA) or 4 mM APDR (for ADPR-RNA) or 1 mM Ap4A (for Ap4A-RNA), 500 U T7 RNA polymerase and 240 U RNase Inhibitor Murine in transcription buffer (40 mM HEPES/KOH pH 8.0, 22 mM MgCl₂, 5 mM dithiothreitol (DTT), 5% DMSO). Reactions were incubated for 2-3h at 37°C, followed by the addition of 10 U DNase I and another 30 min incubation. IVT reactions were subsequently cleaned up using the NEB Monarch RNA Cleanup Kit (50 µg) and RNA was fluorometrically quantified.

4.5.6 RNA sequencing

4.5.6.1 Detection of the circular SRP RNA

S. acidocaldarius DSM639 MW001 cells carrying the plasmid pSVAaraFX-Stop + SACI_RS00445_{perma}388g were grown to the stationary phase in Brock media supplied with 0.1% (w/v) NZ-Amine and 0.2% (w/v) dextrin at 75°C, 120 rpm, and 2 ml cell culture was pelleted by centrifugation for 15 min at max. speed and RT in a tabletop centrifuge. Total RNA was extracted and purified as described previously (section

4.5.2.). RNA samples were subsequently treated with 1 U of Terminator™ 5'-Phosphate-Dependent Exonuclease (TEX) according to the manufacturer's instructions, followed by another column-based cleanup with the Monarch® RNA Cleanup Kit (10 µg). Successful removal of rRNAs by TEX was visualized via gel electrophoresis (section 4.4.4.) and RNA samples were fluorometrically quantified (section 4.5.3.2.). The cDNA libraries were generated using the NEBNext® Ultra™ II Directional RNA Library Prep Kit for Illumina® according to the manufacturer's instructions. All clean up steps were conducted using Solid Phase Reversible Immobilization (SPRI) beads. Library size distribution and quality control was performed using the High Sensitivity DNA Assay for Bioanalyzer and final concentration was fluorometrically determined (section 4.5.3.2.). Sequencing was performed as 150 nt single reads on an Illumina® MiniSeq by Dr. José Vicente Gomes-Filho at the Max Planck Institute for Terrestrial Biology, Marburg.

4.5.6.2 Transcriptomic analysis of Nudix deletion strains

S. acidocaldarius DSM639 MW001 wild type and Nudix single and double deletion strains were grown in duplicates in Brock media supplied with 0.1% (w/v) NZ-Amine, 0.2% (w/v) dextrin and 10 µg/ml uracil at 75°C, 120 rpm, to an OD₆₀₀=0.3 and OD₆₀₀=0.7, corresponding to mid-log and early stationary growth phases, respectively. Cells were pelleted by centrifugation for 15 min at max. speed, RT, and total RNA was extracted and purified as described previously (section 4.5.2.). Ribosomal RNAs were depleted using the Pan-Archaea riboPOOL probes and streptavidin-coated magnetic beads according to the manufacturer's instructions. Briefly, riboPOOL probes are single-stranded 3'-biotinylated DNA probes which specifically hybridize the cytoplasmic and mitochondrial rRNAs, thereby allowing for their removal using streptavidin-coated magnetic beads and a magnetic rack. Depleted RNA samples were cleaned up with the Monarch® RNA Cleanup Kit (10 µg) and successful rRNA depletion in all samples was verified with the RNA 6000 Pico Assay for the Agilent Bioanalyzer according to the manufacturer's instructions. The preparation of cDNA libraries from rRNA-depleted total RNA was performed using the NEBNext® Ultra™ II Directional RNA Library Prep Kit for Illumina®, SPRI beads and NEBNext® Multiplex Oligos for Illumina® (Index Primers Set 1-3), following the instructions of the NEBNext Library Prep Kit. Quality control and size distribution of the cDNA libraries was assessed with the High Sensitivity DNA Assay for Bioanalyzer. The library mix was

assembled according to the instructions of the sequencing facility and quantified using a fluorometer (section 4.5.3.2.). Sequencing was performed as 150 nt single reads on an Illumina® NextSeq550 at the Genomics Core Facility of the Philipps University Marburg.

4.6 Biochemical methods

4.6.1 Heterologous production of *S. acidocaldarius* proteins in *E. coli*

S. acidocaldarius proteins were produced from the recombinant plasmids listed in Table 4.5. All plasmids were cloned on a pRSFDuet-1 backbone where gene expression is under the control of the T7 promoter. Expression was performed by the *E. coli* strain Rosetta 2 DE3 pLysS, where expression of the T7 RNA Polymerase is under control of the IPTG-inducible *lac* promoter. Thereby, addition of IPTG to the media induces T7 RNA Polymerase expression which in turn allows for production of the protein of interest. Additionally, this strain encodes the T7 lysozyme on the pLysS plasmid, which inhibits the T7 RNA Polymerase to ensure minimal expression of the target gene before induction. Furthermore, the pLysS plasmid encodes tRNAs rarely used in *E. coli* (RARE2) to optimize expression of proteins from source organisms with widely different codon usage.

4.6.2 Expression and purification of *S. acidocaldarius* proteins in *E. coli*

1 liter LB medium supplied with the appropriate antibiotic were inoculated from an overnight culture to an $OD_{600}=0.05$ and grown at 37°C and 200 rpm until $OD_{600}=0.6-0.8$. At this point protein induction was induced by addition of 1mM IPTG (SACI_RS00730, Saci_NudT5, SACI_RS04105 + SACI_RS03165) or 0.1 mM IPTG (SACI_RS00575) and cultures were incubated for another 3–4h at 37°C, 200 rpm (SACI_RS00730, Saci_NudT5, SACI_RS04105 + SACI_RS03165) or overnight at 18°C, 200 rpm (SACI_RS00575). Cells were harvested by centrifugation for 15 min at 12.000×g, 4°C and pellets were stored at -80°C until further use. Pellets were resuspended in 5 ml/g Wash Buffer (50 mM TrisHCl, 1 M NaCl, 20 mM Imidazole, 10 mM MgCl₂, 1 mM DTT, 10% (v/v) glycerol, pH 8.0) and 1,5 mg lysozyme per gram cells was added to the suspension. After resting on ice for 30 min, the cells were cracked by sonication 6-8x for 30 sec, at duty cycle 40% and output control 4. Afterwards, the solution was centrifuged for 20 min at 30.000×g, 4°C, and the lysate was subsequently transferred into 2 ml aliquots and incubated for 15 min at 75°C, 500

rpm, to denature the *E. coli* proteins. After another centrifugation step of 15 min at max. speed (14.800 rpm), RT, the lysate was filtered using a Rotilabo® syringe filter (pore size 0.45 µm) and loaded onto a prepared drop column. One Pierce Centrifuge Column per protein was prepared by washing with several column volumes (cv) of 20% ethanol and loaded with Ni-NTA agarose (stored in 20% ethanol) until each column was filled with approx. 2 ml resin. The columns were then washed with 10 cv double-distilled water (ddH₂O) and equilibrated with 10 cv Wash Buffer. The filtered lysate was loaded into the column and the output was caught and stored in a falcon. To remove unspecifically bound protein, columns were washed with 10 cv Wash Buffer and the flowthrough fraction was caught in a fresh falcon. For elution of the His_{6x}-tagged proteins, columns were subsequently washed with 2 x 2 cv Elution Buffer 1 (WB with 100 mM Imidazole), 4 x 2 cv Elution Buffer 2 (WB with 250mM Imidazole) and 3 x 2 cv Elution Buffer 3 (WB with 500mM Imidazole), while catching each elution fraction in a 2 ml aliquot. Finally, columns were subsequently washed with 10 cv Elution Buffer 3, 10 cv ddH₂O and 10 cv 20% ethanol. Elution fractions were analyzed via SDS-PAGE (section 4.6.5.) and protein concentration was fluorometrically determined (section 4.6.6.). Proteins samples were stored at 4°C for short-term use.

4.6.3 Cell-free *in vitro* protein synthesis

The *S. acidocaldarius* proteins SACI_RS02625 and its Nudix domain-mutant were produced by cell-free protein expression from the plasmids pRSF+SACI_RS02625 and pRSF+SACI_RS02625_E55A_E58A_E59A, respectively, using the NEBExpress® Cell-free *E. coli* Protein Synthesis System. Reactions were set up and conducted and protein was purified with the NEBExpress® Ni Spin Columns according to the instructions of the NEBExpress® Cell-free *E. coli* Protein Synthesis System manual. Briefly, this *in vitro* protein synthesis system is based on *E. coli* S30 extract and enables the production of proteins from the T7 RNA Polymerase and template plasmid or linear DNA as well as mRNA. The *in vitro* synthesized His_{6x}-tagged protein is then cleaned up by affinity purification using the pre-packed Ni Spin Columns and elution fractions are analyzed via SDS-PAGE (section 4.6.5.).

4.6.4 Expression and purification of human NudT5

The plasmid pET28a+hNudT5 (gift of Dr. Katharina Höfer, MPI Marburg) was transformed into the *E. coli* expression strain BL21 (DE3). Cell cultures were grown in LB medium supplied with 30 µg/ml Kanamycin at 37°C, 200 rpm, until OD₆₀₀=0.8. At

this point, cells were induced with 500 mM IPTG, grown for another 3h at 37°C, 200 rpm, and harvested by centrifugation for 30 min at 8000 rpm, 4°C. Pellets were resuspended in 5 ml/g HisTrap buffer A (25 mM Tris-HCl pH 8.0, 150 mM NaCl, 5 mM imidazole, 1 mM DTT), lysed by sonication (5 x 30 sec at 50% power) and the lysate was cleared by centrifugation for 40 min at 14,000 rpm and 4°C. The supernatant was filtered using a syringe-driven filter unit (pore size 0.22 µm) and subsequently applied to a 1ml HisTrap column and the protein was gradually eluted using HisTrap buffer B (HisTrap buffer A with 500 mM imidazole). Elution fractions were analyzed via SDS-PAGE. The peak fraction was then loaded onto a Superose™ 6 Increase 30/100 GL column for further purification via size exclusion chromatography with gel filtration buffer (25 mM Tris-HCl pH 8.0, 150 mM NaCl). Protein samples were stored in 5% (v/v) glycerol at -20°C.

4.6.5 SDS-polyacrylamide gel electrophoresis

Production of recombinant proteins from *E. coli* cells was assessed using SDS-polyacrylamide gel electrophoresis (SDS-PAGE). Samples were mixed with 2X SDS loading dye (150 mM Tris-HCl pH 6.8, 1.2% (w/v) SDS, 0.002% (w/v) bromophenol blue, 30% (v/v) glycerol, 2 M β-mercaptoethanol), boiled for 5 min at 95°C and subsequently loaded onto a polyacrylamide gel comprised of an upper stacking gel (125 mM TrisHCl pH 6.8, 4% (v/v) polyacrylamide (acrylamide/bisacrylamide, ratio 37.5:1), 0.1% (v/v) SDS, 0.1% (v/v) APS, 0.001% (v/v) TEMED) and a lower separating gel (375 mM TrisHCl pH 8.8, 15% (v/v) polyacrylamide, 0.1% (v/v) SDS, 0.1% (v/v) APS und 0.001% (v/v) TEMED). Gels were placed into a Mini-PROTEAN Tetra Cell chamber filled with electrophoresis buffer (25 mM TrisHCl pH 8.0, 0.1% (w/v) SDS, 200 mM glycine) and run for 50 min at 200V. The marker Color Prestained Protein Standard, Broad Range (11 - 245 kDa), was run with all samples to enable molecular weight determination. Gels were subsequently stained using ReadyBlue™ protein staining solution according to the manufacturer's instructions and destained with distilled water to visualize protein bands.

4.6.6 Fluorometric protein quantitation

High-sensitivity quantification of protein samples was performed using the Qubit® 2.0 fluorometer. Sample concentration is determined using a fluorescent dye which emits a signal only when bound to its specific target. Quantitation of protein samples was

performed using the Qubit™ Protein Assay kit and measurements and calibrations were conducted according to the manufacturer's protocol.

4.6.7 Splicing Assays

To assess the activity of the *S. acidocaldarius* tRNA splicing endonuclease on the BHB motif of the permuted variant of its SRP RNA gene, splicing assays were conducted. To this end, 0.3 μ M substrate was incubated with increasing concentrations of protein to achieve different molar ratios as indicated in the figure of the corresponding assay. The two subunits of the tRNA splicing endonuclease (SACI_RS04105 and SACI_RS03165) were cloned into the vector pRSFDuet-1 and heterologously expressed in *E. coli* as described in section 4.6.2. The substrate was a 42 nt-long RNA oligonucleotide with the sequence 5'-GAUUGGCUCCGAAGGAGCA-GUAGUGCUCGGGAGAGCCAAUC-3', designed to form the BHB upon self-hybridization. Here, the sequence corresponds to the sequences of the 5' and 3' intron halves of the permuted SRP RNA gene variant with the addition of a GUAG loop. Additionally, the RNA oligo was fluorescently 5'-labeled using Fluorescein (6-FAM™, excitation at 495 nm, emission at 520 nm) to allow for non-radioactive detection and visualization. Prior to the assay, the RNA was incubated for 5 min at 95°C, followed by cooling down to 4°C, ramp rate 0.2°C/sec, to enable self-hybridization and BHB formation. Hybridized RNA substrate and protein were incubated in 1X splicing assay buffer (40 mM TrisHCl pH 8.0, 2 mM MgCl₂, 1 mM EDTA) for 30 min at 65°C and reactions were stopped by addition of 2X formamide loading dye (95% (v/v) formamide, 0.025% (w/v) bromophenol blue, 0.025% (w/v) xylene cyanol, 5 mM EDTA pH 8.0) and boiling for 5 min at 95°C. Samples were subsequently analysed via denaturing polyacrylamide gel electrophoresis by running on a 10% polyacrylamide gel containing 8.3 M Urea (40% (v/v) Rotiphorese® sequencing gel concentrate, 50% (v/v) Rotiphorese® sequencing gel diluter, 10% (v/v) Rotiphorese® sequencing buffer concentrate, 0.7% APS, 0.07% TEMED) in 1X TBE running buffer (90 mM Tris pH 8.0, 90 mM boric acid, 2 mM EDTA) for 40 min at 200V in a Mini-PROTEAN Tetra Cell chamber. Gels were stained using SYBR™ Gold nucleic acid stain in 1X TBE buffer (1 μ l per 10 ml buffer) and visualized using the BlueFAM (488 nm) laser of a Typhoon Trio Imager located at the Max Planck Institute for Terrestrial Microbiology, Marburg.

4.6.8 Decapping assays

Decapping assays were conducted with the *S. acidocaldarius* Nudix hydrolases SACI_RS00730, Saci_NudT5, SACI_RS02625 and SACI_RS00575 (wild type and Nudix domain-mutant variants), as well as NudC and RppH from *E. coli* and human NudT5. The substrate was a 38 nt-long RNA carrying either NAD, ADPR or Ap4A at its 5' end (Table 4.14). Each reaction contained 15 pmol RNA substrate, 15 pmol of the respective enzyme, 10X NEBuffer™ r3.1 (100 mM NaCl, 50 mM Tris-HCl, 10 mM MgCl₂, 100 µg/ml Recombinant Albumin, pH 7.9) and nuclease-free water up to 5 µl. A no enzyme-control was included for each sample. Reactions were incubated for 5-15 minutes at 65°C (for Nudix enzymes from *S. acidocaldarius*) or 37°C (for NudC, RppH and hNudT5) and stopped by addition of 2X APB loading dye (8 M urea, 10 mM Tris-HCl pH 8.0, 50 mM EDTA, 0.025% (w/v) bromophenol blue, 0.025% (w/v) xylene cyanol). NAD-RNA and ADPR-RNA decapping reactions were resolved on a denaturing APB-PAA gel (8 M urea, 6% polyacrylamide (acrylamide/bisacrylamide, ratio 29:1), 0.2% acryloylaminophenyl boronic acid (APB) in 1X TAE) which were placed in a Mini-PROTEAN Tetra Cell chamber and run in 1X TAE running buffer (40 mM Tris-Acetate, 1 mM EDTA, 20 mM acetic acid pH 8.0) for 35 min at 200 V. Ap4A-RNA decapping reactions were resolved via denaturing PAGE (8 M urea, 10% polyacrylamide (acrylamide/bisacrylamide, ratio 29:1) in 1X TAE) and gels were run according to the aforementioned conditions. To test substrate competition between the Nudix hydrolases, each 20 µM of Saci_NudT5 and another Nudix hydrolase was incubated with 150 ng NAD- or ADPR-RNA substrate in NEBuffer r3.1 for 5 min at 65°C. Reaction were subsequently resolved on denaturing APB-PAA gels as mentioned above. All gels were subsequently stained using SYBR™ Gold and visualized under UV light (254 nm) using a gel documentation system.

4.6.9 Malachite Green Assays

To determine activity and specificity of the recombinant archaeal Nudix hydrolases, phosphate release from different substrates was measured using the Malachite Green Phosphate Assay Kit according to the manufacturer's instructions. Briefly, 1 mM protein (wild-type and Nudix domain-mutant variants) was incubated with 0.125 mM substrate (ATP, dATP, dGTP, ADPR, NAD, Ap4A) in assay buffer (40 mM Tris, 80 mM NaCl, 8 mM MgAc₂, 1 mM EDTA, pH 7.5) for 10 min at 65°C and immediately afterwards frozen at -20°C, typically overnight. Reactions were subsequently thawed, coupling enzyme (0.1 U Inorganic pyrophosphatase (PPase) from *E. coli* for ATP,

dATP and dGTP or 20 U Alkaline Phosphatase (AP) for ADPR, NAD and Ap4A) was added and reactions were incubated for 20 min at 25°C or 37°C for PPase or AP, respectively. Phosphate standards and working reagent were prepared according to the manufacturer's instructions. All reactions, including standards and controls, were transferred into a 96 well-plate and after addition of dye incubated for 30 min at RT. Absorbance at 620 nm was measured in a microplate reader. Phosphate standards were used to plot a standard curve to calculate the amount of phosphate released during the reactions (Supplementary Figures S2 and S3). Substrate in assay buffer was set up as heat control and substrate with coupling enzyme as coupling reaction control. All reactions, controls and standards were run in duplicates and all reagents and assay components were tested for free phosphate prior to the assay. If necessary, background controls were established by assembling reaction components without incubation time and immediate transfer to -20°C.

4.7 Bioinformatical methods

4.7.1 Analysis of Illumina RNA-Seq data

Briefly, raw reads were adapter and quality trimmed using Cutadapt (v2.8) and checked with FASTQC (v0.11.9) (FastQC, 2015). Processed reads (≥ 18 nt) were mapped to the reference genome of *S. acidocaldarius* using Hisat2 (v2.2.1) (Kim et al., 2019). Multiple mapped reads with the exact match score were randomly distributed. After the strand-specific screening, HTSeq (v2.0.2) was used to count gene hits (Anders et al., 2015). Statistical and differential expression analyses were performed with DESeq2 (v1.36.0) (Love et al., 2014). The Integrative Genomics Viewer (IGV, v2.13.2) was used for data inspection (Robinson et al., 2011).

The detection of the circular version of the *S. acidocaldarius* SRP RNA was achieved by searching the expected junction sequence (5'-CCACGTTGACCGGGGAA-CCGGCCAGGCCCGGGAGGGAGCAACCGTGCCCGGCTATCCGCGTTCGTCCGGTCT-3') or for the reverse complement (5'-AGACCGACGAACGCGGATAGCCGGGCACGGTTGCTCCCTCCCGGGCCTGGCCGGTTCGCCCGGTCAACGTGG-3') amongst all obtained reads.

5 References

- Abdelraheim, S. R., Spiller, D. G., & McLennan, A. G. (2003). Mammalian NADH diphosphatases of the Nudix family: Cloning and characterization of the human peroxisomal NUDT12 protein. *Biochemical Journal*, *374*(2), 329–335. <https://doi.org/10.1042/BJ20030441>
- Achsel, T., Stark, H., & Lührmann, R. (2001). The Sm domain is an ancient RNA-binding motif with oligo(U) specificity. *Proceedings of the National Academy of Sciences of the United States of America*, *98*(7), 3685–3689.
- Aittaleb, M., Rashid, R., Chen, Q., Palmer, J. R., Daniels, C. J., & Li, H. (2003). Structure and function of archaeal box C/D sRNP core proteins. *Nature Structural Biology*, *10*(4), 256–263. <https://doi.org/10.1038/nsb905>
- Alm, E. J., Huang, K. H., Price, M. N., Koche, R. P., Keller, K., Dubchak, I. L., & Arkin, A. P. (2005). The MicrobesOnline Web site for comparative genomics. *Genome Research*, *15*(7), 1015–1022. <https://doi.org/10.1101/GR.3844805>
- Anders, S., Pyl, P. T., & Huber, W. (2015). HTSeq—a Python framework to work with high-throughput sequencing data. *Bioinformatics*, *31*(2), 166–169. <https://doi.org/10.1093/BIOINFORMATICS/BTU638>
- Anderson, B. M., & Anderson, C. D. (1963). The effect of buffers on nicotinamide adenine dinucleotide hydrolysis. *The Journal of Biological Chemistry*, *238*(4), 1475–1478. [https://doi.org/10.1016/s0021-9258\(18\)81208-x](https://doi.org/10.1016/s0021-9258(18)81208-x)
- Arimori, T., Tamaoki, H., Nakamura, T., Kamiya, H., Ikemizu, S., Takagi, Y., Ishibashi, T., Harashima, H., Sekiguchi, M., & Yamagata, Y. (2011). Diverse substrate recognition and hydrolysis mechanisms of human NUDT5. *Nucleic Acids Research*, *39*(20), 8972. <https://doi.org/10.1093/NAR/GKR575>
- Baes, R., Lemmens, L., Mignon, K., Carlier, M., & Peeters, E. (2020). Defining heat shock response for the thermoacidophilic model crenarchaeon *Sulfolobus acidocaldarius*. *Extremophiles: Life under Extreme Conditions*, *24*(5), 681–692. <https://doi.org/10.1007/S00792-020-01184-Y>
- Baker, D. L., Youssef, O. A., Chastkofsky, M. I. R., Dy, D. A., Terns, R. M., & Terns, M. P. (2005). RNA-guided RNA modification: functional organization of the archaeal H/ACA RNP. *Genes & Development*, *19*(10), 1238–1248. <https://doi.org/10.1101/gad.1309605>
- Batey, R. T., Rambo, R. P., Lucast, L., Rha, B., & Doudna, J. A. (2000). Crystal structure of the ribonucleoprotein core of the signal recognition particle. *Science (New York, N.Y.)*, *287*(5456), 1232–1239. <https://doi.org/10.1126/SCIENCE.287.5456.1232>
- Baykov, A. A., Evtushenko, O. A., & Avaeva, S. M. (1988). A malachite green procedure for orthophosphate determination and its use in alkaline phosphatase-based enzyme immunoassay. *Analytical Biochemistry*, *171*(2), 266–270. [https://doi.org/10.1016/0003-2697\(88\)90484-8](https://doi.org/10.1016/0003-2697(88)90484-8)
- Becker, H. F., Héliou, A., Djaout, K., Lestini, R., Regnier, M., & Myllykallio, H. (2017). High-throughput sequencing reveals circular substrates for an archaeal RNA ligase. *RNA Biology*, *14*(8), 1075–1085. <https://doi.org/10.1080/15476286.2017.1302640>
- Becker, H. F., L'Hermitte-Stead, C., & Myllykallio, H. (2019). Diversity of circular RNAs and RNA ligases in archaeal cells. *Biochimie*, *164*, 37–44. <https://doi.org/10.1016/j.biochi.2019.06.011>
- Berkner, S., Grogan, D., Albers, S. V., & Lipps, G. (2007). Small multicopy, non-integrative shuttle vectors based on the plasmid pRN1 for *Sulfolobus acidocaldarius* and *Sulfolobus solfataricus*, model organisms of the (cren-)archaea. *Nucleic Acids Research*, *35*(12), 1–12. <https://doi.org/10.1093/nar/gkm449>

- Bessman, M. J. (2019). A cryptic activity in the Nudix hydrolase superfamily. *Protein Science*, 28(8), 1494–1500. <https://doi.org/10.1002/pro.3666>
- Bessman, M. J., Frick, D. N., & O'Handley, S. F. (1996). The MutT proteins or “Nudix” hydrolases, a family of versatile, widely distributed, “housecleaning” enzymes. *Journal of Biological Chemistry*, 271(41), 25059–25062. <https://doi.org/10.1074/jbc.271.41.25059>
- Bhuiyan, S. H., Gowda, K., Hotokezaka, H., & Zwieb, C. (2000). Assembly of archaeal signal recognition particle from recombinant components. *Nucleic Acids Research*, 28(6), 1365–1373. <https://doi.org/10.1093/nar/28.6.1365>
- Bird, J. G., Zhang, Y., Tian, Y., Panova, N., Barvík, I., Greene, L., Liu, M., Buckley, B., Krásný, L., Lee, J. K., Kaplan, C. D., Ebright, R. H., & Nickels, B. E. (2016). The mechanism of RNA 5' capping with NAD⁺, NADH and desphospho-CoA. *Nature*, 535(7612), 444–447. <https://doi.org/10.1038/nature18622>
- Birkedal, U., Beckert, B., Wilson, D. N., & Nielsen, H. (2020). The 23S Ribosomal RNA From *Pyrococcus furiosus* Is Circularly Permuted. *Frontiers in Microbiology*, 11(December). <https://doi.org/10.3389/fmicb.2020.582022>
- Bischof, L. F., Haurat, M. F., Hoffmann, L., Albersmeier, A., Wolf, J., Neu, A., Pham, T. K., Albaum, S. P., Jakobi, T., Schouten, S., Neumann-Schaal, M., Wright, P. C., Kalinowski, J., Siebers, B., & Albers, S. V. (2019). Early response of *Sulfolobus acidocaldarius* to nutrient limitation. *Frontiers in Microbiology*, 10(JAN), 1–17. <https://doi.org/10.3389/fmicb.2018.03201>
- Boccaletto, P., Stefaniak, F., Ray, A., Cappannini, A., Mukherjee, S., Purta, E., Kurkowska, M., Shirvanizadeh, N., Destefanis, E., Groza, P., Avşar, G., Romitelli, A., Pir, P., Dassi, E., Conticello, S. G., Aguilo, F., & Bujnicki, J. M. (2022). MODOMICS: a database of RNA modification pathways. 2021 update. *Nucleic Acids Research*, 50(D1), D231. <https://doi.org/10.1093/NAR/GKAB1083>
- Brinkman, A. B., Bell, S. D., Lebbink, R. J., De Vos, W. M., & Der Van Oost, J. (2002). The *Sulfolobus solfataricus* Lrp-like protein LysM regulates lysine biosynthesis in response to lysine availability. *Journal of Biological Chemistry*, 277(33), 29537–29549. <https://doi.org/10.1074/jbc.M203528200>
- Brock, T. D., Brock, K. M., Belly, R. T., & Weiss, R. L. (1972). *Sulfolobus*: A new genus of sulfur-oxidizing bacteria living at low pH and high temperature. *Archiv Für Mikrobiologie*, 84(1), 54–68. <https://doi.org/10.1007/BF00408082>
- Cahová, H., Winz, M. L., Höfer, K., Nübel, G., & Jäschke, A. (2015). NAD captureSeq indicates NAD as a bacterial cap for a subset of regulatory RNAs. *Nature*, 519(7543), 374–377. <https://doi.org/10.1038/nature14020>
- Calvin, K., Hall, M. D., Xu, F., Xue, S., & Li, H. (2005). Structural characterization of the catalytic subunit of a novel RNA splicing endonuclease. *Journal of Molecular Biology*, 353(5), 952–960. <https://doi.org/10.1016/j.jmb.2005.09.035>
- Carter, M., Jemth, A. S., Hagenkört, A., Page, B. D. G., Gustafsson, R., Griese, J. J., Gad, H., Valerie, N. C. K., Desroses, M., Boström, J., Warpman Berglund, U., Helleday, T., & Stenmark, P. (2015). Crystal structure, biochemical and cellular activities demonstrate separate functions of MTH1 and MTH2. *Nature Communications*, 6, 4–13. <https://doi.org/10.1038/ncomms8871>
- Cervantes-Laurean, D., Jacobson, E. L., & Jacobson, M. K. (1996). Glycation and glycooxidation of histones by ADP-ribose. *Journal of Biological Chemistry*, 271(18), 10461–10469. <https://doi.org/10.1074/jbc.271.18.10461>
- Chan, P. P., & Lowe, T. M. (2009). GtRNAdb: a database of transfer RNA genes detected in genomic

- sequence. *Nucleic Acids Research*, 37(Database issue), D93.
<https://doi.org/10.1093/NAR/GKN787>
- Chang, J. H., Jiao, X., Chiba, K., Oh, C., Martin, C. E., Kiledjian, M., & Tong, L. (2012). Dxo1 is a new type of eukaryotic enzyme with both decapping and 5'-3' exoribonuclease activity. *Nature Structural & Molecular Biology*, 19(10), 1011–1017. <https://doi.org/10.1038/nsmb.2381>
- Charpentier, B., Muller, S., & Branlant, C. (2005). Reconstitution of archaeal H/ACA small ribonucleoprotein complexes active in pseudouridylation. *Nucleic Acids Research*, 33(10), 3133–3144. <https://doi.org/10.1093/nar/gki630>
- Chauhan, S. M., Poudel, S., Rychel, K., Lamoureux, C., Yoo, R., Al Bulushi, T., Yuan, Y., Palsson, B. O., & Sastry, A. V. (2021). Machine Learning Uncovers a Data-Driven Transcriptional Regulatory Network for the Crenarchaeal Thermoacidophile *Sulfolobus acidocaldarius*. *Frontiers in Microbiology*, 12. <https://doi.org/10.3389/fmicb.2021.753521>
- Chen, R., Wang, S. K., Belk, J. A., Amaya, L., Li, Z., Cardenas, A., Abe, B. T., Chen, C. K., Wender, P. A., & Chang, H. Y. (2022). Engineering circular RNA for enhanced protein production. *Nature Biotechnology* 2022, 1–11. <https://doi.org/10.1038/s41587-022-01393-0>
- Chen, Y. G., Kowtoniuk, W. E., Agarwal, I., Shen, Y., & Liu, D. R. (2009). LC/MS analysis of cellular RNA reveals NAD-linked RNA. *Nature Chemical Biology*, 5(12), 879–881.
<https://doi.org/10.1038/nchembio.235>
- Ciammaruconi, A., & Londei, P. (2001). *In Vitro* Processing of the 16S rRNA of the Thermophilic Archaeon *Sulfolobus solfataricus*. *Journal of Bacteriology*, 183(13), 3866.
<https://doi.org/10.1128/JB.183.13.3866-3874.2001>
- Contursi, P., Fusco, S., Limauro, D., & Fiorentino, G. (2013). Host and viral transcriptional regulators in *Sulfolobus*: An overview. *Extremophiles*, 17(6), 881–895. <https://doi.org/10.1007/s00792-013-0586-9>
- Danan, M., Schwartz, S., Edelheit, S., & Sorek, R. (2012). Transcriptome-wide discovery of circular RNAs in Archaea. *Nucleic Acids Research*, 40(7), 3131–3142.
<https://doi.org/10.1093/nar/gkr1009>
- Daume, M. (2017). *L7Ae- and LSm-RNA interactomes of Sulfolobus acidocaldarius* (Dissertation).
- Daume, M., Uhl, M., Backofen, R., & Randau, L. (2017). RIP-Seq Suggests Translational Regulation by L7Ae in Archaea. *MBio*, 8(4), 1–14.
- Deana, A., Celesnik, H., & Belasco, J. G. (2008). The bacterial enzyme RppH triggers messenger RNA degradation by 5' pyrophosphate removal. *Nature*, 451(7176), 355–358.
<https://doi.org/10.1038/nature06475>
- Decatur, W. A., & Fournier, M. J. (2002). rRNA modifications and ribosome function. *Trends in Biochemical Sciences*, 27(7), 344–351. [https://doi.org/10.1016/S0968-0004\(02\)02109-6](https://doi.org/10.1016/S0968-0004(02)02109-6)
- Dennis, P. P., & Omer, A. (2005). Small non-coding RNAs in Archaea. *Current Opinion in Microbiology*, 8(6), 685–694. <https://doi.org/10.1016/J.MIB.2005.10.013>
- Dennis, P. P., Tripp, V., Lui, L., Lowe, T., & Randau, L. (2015). C/D box sRNA-guided 2'-O-methylation patterns of archaeal rRNA molecules. *BMC Genomics*, 16(1), 1–12.
<https://doi.org/10.1186/s12864-015-1839-z>
- Doamekpor, S. K., Sharma, S., Kiledjian, M., & Tong, L. (2022). Recent insights into noncanonical 5' capping and decapping of RNA. *Journal of Biological Chemistry*, 298(8), 102171.
<https://doi.org/10.1016/j.jbc.2022.102171>

- Dunckley, T., & Parker, R. (1999). The DCP2 protein is required for mRNA decapping in *Saccharomyces cerevisiae* and contains a functional MutT motif. *EMBO Journal*, *18*(19), 5411–5422. <https://doi.org/10.1093/emboj/18.19.5411>
- Dunn, C. A., O'Handley, S. F., Frick, D. N., & Bessman, M. J. (1999). Studies on the ADP-ribose pyrophosphatase subfamily of the Nudix hydrolases and tentative identification of *trgB*, a gene associated with tellurite resistance. *Journal of Biological Chemistry*, *274*(45), 32318–32324. <https://doi.org/10.1074/jbc.274.45.32318>
- Duong-Ly, K. C., Gabelli, S. B., Xu, W. L., Dunn, C. A., Schoeffield, A. J., Bessman, M. J., & Amzel, L. M. (2011). The Nudix hydrolase CDP-chase, a CDP-choline pyrophosphatase, is an asymmetric dimer with two distinct enzymatic activities. *Journal of Bacteriology*, *193*(13), 3175–3185. <https://doi.org/10.1128/JB.00089-11>
- Englert, M., Sheppard, K., Aslanian, A., Yates, J. R., & Söll, D. (2011). Archaeal 3'-phosphate RNA splicing ligase characterization identifies the missing component in tRNA maturation. *Proceedings of the National Academy of Sciences of the United States of America*, *108*(4), 1290–1295. <https://doi.org/10.1073/pnas.1018307108>
- FastQC. (2015). Available Online at <https://qubeshub.org/resources/fastqc>.
- Ferguson, F., McLennan, A. G., Urbaniak, M. D., Jones, N. J., & Copeland, N. A. (2020). Re-evaluation of Diadenosine Tetraphosphate (Ap4A) From a Stress Metabolite to Bona Fide Secondary Messenger. *Frontiers in Molecular Biosciences*, *7*, 332. <https://doi.org/10.3389/FMOLB.2020.606807/BIBTEX>
- Fischer, S., Benz, J., Späth, B., Maier, L. K., Straub, J., Granzow, M., Raabe, M., Urlaub, H., Hoffmann, J., Brutschy, B., Allers, T., Soppa, J., & Marchfelder, A. (2010). The archaeal Ism protein binds to small RNAs. *Journal of Biological Chemistry*, *285*(45), 34429–34438. <https://doi.org/10.1074/jbc.M110.118950>
- Frick, D. N., & Bessman, M. J. (1995). Cloning, purification, and properties of a novel NADH pyrophosphatase. Evidence for a nucleotide pyrophosphatase catalytic domain in MutT-like enzymes. *The Journal of Biological Chemistry*, *270*(4), 1529–1534. <https://doi.org/10.1074/JBC.270.4.1529>
- Frindert, J., Zhang, Y., Nübel, G., Kahloon, M., Kolmar, L., Hotz-Wagenblatt, A., Burhenne, J., Haefeli, W. E., & Jäschke, A. (2018). Identification, Biosynthesis, and Decapping of NAD-Capped RNAs in *B. subtilis*. *Cell Reports*, *24*(7), 1890-1901.e8. <https://doi.org/10.1016/j.celrep.2018.07.047>
- Fujishima, K., Sugahara, J., Miller, C. S., Baker, B. J., Di Giulio, M., Takesue, K., Sato, A., Tomita, M., Banfield, J. F., & Kanai, A. (2011). A novel three-unit tRNA splicing endonuclease found in ultrasmall Archaea possesses broad substrate specificity. *Nucleic Acids Research*, *39*(22), 9695. <https://doi.org/10.1093/NAR/GKR692>
- Furuichi, Y., Morgan, M., Muthukrishnan, S., & Shatkin, A. J. (1975). Reovirus messenger RNA contains a methylated, blocked 5'-terminal structure: m-7G(5')ppp(5')G-MpCp-. *Proceedings of the National Academy of Sciences of the United States of America*, *72*(1), 362–366. <https://doi.org/10.1073/PNAS.72.1.362>
- Furuichi, Yasuhiro, LaFiandra, A., & Shatkin, A. J. (1977). 5'-Terminal structure and mRNA stability. *Nature*, *266*(5599), 235–239. <https://doi.org/10.1038/266235a0>
- Gabelli, S. B., Bianchet, M. A., Xu, W. L., Dunn, C. A., Niu, Z. D., Amzel, L. M., & Bessman, M. J. (2007). Structure and Function of the *E. coli* Dihydroneopterin Triphosphate Pyrophosphatase: A Nudix Enzyme Involved in Folate Biosynthesis. *Structure*, *15*(8), 1014–1022.

<https://doi.org/10.1016/J.STR.2007.06.018>

- Ganot, P., Bortolin, M.-L., & Kiss, T. (1997). Site-Specific Pseudouridine Formation in Preribosomal RNA Is Guided by Small Nucleolar RNAs. *Cell*, *89*(5), 799–809. [https://doi.org/10.1016/S0092-8674\(00\)80263-9](https://doi.org/10.1016/S0092-8674(00)80263-9)
- Gaspin, C., Cavallé, J., Erauso, G., & Bachellerie, J.-P. (2000). Archaeal homologs of eukaryotic methylation guide small nucleolar RNAs: lessons from the *Pyrococcus* genomes. *Journal of Molecular Biology*, *297*(4), 895–906. <https://doi.org/10.1006/JMBI.2000.3593>
- Gibson, D. G., Young, L., Chuang, R., Venter, J. C., Hutchison, C. A., & Smith, H. O. (2009). Enzymatic assembly of DNA molecules up to several hundred kilobases. *Nature Methods*, *6*(5), 343–345. <https://doi.org/10.1038/nmeth.1318>
- Gomes-Filho, J. V., Daume, M., & Randau, L. (2018). Unique Archaeal Small RNAs. *Annual Review of Genetics*, *52*(1), 465–487. <https://doi.org/10.1146/annurev-genet-120417-031300>
- Grogan, D. W. (2003). Cytosine methylation by the SuaI restriction-modification system: implications for genetic fidelity in a hyperthermophilic archaeon. *Journal of Bacteriology*, *185*(15), 4657–4661. <https://doi.org/10.1128/JB.185.15.4657-4661.2003>
- Grudzien-Nogalska, E., Wu, Y., Jiao, X., Cui, H., Mateyak, M. K., Hart, R. P., Tong, L., & Kiledjian, M. (2019). Structural and mechanistic basis of mammalian Nudt12 RNA deNADding. *Nature Chemical Biology*, *15*(6), 575–582. <https://doi.org/10.1038/s41589-019-0293-7>
- Gu, H., Yoshinari, S., Ghosh, R., Ignatichkina, A. V., Gollnick, P. D., Murakami, K. S., & Ho, C. K. (2016). Structural and mutational analysis of archaeal ATP-dependent RNA ligase identifies amino acids required for RNA binding and catalysis. *Nucleic Acids Research*, *44*(5), 2337–2347. <https://doi.org/10.1093/nar/gkw094>
- Gundelfinger, E. D., Krause, E., Melli, M., & Dobberstein, B. (1983). The organization of the 7SL RNA in the signal recognition particle. *Nucleic Acids Research*, *11*(21), 7363–7374.
- Guy, L., & Ettema, T. J. G. (2011). The archaeal ‘TACK’ superphylum and the origin of eukaryotes. *Trends in Microbiology*, *19*(12), 580–587. <https://doi.org/10.1016/J.TIM.2011.09.002>
- Hachisuka, Shin-ichi, Sato, T., & Atomi, H. (2017). Metabolism Dealing with Thermal Degradation of NAD⁺ in the Hyperthermophilic Archaeon *Thermococcus kodakarensis*. *Journal of Bacteriology*, *199*(19), 1–14. <https://doi.org/https://doi.org/10.1128/JB.00162-17>.
- Hachisuka, Shin ichi, Sato, T., & Atomi, H. (2018). Hyperthermophilic archaeon *Thermococcus kodakarensis* utilizes a four-step pathway for NAD⁺ salvage through nicotinamide deamination. *Journal of Bacteriology*, *200*(11). <https://doi.org/10.1128/JB.00785-17>
- Hainzl, T., Huang, S., & Sauer-Eriksson, A. E. (2002). Structure of the SRP19–RNA complex and implications for signalrecognition particle assembly. *Nature*, *417*(6890), 767–771. <https://doi.org/10.1038/nature00768>
- Hanahan, D. (1983). Studies on transformation of *Escherichia coli* with plasmids. *Journal of Molecular Biology*, *166*(4), 557–580. [https://doi.org/10.1016/S0022-2836\(83\)80284-8](https://doi.org/10.1016/S0022-2836(83)80284-8)
- Helm, M., & Alfonzo, J. D. (2014). Post-transcriptional RNA modifications: Playing metabolic games in a cell’s chemical legoland. *Chemistry & Biology*, *21*(2), 174. <https://doi.org/10.1016/J.CHEMBIOL.2013.10.015>
- Hendrickson, E. L., Liu, Y., Rosas-Sandoval, G., Porat, I., Söll, D., Whitman, W. B., & Leigh, J. A. (2008). Global responses of *Methanococcus maripaludis* to specific nutrient limitations and growth rate. *Journal of Bacteriology*, *190*(6), 2198–2205. <https://doi.org/10.1128/JB.01805-07>

- Hirata, A., Kitajima, T., & Hori, H. (2011). Cleavage of intron from the standard or non-standard position of the precursor tRNA by the splicing endonuclease of *Aeropyrum pernix*, a hyperthermophilic Crenarchaeon, involves a novel RNA recognition site in the Crenarchaea specific loop. *Nucleic Acids Research*, *39*(21), 9376–9389. <https://doi.org/10.1093/nar/gkr615>
- Ho, S. N., Hunt, H. D., Horton, R. M., Pullen, J. K., & Pease, L. R. (1989). Site-directed mutagenesis by overlap extension using the polymerase chain reaction. *Gene*, *77*(1), 51–59. [https://doi.org/10.1016/0378-1119\(89\)90358-2](https://doi.org/10.1016/0378-1119(89)90358-2)
- Höfer, K., & Jäschke, A. (2018). Epitranscriptomics: RNA Modifications in Bacteria and Archaea. *Microbiology Spectrum*, *6*(3). <https://doi.org/10.1128/microbiolspec.RWR-0015-2017>
- Höfer, K., Li, S., Abele, F., Frindert, J., Schlotthauer, J., Grawenhoff, J., Du, J., Patel, D. J., & Jäschke, A. (2016). Structure and function of the bacterial decapping enzyme NudC. *Nature Chemical Biology*, *12*(9), 730–734. <https://doi.org/10.1038/nchembio.2132>
- Hori, M., Fujikawa, K., Kasai, H., Harashima, H., & Kamiya, H. (2005). Dual hydrolysis of diphosphate and triphosphate derivatives of oxidized deoxyadenosine by Orf17 (NtpA), a MutT-type enzyme. *DNA Repair*, *4*(1), 33–39. <https://doi.org/10.1016/J.DNAREP.2004.07.010>
- Hudeček, O., Benoni, R., Reyes-Gutierrez, P. E., Culka, M., Šanderová, H., Hubálek, M., Rulíšek, L., Cvačka, J., Krásný, L., & Cahová, H. (2020). Dinucleoside polyphosphates act as 5'-RNA caps in bacteria. *Nature Communications*, *11*(1). <https://doi.org/10.1038/s41467-020-14896-8>
- Inoue, H., Nojima, H., & Okayama, H. (1990). High efficiency transformation of *Escherichia coli* with plasmids. *Gene*, *96*(1), 23–28. [https://doi.org/10.1016/0378-1119\(90\)90336-P](https://doi.org/10.1016/0378-1119(90)90336-P)
- Ishibashi, T., Hayakawa, H., & Sekiguchi, M. (2003). A novel mechanism for preventing mutations caused by oxidation of guanine nucleotides. *EMBO Reports*, *4*(5), 479–483. <https://doi.org/10.1038/SJ.EMBOR.EMBOR838>
- Ito, R., Sekiguchi, M., Setoyama, D., Nakatsu, Y., Yamagata, Y., & Hayakawa, H. (2011). Cleavage of oxidized guanine nucleotide and ADP sugar by human NUDT5 protein. *The Journal of Biochemistry*, *149*(6), 731–738. <https://doi.org/10.1093/JB/MVR028>
- J. Sambrook, E. F. Fritsch, & T. Maniatis. (1989). Molecular Cloning. A Laboratory Manual. In *Biologie in unserer Zeit* (2nd ed., Issue 6). Cold Spring Harbor Laboratory Press. <https://onlinelibrary.wiley.com/doi/10.1002/biuz.19900200607>
- Jacobson, E. L., Cervantes-Laurean, D., & Jacobson, M. K. (1994). Glycation of proteins by ADP-ribose. In *ADP-Ribosylation: Metabolic Effects and Regulatory Functions* (pp. 207–212). Springer US. https://doi.org/10.1007/978-1-4615-2614-8_27
- Jiao, X., Chang, J. H., Kilic, T., Tong, L., & Kiledjian, M. (2013). A Mammalian Pre-mRNA 5' End Capping Quality Control Mechanism and an Unexpected Link of Capping to Pre-mRNA Processing. *Molecular Cell*, *50*(1), 104–115. <https://doi.org/10.1016/J.MOLCEL.2013.02.017>
- Jiao, X., Doamekpor, S. K., Bird, J. G., Nickels, B. E., Tong, L., Hart, R. P., & Kiledjian, M. (2017). 5' End Nicotinamide Adenine Dinucleotide Cap in Human Cells Promotes RNA Decay through DXO-Mediated deNADding. *Cell*, *168*(6), 1015–1027.e10. <https://doi.org/10.1016/J.CELL.2017.02.019>
- Jiao, X., Xiang, S., Oh, C., Martin, C. E., Tong, L., & Kiledjian, M. (2010). Identification of a quality-control mechanism for mRNA 5'-end capping. *Nature*, *467*(7315), 608–611. <https://doi.org/10.1038/nature09338>
- Julius, C., & Yuzenkova, Y. (2017). Bacterial RNA polymerase caps RNA with various cofactors and cell wall precursors. *Nucleic Acids Research*, *45*(14), 8282–8290.

<https://doi.org/10.1093/nar/gkx452>

- Jumper, J., Evans, R., Pritzel, A., Green, T., Figurnov, M., Ronneberger, O., Tunyasuvunakool, K., Bates, R., Žídek, A., Potapenko, A., Bridgland, A., Meyer, C., Kohl, S. A. A., Ballard, A. J., Cowie, A., Romera-Paredes, B., Nikolov, S., Jain, R., Adler, J., Back, T., Petersen, S., Reiman, D., Clancy, E., Zielinski, M., Steinegger, M., Pacholska, M., Berghammer, T., Bodenstein, S., Silver, D., Vinyals, O., Senior, A. W., Kavukcuoglu, K., Kohli, P., Hassabis, D. (2021). Highly accurate protein structure prediction with AlphaFold. *Nature* 2021 596:7873, 596(7873), 583–589. <https://doi.org/10.1038/s41586-021-03819-2>
- Jüttner, M., Weiß, M., Ostheimer, N., Reglin, C., Kern, M., Knüppel, R., & Ferreira-Cerca, S. (2020). A versatile cis-acting element reporter system to study the function, maturation and stability of ribosomal RNA mutants in archaea. *Nucleic Acids Research*, 48(4), 2073–2090. <https://doi.org/10.1093/nar/gkz1156>
- Kaine, B. P. (1987). Intron-containing tRNA genes of *Sulfolobus solfataricus*. *Journal of Molecular Evolution*, 25(3), 248–254. <https://doi.org/10.1007/BF02100018>
- Kaine, B. P., Gupta, R., & Woese, C. R. (1983). Putative introns in tRNA genes of prokaryotes. *Proceedings of the National Academy of Sciences of the United States of America*, 80(11), 3309–3312. <https://doi.org/10.1073/PNAS.80.11.3309>
- Kaplan, N. O., Colowick, S. P., & Barnes, C. C. (1951). Effect of alkali on diphosphopyridine nucleotide. *The Journal of Biological Chemistry*, 191(2), 461–472. [https://doi.org/10.1016/s0021-9258\(18\)55951-2](https://doi.org/10.1016/s0021-9258(18)55951-2)
- Karijolich, J., & Yu, Y. T. (2011). Converting nonsense codons into sense codons by targeted pseudouridylation. *Nature* 2011 474:7351, 474(7351), 395–398. <https://doi.org/10.1038/nature10165>
- Kashefi, K., & Lovley, D. R. (2003). Extending the upper temperature limit for life. *Science*, 301(5635), 934. <https://doi.org/10.1126/science.1086823>
- Kierzek, E., Malgowska, M., Lisowiec, J., Turner, D. H., Gdaniec, Z., & Kierzek, R. (2014). The contribution of pseudouridine to stabilities and structure of RNAs. *Nucleic Acids Research*, 42(5), 3492–3501. <https://doi.org/10.1093/nar/gkt1330>
- Kiledjian, M. (2018). Eukaryotic RNA 5'-end NAD⁺ Capping and deNADding. *Trends in Cell Biology*, 28(5). <https://doi.org/10.1016/j.physbeh.2017.03.040>
- Kim, D., Paggi, J. M., Park, C., Bennett, C., & Salzberg, S. L. (2019). Graph-based genome alignment and genotyping with HISAT2 and HISAT-genotype. *Nature Biotechnology*, 37(8), 907–915. <https://doi.org/10.1038/S41587-019-0201-4>
- Kiss-László, Z., Henry, Y., Bachelierie, J.-P., Caizergues-Ferrer, M., & Kiss, T. (1996). Site-Specific Ribose Methylation of Preribosomal RNA: A Novel Function for Small Nucleolar RNAs. *Cell*, 85(7), 1077–1088. [https://doi.org/10.1016/S0092-8674\(00\)81308-2](https://doi.org/10.1016/S0092-8674(00)81308-2)
- Kiss-Laszlo, Z., Henry, Y. H., & Kiss, T. (1998). Sequence and structural elements of methylation guide snoRNAs essential for site-specific ribose methylation of pre-rRNA. *The EMBO Journal*, 17(3), 797–807. <https://doi.org/10.1093/emboj/17.3.797>
- Klein, R. J., Misulovin, Z., & Eddy, S. R. (2002). Noncoding RNA genes identified in AT-rich hyperthermophiles. *Proceedings of the National Academy of Sciences of the United States of America*, 99(11), 7542–7547.
- Komorowski, L., Verheyen, W., & Schäfer, G. (2002). The archaeal respiratory supercomplex SoxM from *S. acidocaldarius* combines features of quinole and cytochrome c oxidases. *Biological*

- Chemistry*, 383(11), 1791–1799. <https://doi.org/10.1515/BC.2002.200>
- Kowtoniuk, W. E., Shen, Y., Heemstra, J. M., Agarwal, I., & Liu, D. R. (2009). A chemical screen for biological small molecule-RNA conjugates reveals CoA-linked RNA. *Proceedings of the National Academy of Sciences of the United States of America*, 106(19), 7768–7773. <https://doi.org/10.1073/pnas.0900528106>
- Kuhn, J. F., Tran, E. J., & Maxwell, E. S. (2002). Archaeal ribosomal protein L7 is a functional homolog of the eukaryotic 15.5kD/Snu13p snoRNP core protein. *Nucleic Acids Research*, 30(4), 931–941. <https://doi.org/10.1093/nar/30.4.931>
- Lai, S. M., Lai, L. B., Foster, M. P., & Gopalan, V. (2014). The L7Ae protein binds to two kink-turns in the *Pyrococcus furiosus* RNase P RNA. *Nucleic Acids Research*, 42(21), 13328–13338. <https://doi.org/10.1093/NAR/GKU994>
- Lassak, K., Peeters, E., Wróbel, S., & Albers, S. (2013). The one-component system ArnR : a membrane-bound activator of the crenarchaeal archaeellum. *Molecular Microbiology*, 88(March), 125–139. <https://doi.org/10.1111/mmi.12173>
- Lemmens, L., Tilleman, L., De Koning, E., Valegård, K., Lindås, A. C., Van Nieuwerburgh, F., Maes, D., & Peeters, E. (2019). YtrASa, a GntR-Family Transcription Factor, Represses Two Genetic Loci Encoding Membrane Proteins in *Sulfolobus acidocaldarius*. *Frontiers in Microbiology*, 10, 2084. <https://doi.org/10.3389/fmicb.2019.02084>
- Li, H., & Abelson, J. (2000). Crystal structure of a dimeric archaeal splicing endonuclease. *Journal of Molecular Biology*, 302(3), 639–648. <https://doi.org/10.1006/JMBI.2000.3941>
- Li, H., Trotta, C. R., & Abelson, J. (1998). Crystal structure and evolution of a transfer RNA splicing enzyme. *Science*, 280(5361), 279–284.
- Li, Yingjun, Pan, S., Zhang, Y., Ren, M., Feng, M., Peng, N., Chen, L., Liang, Y. X., & She, Q. (2016). Harnessing Type I and Type III CRISPR-Cas systems for genome editing. *Nucleic Acids Research*, 44(4), 1–12. <https://doi.org/10.1093/nar/gkv1044>
- Li, You, Song, M., & Kiledjian, M. (2011). Differential utilization of decapping enzymes in mammalian mRNA decay pathways. *RNA*, 17(3), 419–428. <https://doi.org/10.1261/rna.2439811>
- Liang, X.-H., Liu, Q., & Fournier, M. J. (2009). Loss of rRNA modifications in the decoding center of the ribosome impairs translation and strongly delays pre-rRNA processing. *RNA*, 15(9), 1716–1728. <https://doi.org/10.1261/rna.1724409>
- Litke, J. L., & Jaffrey, S. R. (2019). Highly efficient expression of circular RNA aptamers in cells using autocatalytic transcripts. *Nature Biotechnology*, 37(6), 667. <https://doi.org/10.1038/S41587-019-0090-6>
- Lorenz, C., Lünse, C. E., & Mörl, M. (2017). tRNA Modifications: Impact on Structure and Thermal Adaptation. *Biomolecules*, 7(2). <https://doi.org/10.3390/BIOM7020035>
- Love, M. I., Huber, W., & Anders, S. (2014). Moderated estimation of fold change and dispersion for RNA-seq data with DESeq2. *Genome Biology*, 15(12), 1–21. <https://doi.org/10.1186/s13059-014-0550-8>
- Luciano, D. J., Levenson-Palmer, R., & Belasco, J. G. (2019). Stresses that Raise Np4A Levels Induce Protective Nucleoside Tetraphosphate Capping of Bacterial RNA. *Molecular Cell*, 75(5), 957-966.e8. <https://doi.org/10.1016/j.molcel.2019.05.031>
- Lykke-Andersen, J. (2002). Identification of a Human Decapping Complex Associated with hUpf Proteins in Nonsense-Mediated Decay. *Molecular and Cellular Biology*, 22(23), 8114–8121.

<https://doi.org/10.1128/mcb.22.23.8114-8121.2002>

- Lykke-Andersen, Jens, & Garrett, R. A. (1997). RNA–protein interactions of an archaeal homotetrameric splicing endoribonuclease with an exceptional evolutionary history. *The EMBO Journal*, *16*(20), 6290–6300. <https://doi.org/10.1093/EMBOJ/16.20.6290>
- Maezato, Y., Daugherty, A., Dana, K., Soo, E., Cooper, C., Tachdjian, S., Kelly, R. M., & Blum, P. (2011). VapC6, a ribonucleolytic toxin regulates thermophilicity in the crenarchaeote *Sulfolobus solfataricus*. *RNA*, *17*(7), 1381. <https://doi.org/10.1261/RNA.2679911>
- Makarova, K. S., Wolf, Y. I., & Koonin, E. V. (2015). Archaeal Clusters of Orthologous Genes (arCOGs): An Update and Application for Analysis of Shared Features between Thermococcales, Methanococcales, and Methanobacteriales. *Life*, *5*(1), 818. <https://doi.org/10.3390/LIFE5010818>
- Malygin, A. G., Shemyakin, M. F., & Shemakin, M. M. (1979). Adenosine, NAD and FAD can initiate template-dependent RNA synthesis catalyzed by *Escherichia coli* RNA Polymerase. *FEBS Letters*, *102*(1), 51–54.
- Marck, C., & Grosjean, H. (2003). Identification of BHB splicing motifs in intron-containing tRNAs from 18 archaea: Evolutionary implications. *Rna*, *9*(12), 1516–1531. <https://doi.org/10.1261/rna.5132503>
- Märtens, B., Hou, L., Amman, F., Wolfinger, M. T., Evguenieva-Hackenberg, E., & Bi Asi, U. (2017). The SmAP1/2 proteins of the crenarchaeon *Sulfolobus solfataricus* interact with the exosome and stimulate A-rich tailing of transcripts. *Nucleic Acids Research*, *45*(13), 7938–7949. <https://doi.org/10.1093/nar/gkx437>
- Märtens, B., Sharma, K., Urlaub, H., & Bläsi, U. (2017). The SmAP2 RNA binding motif in the 3'UTR affects mRNA stability in the crenarchaeum *Sulfolobus solfataricus*. *Nucleic Acids Research*, *45*(15), 8957–8967. <https://doi.org/10.1093/NAR/GKX581>
- McLennan, A. G. (2006). The Nudix hydrolase superfamily. *Cellular and Molecular Life Sciences*, *63*(2), 123–143. <https://doi.org/10.1007/s00018-005-5386-7>
- McLennan, Alexander G. (2013). Substrate ambiguity among the nudix hydrolases: biologically significant, evolutionary remnant, or both? *Cellular and Molecular Life Sciences*, *70*(3), 373–385. <https://doi.org/10.1007/s00018-012-1210-3>
- Miralles, F. (2010). Compositional properties and thermal adaptation of SRP-RNA in bacteria and archaea. *Journal of Molecular Evolution*, *70*(2), 181–189. <https://doi.org/10.1007/s00239-009-9319-1>
- Mitchell, M., Xue, S., Erdman, R., Randau, L., Söll, D., & Li, H. (2009). Crystal structure and assembly of the functional *Nanoarchaeum equitans* tRNA splicing endonuclease. *Nucleic Acids Research*, *37*(17), 5793. <https://doi.org/10.1093/NAR/GKP537>
- Mukhopadhyay, B., Johnson, E. F., & Wolfe, R. S. (2000). A novel P(H2) control on the expression of flagella in the hyperthermophilic strictly hydrogenotrophic methanarchaeon *Methanococcus jannaschii*. *Proceedings of the National Academy of Sciences of the United States of America*, *97*(21), 11522–11527. <https://doi.org/10.1073/pnas.97.21.11522>
- Mullis, K., Faloona, F., Scharf, S., Saiki, R., Horn, G., & Erlich, H. (1986). Specific enzymatic amplification of DNA in vitro: The polymerase chain reaction. *Cold Spring Harbor Symposia on Quantitative Biology*, *51*(1), 263–273. <https://doi.org/10.1101/sqb.1986.051.01.032>
- Munir, A., Banerjee, A., & Shuman, S. (2018). NAD⁺-dependent synthesis of a 5'-phospho-ADP-ribosylated RNA/DNA cap by RNA 2'-phosphotransferase Tpt1. *Nucleic Acids Research*, *46*(18),

- 9617–9624. <https://doi.org/10.1093/NAR/GKY792>
- Munnur, D., Bartlett, E., Mikočević, P., Kirby, I. T., Rack, J. G. M., Mikoč, A., Cohen, M. S., & Ahel, I. (2019). Reversible ADP-ribosylation of RNA. *Nucleic Acids Research*, *47*(11), 5658–5669. <https://doi.org/10.1093/NAR/GKZ305>
- Ni, J., Tien, A. L., & Fournier, M. J. (1997). Small Nucleolar RNAs Direct Site-Specific Synthesis of Pseudouridine in Ribosomal RNA. *Cell*, *89*(4), 565–573. [https://doi.org/10.1016/S0092-8674\(00\)80238-X](https://doi.org/10.1016/S0092-8674(00)80238-X)
- Noon, K. R., Bruenger, E., & McCloskey, J. A. (1998). Posttranscriptional modifications in 16S and 23S rRNAs of the archaeal hyperthermophile *Sulfolobus solfataricus*. *Journal of Bacteriology*, *180*(11), 2883–2888. <https://doi.org/10.1128/jb.180.11.2883-2888.1998>
- Nübel, G., Sorgenfrei, F. A., & Jäschke, A. (2017). Boronate affinity electrophoresis for the purification and analysis of cofactor-modified RNAs. *Methods*, *117*, 14–20. <https://doi.org/10.1016/j.ymeth.2016.09.008>
- Ofengand, J., & Bakin, A. (1997). Mapping to nucleotide resolution of pseudouridine residues in large subunit ribosomal RNAs from representative eukaryotes, prokaryotes, archaeobacteria, mitochondria and chloroplasts. *Journal of Molecular Biology*, *266*(2), 246–268. <https://doi.org/10.1006/JMBI.1996.0737>
- Omer, A. D., Lowe, T. M., Russell, A. C., Ehardt, H., Eddy, S. R., & Dennis, P. P. (2000). Homologs of small nucleolar RNAs in Archaea. *Science*, *288*(5465), 517–522. <https://doi.org/10.1126/science.288.5465.517>
- Omer, A. D., Ziesche, S., Ehardt, H. A., & Dennis, P. P. (2002). *In vitro* reconstitution and activity of a C/D box methylation guide ribonucleoprotein complex. *Proceedings of the National Academy of Sciences of the United States of America*, *99*(8), 5289–5294. <https://doi.org/10.1073/pnas.082101999>
- Ouchi, T., Tomita, T., Horie, A., Yoshida, A., Takahashi, K., Nishida, H., Lassak, K., Taka, H., Mineki, R., Fujimura, T., Kosono, S., Nishiyama, C., Masui, R., Kuramitsu, S., Albers, S. V., Kuzuyama, T., & Nishiyama, M. (2013). Lysine and arginine biosyntheses mediated by a common carrier protein in *Sulfolobus*. *Nature Chemical Biology* *2013* 9:4, *9*(4), 277–283. <https://doi.org/10.1038/nchembio.1200>
- Perera, I. C., & Grove, A. (2010). Molecular mechanisms of ligand-mediated attenuation of DNA binding by MarR family transcriptional regulators. *Journal of Molecular Cell Biology*, *2*(5), 243–254. <https://doi.org/10.1093/jmcb/mjq021>
- Pérez-Rueda, E., & Collado-Vides, J. (2001). Common History at the Origin of the Position–Function Correlation in Transcriptional Regulators in Archaea and Bacteria. *Journal of Molecular Evolution* *2001* 53:3, *53*(3), 172–179. <https://doi.org/10.1007/S002390010207>
- Plagens, A., Daume, M., Wiegel, J., & Randau, L. (2015). Circularization restores signal recognition particle RNA functionality in *Thermoproteus*. *ELife*. <https://doi.org/10.7554/eLife.11623.001>
- Qi, L., Li, J., Jia, J., Yue, L., & Dong, X. (2020). Comprehensive analysis of the pre-ribosomal RNA maturation pathway in a methanoarchaeon exposes the conserved circularization and linearization mode in archaea. *RNA Biology*, *17*(10), 1427–1441. <https://doi.org/10.1080/15476286.2020.1771946>
- Rachel, R., Bettstetter, M., Hedlund, B. P., Häring, M., Kessler, A., Stetter, K. O., & Prangishvili, D. (2002). Remarkable morphological diversity of viruses and virus-like particles in hot terrestrial environments. *Archives of Virology* *2002* 147:12, *147*(12), 2419–2429. <https://doi.org/10.1007/S00705-002-0895-2>

- Randau, L. (2012). RNA processing in the minimal organism *Nanoarchaeum equitans*. *Genome Biology*, 13(7). <https://doi.org/10.1186/gb-2012-13-7-r63>
- Randau, L., Calvin, K., Hall, M., Yuan, J., Podar, M., Li, H., & Söll, D. (2005). The heteromeric *Nanoarchaeum equitans* splicing endonuclease cleaves noncanonical bulge-helix-bulge motifs of joined tRNA halves. *Proceedings of the National Academy of Sciences of the United States of America*, 102(50), 17934–17939. <https://doi.org/10.1073/pnas.0509197102>
- Randau, L., Münch, R., Hohn, M. J., Jahn, D., & Söll, D. (2005). *Nanoarchaeum equitans* creates functional tRNAs from separate genes for their 5'- and 3'-halves. *Nature*, 433(7025), 537–541. <https://doi.org/10.1038/nature03233>
- Randau, L., & Söll, D. (2008). Transfer RNA genes in pieces. *EMBO Reports*, 9(7), 623–628. <https://doi.org/10.1038/embor.2008.101>
- Reimann, J., Lassak, K., Khadouma, S., Ettema, T. J. G., Yang, N., Driessen, A. J. M., Klingl, A., & Albers, S. V. (2012). Regulation of archaeella expression by the FHA and von Willebrand domain-containing proteins ArnA and ArnB in *Sulfolobus acidocaldarius*. *Molecular Microbiology*, 86(1), 24–36. <https://doi.org/10.1111/j.1365-2958.2012.08186.x>
- Rice, G., Stedman, K., Snyder, J., Wiedenheft, B., Willits, D., Brumfield, S., McDermott, T., & Young, M. J. (2001). Viruses from extreme thermal environments. *Proceedings of the National Academy of Sciences of the United States of America*, 98(23), 13341–13345.
- Richards, J., Liu, Q., Pellegrini, O., Celesnik, H., Yao, S., Bechhofer, D. H., Condon, C., & Belasco, J. G. (2011). An RNA Pyrophosphohydrolase Triggers 5'-Exonucleolytic Degradation of mRNA in *Bacillus subtilis*. *Molecular Cell*, 43(6), 940–949. <https://doi.org/10.1016/J.MOLCEL.2011.07.023>
- Robinson, J. T., Thorvaldsdóttir, H., Winckler, W., Guttman, M., Lander, E. S., Getz, G., & Mesirov, J. P. (2011). Integrative genomics viewer. *Nature Biotechnology* 2011 29:1, 29(1), 24–26. <https://doi.org/10.1038/nbt.1754>
- Rodionov, D. A., De Ingeniis, J., Mancini, C., Cimadamore, F., Zhang, H., Osterman, A. L., & Raffaelli, N. (2008). Transcriptional regulation of NAD metabolism in bacteria: NrtR family of Nudix-related regulators. *Nucleic Acids Research*, 36(6), 2047–2059. <https://doi.org/10.1093/nar/gkn047>
- Rose, M. A., & Weeks, K. M. (2001). Visualizing induced fit in early assembly of the human signal recognition particle. *Nature Structural Biology*, 8(6), 515–520. <https://doi.org/10.1038/88577>
- Rozhdestvensky, T. S., Tang, T. H., Tchirkova, I. V., Brosius, J., Bachellerie, J. P., & Hüttenhofer, A. (2003). Binding of L7Ae protein to the K-turn of archaeal snoRNAs: a shared RNA binding motif for C/D and H/ACA box snoRNAs in Archaea. *Nucleic Acids Research*, 31(3), 869–877. <https://doi.org/10.1093/NAR/GKG175>
- Rychel, K., Decker, K., Sastry, A. V., Phaneuf, P. V., Poudel, S., & Palsson, B. O. (2021). iModulonDB: a knowledgebase of microbial transcriptional regulation derived from machine learning. *Nucleic Acids Research*, 49(D1), D112–D120. <https://doi.org/10.1093/NAR/GKAA810>
- Saiki, R. K., Gelfand, D. H., Stoffel, S., Scharf, S. J., Higuchi, R., Horn, G. T., Mullis, K. B., & Erlich, H. A. (1988). Primer-directed enzymatic amplification of DNA with a thermostable DNA polymerase. *Science*, 239(4839), 487–491. <https://doi.org/10.1126/science.2448875>
- Schattner, P. (2002). Searching for RNA genes using base-composition statistics. *Nucleic Acids Research*, 30(9), 2076–2082. <https://doi.org/10.1093/NAR/30.9.2076>
- Schindelin, J., Arganda-Carreras, I., Frise, E., Kaynig, V., Longair, M., Pietzsch, T., Preibisch, S., Rueden, C., Saalfeld, S., Schmid, B., Tinevez, J. Y., White, D. J., Hartenstein, V., Eliceiri, K., Tomancak, P., & Cardona, A. (2012). Fiji: an open-source platform for biological-image analysis.

- Nature Methods* 2012 9:7, 9(7), 676–682. <https://doi.org/10.1038/nmeth.2019>
- Schult, F., Le, T. N., Albersmeier, A., Rauch, B., Blumenkamp, P., Van Der Does, C., Goesmann, A., Kalinowski, J., Albers, S. V., & Siebers, B. (2018). Effect of UV irradiation on *Sulfolobus acidocaldarius* and involvement of the general transcription factor TFB3 in the early UV response. *Nucleic Acids Research*, 46(14), 7179–7192. <https://doi.org/10.1093/NAR/GKY527>
- Schwarz, T. S., Berkemer, S. J., Bernhart, S. H., Weiß, M., Ferreira-Cerca, S., Stadler, P. F., & Marchfelder, A. (2020). Splicing Endonuclease Is an Important Player in rRNA and tRNA Maturation in Archaea. *Frontiers in Microbiology*, 11(November), 1–15. <https://doi.org/10.3389/fmicb.2020.594838>
- Sheikh, S., O'Handley, S. F., Dunn, C. A., & Bessman, M. J. (1998). Identification and characterization of the Nudix hydrolase from the Archaeon, *Methanococcus jannaschii*, as a highly specific ADP-ribose pyrophosphatase. *Journal of Biological Chemistry*, 273(33), 20924–20928. <https://doi.org/10.1074/jbc.273.33.20924>
- Siebers, B., Zaparty, M., Raddatz, G., Tjaden, B., Albers, S.-V., Bell, S. D., Blombach, F., Kletzin, A., Kyrpides, N., Lanz, C., Plagens, A., Rampp, M., Rosinus, A., von Jan, M., Makarova, K. S., Klenk, H.-P., Schuster, S. C., & Hensel, R. (2011). The Complete Genome Sequence of *Thermoproteus tenax*: A Physiologically Versatile Member of the Crenarchaeota. *PLoS ONE*, 6(10), e24222. <https://doi.org/10.1371/journal.pone.0024222>
- Song, M.-G., Bail, S., & Kiledjian, M. (2013). Multiple Nudix family proteins possess mRNA decapping activity. *RNA (New York, N.Y.)*, 19(3), 390–399. <https://doi.org/10.1261/rna.037309.112>
- Song, M.-G., Li, Y., & Kiledjian, M. (2010). Multiple mRNA Decapping Enzymes in Mammalian Cells. *Molecular Cell*, 40(3), 423–432. <https://doi.org/10.1016/j.molcel.2010.10.010>
- Spang, A., Saw, J. H., Jørgensen, S. L., Zaremba-Niedzwiedzka, K., Martijn, J., Lind, A. E., Van Eijk, R., Schleper, C., Guy, L., & Ettema, T. J. G. (2015). Complex archaea that bridge the gap between prokaryotes and eukaryotes. *Nature*, 521(7551), 173. <https://doi.org/10.1038/NATURE14447>
- Srouji, J. R., Xu, A., Park, A., Kirsch, J. F., & Brenner, S. E. (2017). The evolution of function within the Nudix homology clan. *Proteins: Structure, Function and Bioinformatics*, 85(5), 775–811. <https://doi.org/10.1002/prot.25223>
- Starostina, N. G., Marshburn, S., Johnson, L. S., Eddy, S. R., Terns, R. M., & Terns, M. P. (2004). Circular box C/D RNAs in *Pyrococcus furiosus*. *Proceedings of the National Academy of Sciences of the United States of America*, 101(39), 14097–14101. <https://doi.org/10.1073/pnas.0403520101>
- Su, A. A. H., Tripp, V., & Randau, L. (2013). RNA-Seq analyses reveal the order of tRNA processing events and the maturation of C/D box and CRISPR RNAs in the hyperthermophile *Methanopyrus kandleri*. *Nucleic Acids Research*, 41(12), 6250–6258. <https://doi.org/10.1093/nar/gkt317>
- Sugahara, J., Kikuta, K., Fujishima, K., Yachie, N., Tomita, M., & Kanai, A. (2008). Comprehensive analysis of archaeal tRNA genes reveals rapid increase of tRNA introns in the order thermoproteales. *Molecular Biology and Evolution*, 25(12), 2709–2716. <https://doi.org/10.1093/molbev/msn216>
- Szabó, Z., Sani, M., Groeneveld, M., Zolghadr, B., Schelert, J., Albers, S. V., Blum, P., Boekema, E. J., & Driessen, A. J. M. (2007). Flagellar motility and structure in the hyperthermoacidophilic archaeon *Sulfolobus solfataricus*. *Journal of Bacteriology*, 189(11), 4305–4309. <https://doi.org/10.1128/JB.00042-07>

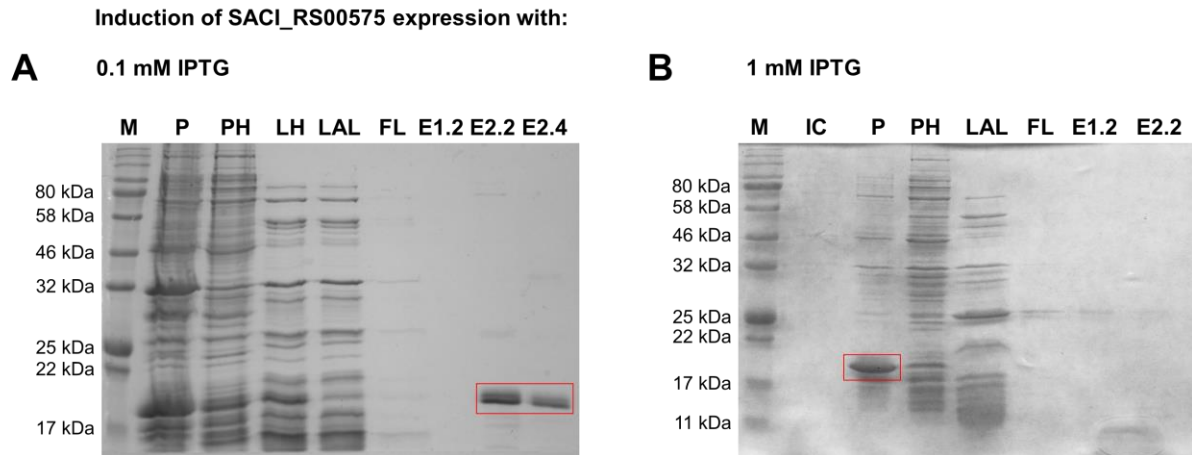
- Tachdjian, S., & Kelly, R. M. (2006). Dynamic metabolic adjustments and genome plasticity are implicated in the heat shock response of the extremely thermoacidophilic archaeon *Sulfolobus solfataricus*. *Journal of Bacteriology*, *188*(12), 4553–4559. <https://doi.org/10.1128/JB.00080-06>
- Takai, K., Nakamura, K., Toki, T., Tsunogai, U., Miyazaki, M., Miyazaki, J., Hirayama, H., Nakagawa, S., Nunoura, T., & Horikoshi, K. (2008). Cell proliferation at 122°C and isotopically heavy CH₄ production by a hyperthermophilic methanogen under high-pressure cultivation. *Proceedings of the National Academy of Sciences*, *105*(31), 10949–10954. <https://doi.org/10.1073/pnas.0712334105>
- Tang, T. H., Rozhdestvensky, T. S., D’Orval, B. C., Bortolin, M. L., Huber, H., Charpentier, B., Branlant, C., Bachelier, J. P., Brosius, J., & Hüttenhofer, A. (2002). RNomics in Archaea reveals a further link between splicing of archaeal introns and rRNA processing. *Nucleic Acids Research*, *30*(4), 921–930. <https://doi.org/10.1093/nar/30.4.921>
- Tatusov, R. L., Galperin, M. Y., Natale, D. A., & Koonin, E. V. (2000). The COG database: a tool for genome-scale analysis of protein functions and evolution. *Nucleic Acids Research*, *28*(1), 33. <https://doi.org/10.1093/NAR/28.1.33>
- Thompson, L. D., & Daniels, C. J. (1990). Recognition of exon-intron boundaries by the *Halobacterium volcanii* tRNA intron endonuclease. *Journal of Biological Chemistry*, *265*(30), 18104–18111. [https://doi.org/10.1016/S0021-9258\(17\)44723-5](https://doi.org/10.1016/S0021-9258(17)44723-5)
- Thompson, Leo D, & Daniels, J. (1988). A tRNA-Trp Intron Endonuclease from *Halobacterium volcanii*. *Journal of Biological Chemistry*, *263*(34), 17951–17959.
- Tocchini-Valentini, G. D., Fruscoloni, P., & Tocchini-Valentini, G. P. (2005a). Coevolution of tRNA intron motifs and tRNA endonuclease architecture in Archaea. *Proceedings of the National Academy of Sciences of the United States of America*, *102*(43), 15418–15422. <https://doi.org/10.1073/pnas.0506750102>
- Tocchini-Valentini, G. D., Fruscoloni, P., & Tocchini-Valentini, G. P. (2005b). Structure, function, and evolution of the tRNA endonucleases of Archaea: An example of subfunctionalization. *Proceedings of the National Academy of Sciences of the United States of America*, *102*(25), 8933–8938. <https://doi.org/10.1073/pnas.88.2.439>
- van der Kolk, N., Wagner, A., Wagner, M., Waßmer, B., Siebers, B., & Albers, S. V. (2020). Identification of XylR, the Activator of Arabinose/Xylose Inducible Regulon in *Sulfolobus acidocaldarius* and Its Application for Homologous Protein Expression. *Frontiers in Microbiology*, *11*, 1066. <https://doi.org/10.3389/fmicb.2020.01066>
- Van Dijk, E., Cougot, N., Meyer, S., Babajko, S., Wahle, E., & Séraphin, B. (2002). Human Dcp2: A catalytically active mRNA decapping enzyme located in specific cytoplasmic structures. *EMBO Journal*, *21*(24), 6915–6924. <https://doi.org/10.1093/emboj/cdf678>
- Varadi, M., Anyango, S., Deshpande, M., Nair, S., Natassia, C., Yordanova, G., Yuan, D., Stroe, O., Wood, G., Laydon, A., Zidek, A., Green, T., Tunyasuvunakool, K., Petersen, S., Jumper, J., Clancy, E., Green, R., Vora, A., Lutfi, M., Figurnov, M., Cowie, A., Hobbs, N., Kohli, P., Kleywegt, G., Birney, E., Hassabis, D. Velankar, S. (2022). AlphaFold Protein Structure Database: massively expanding the structural coverage of protein-sequence space with high-accuracy models. *Nucleic Acids Research*, *50*(D1), D439–D444. <https://doi.org/10.1093/NAR/GKAB1061>
- Wagner, M., van Wolferen, M., Wagner, A., Lassak, K., Meyer, B. H., Reimann, J., & Albers, S. V. (2012). Versatile genetic tool box for the crenarchaeote *Sulfolobus acidocaldarius*. *Frontiers in Microbiology*, *3*(JUN), 1–12. <https://doi.org/10.3389/fmicb.2012.00214>

- Walters, R. W., Matheny, T., Mizoue, L. S., Rao, B. S., Muhlrad, D., & Parker, R. (2017). Identification of NAD⁺ capped mRNAs in *Saccharomyces cerevisiae*. *Proceedings of the National Academy of Sciences of the United States of America*, *114*(3), 480–485. <https://doi.org/10.1073/pnas.1619369114>
- Wang, J., Alvin Chew, B. L., Lai, Y., Dong, H., Xu, L., Balamkundu, S., Cai, W. M., Cui, L., Liu, C. F., Fu, X. Y., Lin, Z., Shi, P. Y., Lu, T. K., Luo, D., Jaffrey, S. R., & Dedon, P. C. (2019). Quantifying the RNA cap epitranscriptome reveals novel caps in cellular and viral RNA. *Nucleic Acids Research*, *47*(20), e130–e130. <https://doi.org/10.1093/NAR/GKZ751>
- Wang, K., Sybers, D., Maklad, H. R., Lemmens, L., Lewyllie, C., Zhou, X., Schult, F., Bräsen, C., Siebers, B., Valegård, K., Lindås, A. C., & Peeters, E. (2019). A TetR-family transcription factor regulates fatty acid metabolism in the archaeal model organism *Sulfolobus acidocaldarius*. *Nature Communications* *2019 10:1*, *10*(1), 1–16. <https://doi.org/10.1038/s41467-019-09479-1>
- Wang, W., Kim, R., Jancarik, J., Yokota, H., & Kim, S. H. (2001). Crystal structure of phosphoserine phosphatase from *Methanococcus jannaschii*, a hyperthermophile, at 1.8 Å resolution. *Structure*, *9*(1), 65–71. [https://doi.org/10.1016/S0969-2126\(00\)00558-X](https://doi.org/10.1016/S0969-2126(00)00558-X)
- Wang, W., & Malcolm, B. A. (1999). Two-stage PCR protocol allowing introduction of multiple mutations, deletions and insertions using QuikChange Site-Directed Mutagenesis. *BioTechniques*, *26*(4), 680–682. <https://doi.org/10.2144/99264st03>
- Wang, Y., & Wang, Z. (2015). Efficient backsplicing produces translatable circular mRNAs. *Rna*, *21*(2), 172–179. <https://doi.org/10.1261/rna.048272.114>
- Wang, Z., Jiao, X., Carr-Schmid, A., & Kiledjian, M. (2002). The hDcp2 protein is a mammalian mRNA decapping enzyme. *Proceedings of the National Academy of Sciences of the United States of America*, *99*(20), 12663–12668. <https://doi.org/10.1073/pnas.192445599>
- Wang, Z., & Kiledjian, M. (2001). Functional Link between the Mammalian Exosome and mRNA Decapping. *Cell*, *107*(6), 751–762. [https://doi.org/10.1016/S0092-8674\(01\)00592-X](https://doi.org/10.1016/S0092-8674(01)00592-X)
- Watanabe, Y., Yokobori, S., Inaba, T., Yamagishi, A., Oshima, T., Kawarabayasi, Y., Kikuchi, H., & Kita, K. (2002). Introns in protein-coding genes in Archaea. *FEBS Letters*, *510*(1–2), 27–30. [https://doi.org/10.1016/S0014-5793\(01\)03219-7](https://doi.org/10.1016/S0014-5793(01)03219-7)
- Wei, C.-M., Gershowitz, A., & Moss, B. (1975). Methylated nucleotides block 5' terminus of HeLa cell messenger RNA. *Cell*, *4*(4), 379–386. [https://doi.org/10.1016/0092-8674\(75\)90158-0](https://doi.org/10.1016/0092-8674(75)90158-0)
- Weixler, L., Feijs, K. L. H., & Zaja, R. (2022). ADP-ribosylation of RNA in mammalian cells is mediated by TRPT1 and multiple PARPs. *Nucleic Acids Research*. <https://doi.org/10.1093/nar/gkac711>
- Wiedermannová, J., Julius, C., & Yuzenkova, Y. (2021). The expanding field of non-canonical RNA capping: new enzymes and mechanisms. *Royal Society Open Science*, *8*(5). <https://doi.org/10.1098/RSOS.201979>
- Winz, M.-L., Cahová, H., Nübel, G., Frindert, J., Höfer, K., & Jäschke, A. (2017). Capture and sequencing of NAD-capped RNA sequences with NAD captureSeq. *Nature Protocols*, *12*(1), 122–149. <https://doi.org/10.1038/nprot.2016.163>
- Woese, C. R., & Fox, G. E. (1977). Phylogenetic structure of the prokaryotic domain: The primary kingdoms. *Proceedings of the National Academy of Sciences of the United States of America*, *74*(11), 5088–5090.
- Woese, Carl R, Kandler, O., & Wheelis, M. L. (1990). Towards a natural system of organisms: Proposal for the domains Archaea, Bacteria, and Eucarya (Euryarchaeota/Crenarchaeota/kingdom/evolution). *Proc. Natl. Acad. Sci. USA*, *87*, 4576–4579.

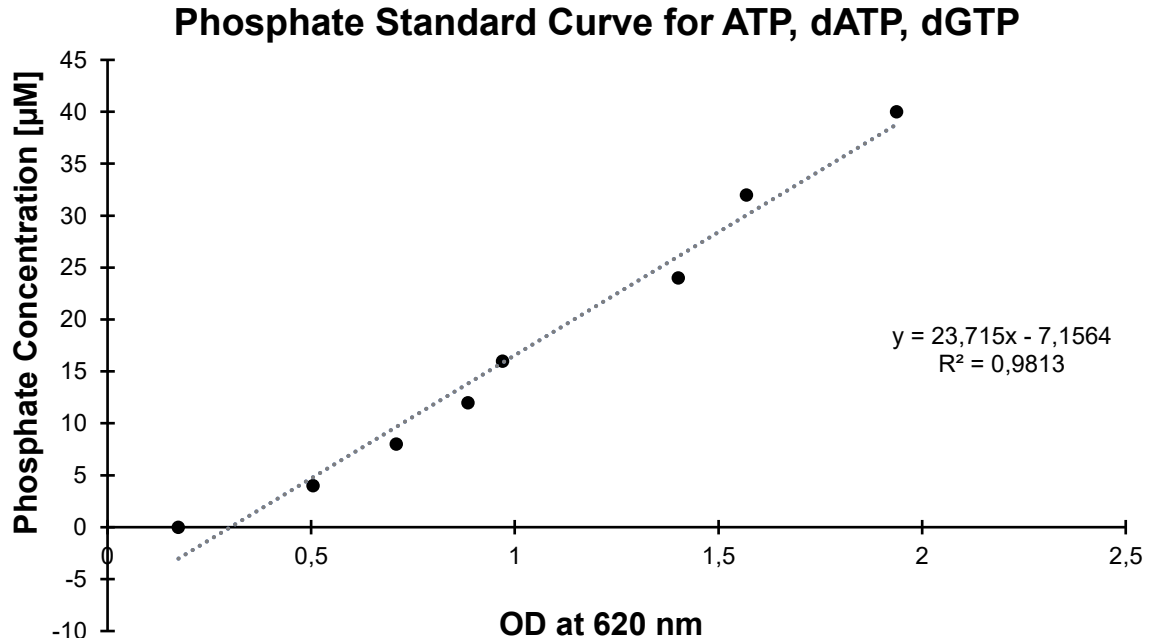
- Xia, Q., Wang, T., Hendrickson, E. L., Lie, T. J., Hackett, M., & Leigh, J. A. (2009). Quantitative proteomics of nutrient limitation in the hydrogenotrophic methanogen *Methanococcus maripaludis*. *BMC Microbiology*, 9, 1–10. <https://doi.org/10.1186/1471-2180-9-149>
- Xiang, S., Cooper-Morgan, A., Jiao, X., Kiledjian, M., Manley, J. L., & Tong, L. (2009). Structure and function of the 5'→3' exoribonuclease Rat1 and its activating partner Rai1. *Nature*, 458(7239), 784–788. <https://doi.org/10.1038/nature07731>
- Xu, A., Desai, A. M., Brenner, S. E., & Kirsch, J. F. (2013). A continuous fluorescence assay for the characterization of Nudix hydrolases. *Analytical Biochemistry*, 437(2), 178–184. <https://doi.org/10.1016/j.ab.2013.02.023>
- Yang, H., Slupska, M. M., Wei, Y. F., Tai, J. H., Luther, W. M., Xia, Y. R., Shih, D. M., Chiang, J. H., Baikalov, C., Fitz-Gibbon, S., Phan, I. T., Conrad, A., & Miller, J. H. (2000). Cloning and characterization of a new member of the nudix hydrolases from human and mouse. *Journal of Biological Chemistry*, 275(12), 8844–8853. <https://doi.org/10.1074/jbc.275.12.8844>
- Yip, W. S. V., Vincent, N. G., & Baserga, S. J. (2013). Ribonucleoproteins in Archaeal Pre-rRNA Processing and Modification. *Archaea*, 2013, 1–14. <https://doi.org/10.1155/2013/614735>
- Yoshinari, S., Fujita, S., Masui, R., Kuramitsu, S., Yokobori, S. I., Kita, K., & Watanabe, Y. I. (2005). Functional reconstitution of a crenarchaeal splicing endonuclease in vitro. *Biochemical and Biophysical Research Communications*, 334(4), 1254–1259. <https://doi.org/10.1016/j.bbrc.2005.07.023>
- Yoshinari, S., Shiba, T., Inaoka, D. K., Itoh, T., Kurisu, G., Harada, S., Kita, K., & Watanabe, Y. I. (2009). Functional importance of Crenarchaea-specific extra-loop revealed by an X-ray structure of a heterotetrameric crenarchaeal splicing endonuclease. *Nucleic Acids Research*, 37(14), 4787–4798. <https://doi.org/10.1093/nar/gkp506>
- Zaremba-Niedzwiedzka, K., Caceres, E. F., Saw, J. H., Bäckström, D., Juzokaite, L., Vancaester, E., Seitz, K. W., Anantharaman, K., Starnawski, P., Kjeldsen, K. U., Stott, M. B., Nunoura, T., Banfield, J. F., Schramm, A., Baker, B. J., Spang, A., & Ettema, T. J. G. (2017). Asgard archaea illuminate the origin of eukaryotic cellular complexity. *Nature* 2017 541:7637, 541(7637), 353–358. <https://doi.org/10.1038/nature21031>
- Zha, M., Zhong, C., Peng, Y., Hu, H., & Ding, J. (2006). Crystal structures of human NUDT5 reveal insights into the structural basis of the substrate specificity. *Journal of Molecular Biology*, 364(5), 1021–1033. <https://doi.org/10.1016/J.JMB.2006.09.078>
- Zhang, D., Liu, Y., Wang, Q., Guan, Z., Wang, J., Liu, J., Zou, T., & Yin, P. (2016). Structural basis of prokaryotic NAD-RNA decapping by NudC. *Cell Research*, 26(9), 1062–1066. <https://doi.org/10.1038/cr.2016.98>
- Zwieb, C., Van Nues, R. W., Rosenblad, M. A., Brown, J. D., & Samuelsson, T. (2005). A nomenclature for all signal recognition particle RNAs. *Spring*, 48, 7–13. <https://doi.org/10.1261/rna.7203605>

6 Appendix

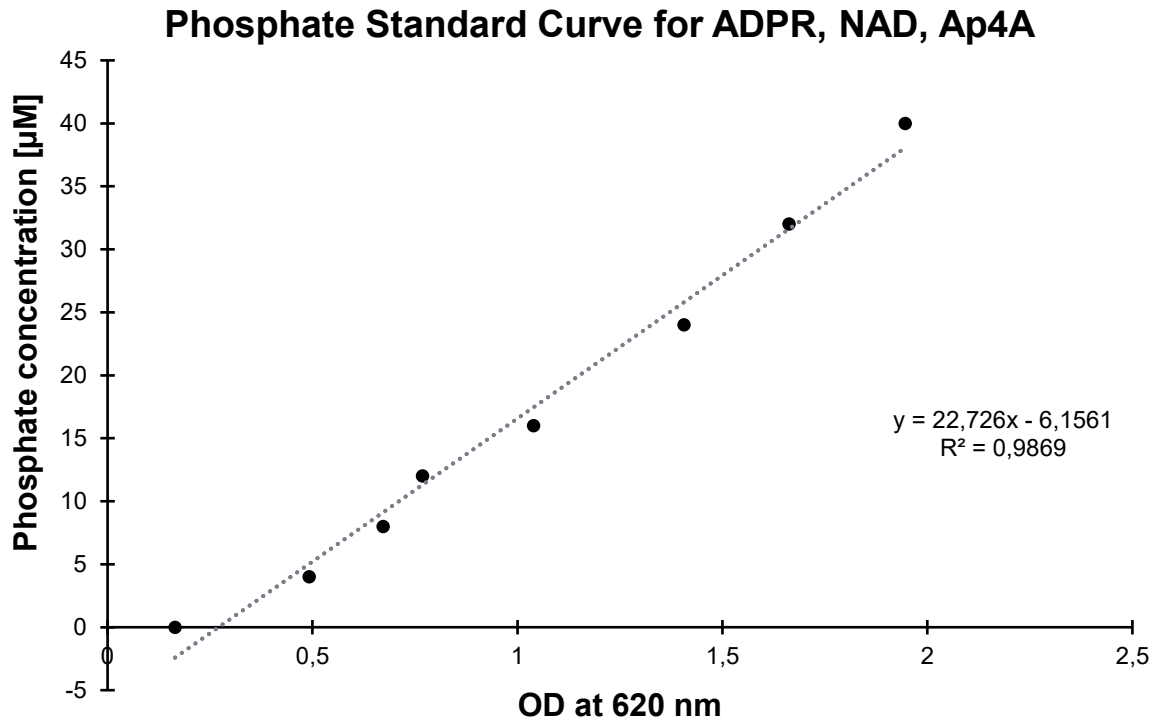
6.1 Supplementary Material



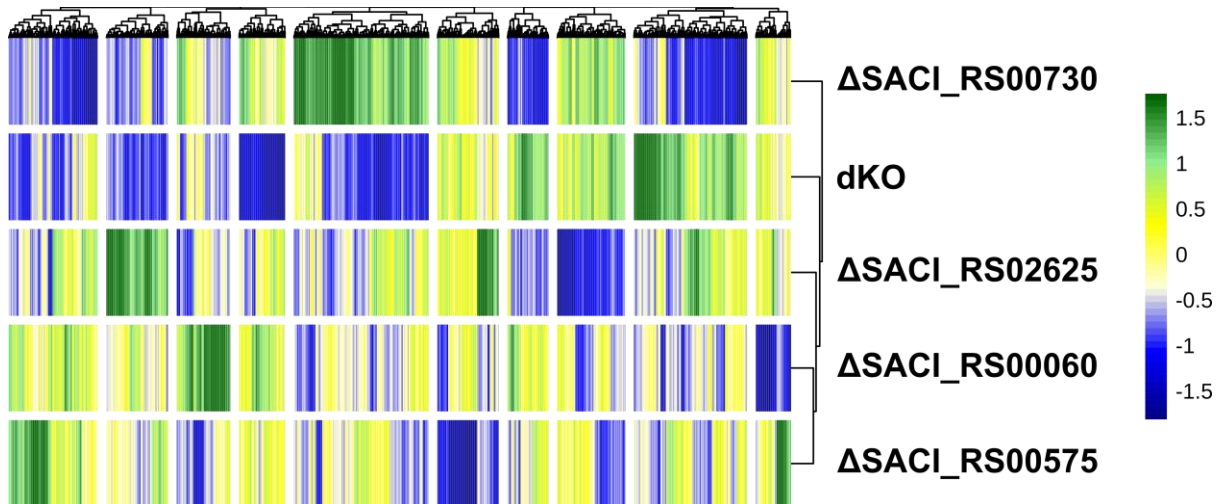
Supplementary Figure S1: Recombinant production of the Nudix family hydrolase SACI_RS00575 from *S. acidocaldarius* using different inducer concentrations. Expression of the recombinant protein in *E. coli* Rosetta 2 DE3 pLysS cells was induced using A) 0.1 mM IPTG and B) 1 mM IPTG. Samples from purification via Ni-NTA chromatography and elution fractions were analyzed via SDS-PAGE. Black arrows indicate the protein band at 18 kDa. M = marker, IC = induction control, P = pellet, PH = pellet after heat treatment, LH = lysate after heat treatment, LAL = lysate after column loading, FL = flowthrough, Ex.x = elution buffer no. x fraction no. x.



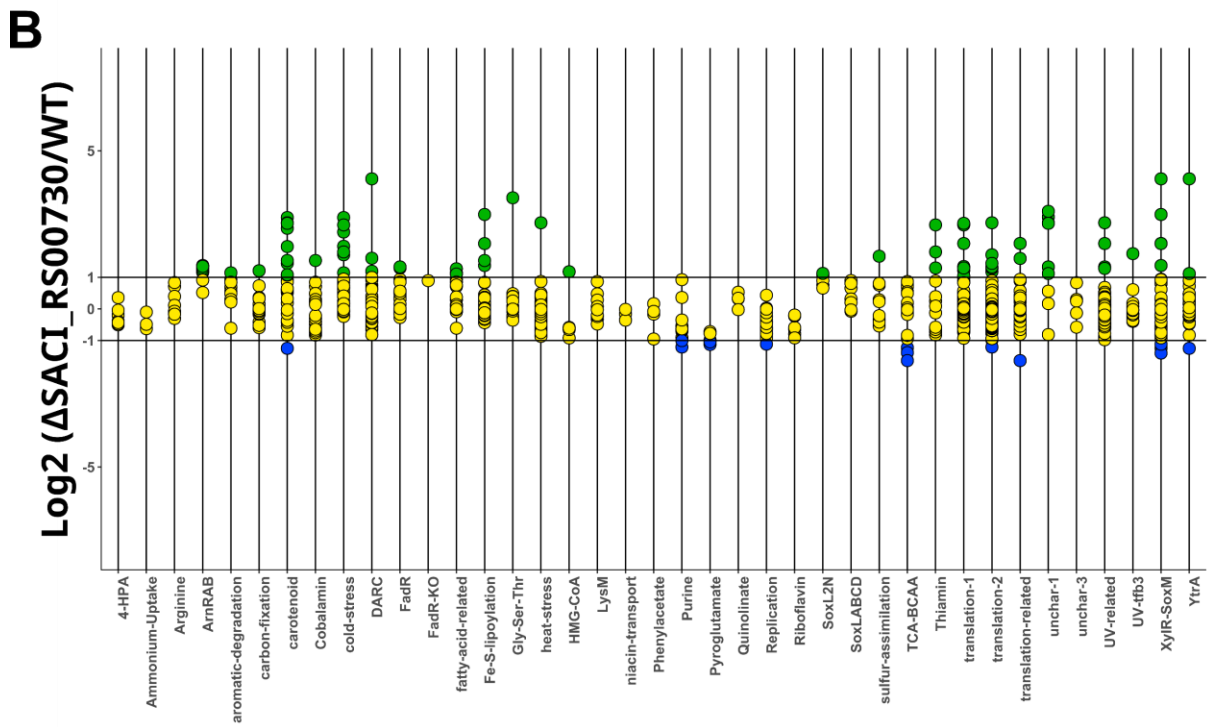
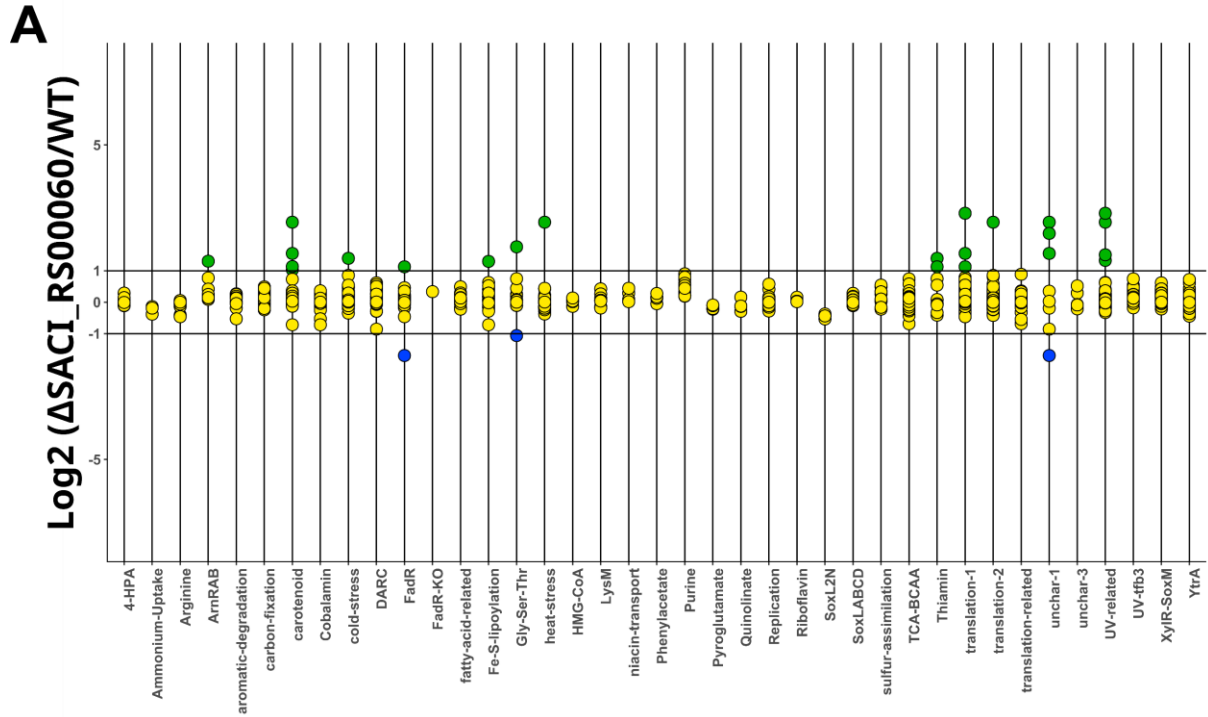
Supplementary Figure S2: Phosphate standard curve for the Malachite Green assays with the substrates ATP, dATP and dGTP. Phosphate standards were prepared in duplicates according to the manufacturer's instructions, absorbance was measured in a plate reader at 620 nm and OD values were plotted against phosphate concentration [µM].



Supplementary Figure S3: Phosphate standard curve for the Malachite Green assays with the substrates NAD, ADPR and Ap4A. Phosphate standards were prepared in duplicates according to the manufacturer's instructions, absorbance was measured in a plate reader at 620 nm and OD values were plotted against phosphate concentration [μM].

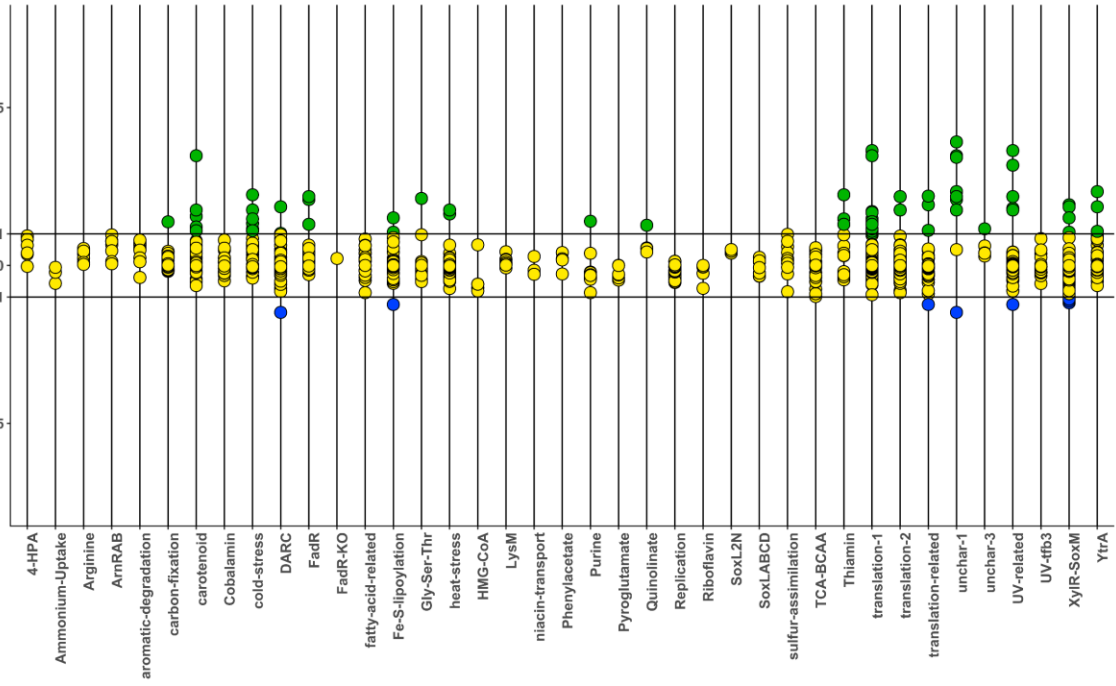


Supplementary Figure S4: Heatmap of the \log_2 (FoldChange) of the transcriptome of the Nudix deletion strains in relation to the WT strain *S. acidocaldarius* DSM639 MW001 in the mid-logarithmic growth phase. Genes were hierarchically clustered according to their expression behavior in the samples. The dendrogram represents Euclidean distances. Green: upregulated genes, blue: downregulated genes, yellow: not affected. Heatmap generated by José Vicente Gomes-Filho.



C

Log2 (Δ SACI_RS02625/WT)



D

Log2 (Δ SACI_RS00575/WT)

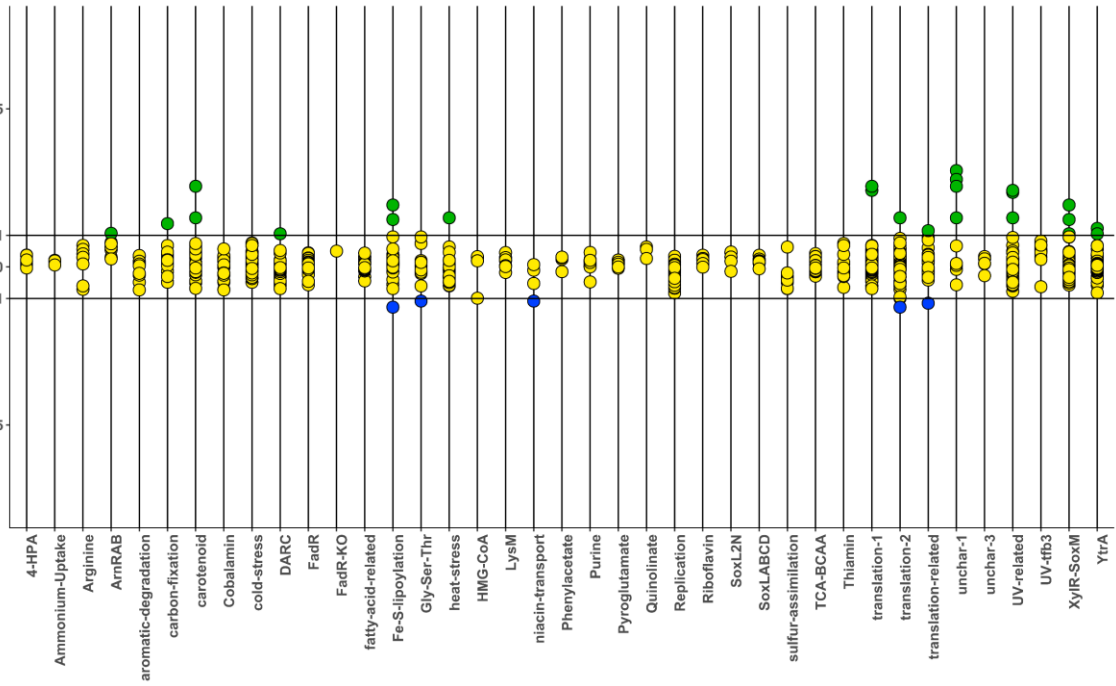
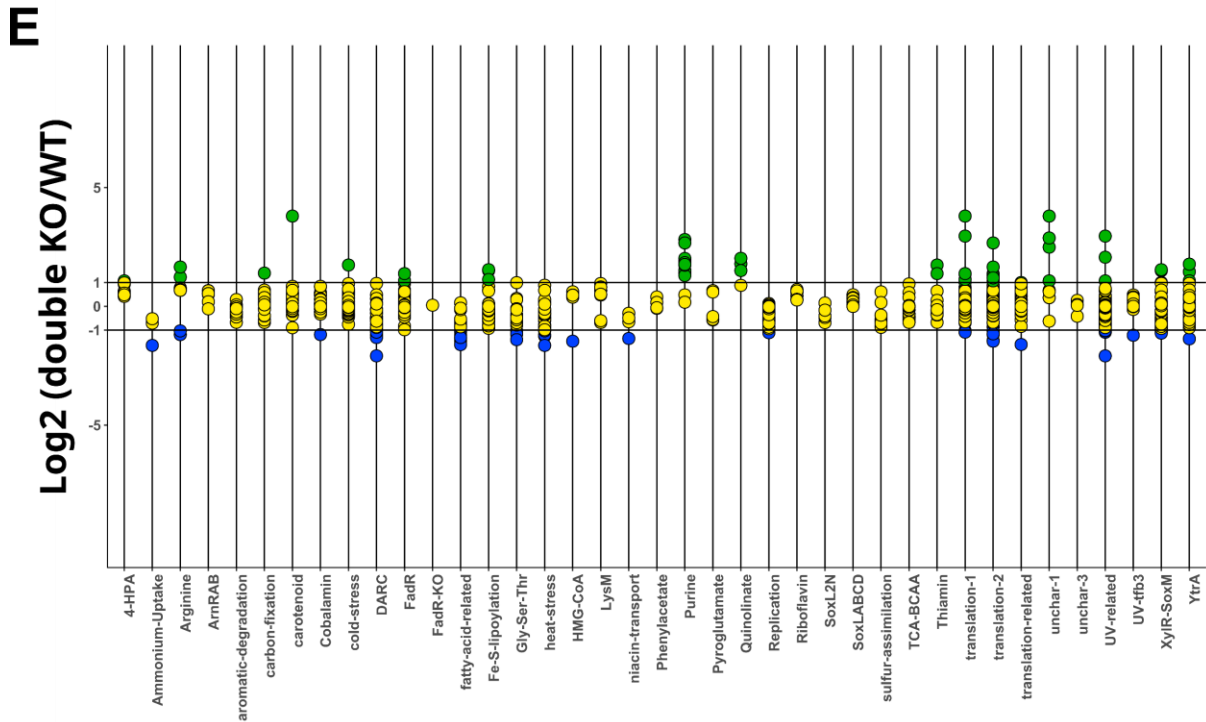


Figure continued on the next page



Supplementary Figure S5: Dot Plots of differentially regulated genes in the Nudix deletion strains in the mid-logarithmic growth phase. Log₂ (FoldChange) in relation to the WT strain *S. acidocaldarius* DSM639 MW001 for A) Δ SACI_RS00730, B) Δ SACI_RS00060, C) Δ SACI_RS02625, D) Δ SACI_RS00575 and E) the double KO strain. Green: upregulated genes, blue: downregulated genes, yellow: not affected. Genes were assembled into clusters of similarly expressed genes based on the iModulonDB database (Chauhan et al., 2021; Rychel et al., 2021). Dot Plots generated by José Vicente Gomes-Filho.

Supplementary Table S1: Overview of iModulons in *S. acidocaldarius* DSM639 with associated regulators and functions. Sourced from imodulondb.org (Chauhan et al., 2021; Rychel et al., 2021).

No.	Name	Regulator	Function	Category	No. of genes in iModulon
0	Pseudogene			Genomic	2
1	Heat-stress			Stress Response	38
2	SoxL2N		Cytochrome Oxidase bc1 complex (SoxL2N-CbsAB-OdsN)	Other Functional	5
3	Fatty-acid-related			Misc Metabolism	17
4	Riboflavin			Vitamin B	6
5	Niacin-transport			Vitamin B	4
6	Cold-stress			Stress Response	38
7	Carbon-fixation			Misc Metabolism	17
8	Fe-S-lipoylation			Other Functional	40
9	HMG-CoA			Misc Metabolism	5
10	Purine			Amino Acid & Nucleotide Biosynthesis	13

Table continued on the next page

11	XylR-SoxM	XylR		Misc Metabolism	47
12	YtrA	YtrA		Other Functional	37
13	LysM	LysM	Lysine biosynthesis	Amino Acid & Nucleotide Biosynthesis	10
14	Phenylacetate			Misc Metabolism	4
15	Single_gene_1			Uncharacterized	1
16	Single_gene_2			Uncharacterized	1
17	Translation-1			Other Functional	122
18	UV-tfb3	tfb3	tfb3-dependent UV stress response	Stress Response	16
19	Arginine		Arginine biosynthesis	Amino Acid & Nucleotide Biosynthesis	8
20	Pyro-glutamate			Amino Acid & Nucleotide Biosynthesis	6
21	Translation-2			Other Functional	146
22	Unchar-1		Unknown Function	Uncharacterized	12
23	Sulfur-assimilation			Amino Acid & Nucleotide Biosynthesis	10
24	FadR-KO		Accounts for fadR knock-out	Genomic	1
25	Cobalamin			Vitamin B	24
26	4-HPA		4-hydroxyphenylacetate	Misc Metabolism	7
27	ArnRAB	ArnR, ArnR1, ArnA, ArnB	Archaeallum formation operon	Other Functional	8
28	Single_gene_3			Uncharacterized	1
29	FadR	FadR	Fatty acid degradation	Misc Metabolism	25
30	SoxLABCD		SoxLABCD terminal oxidase gene cluster	Other Functional	8
31	TCA-BCAA			Amino Acid & Nucleotide Biosynthesis	18
32	UV-related			Stress Response	74
33	DARC		Unknown Function	Uncharacterized	33
34	Replication		Replication and Cell Division	Other Functional	39
35	Translation-related			Other Functional	33
36	Quinolate			Other Functional	4
37	Aromatic-degradation			Misc Metabolism	10
38	Ammonium-Uptake			Other Functional	3
39	Carotenoid			Other Functional	28
40	Single_gene_4			Uncharacterized	1
41	Thiamin			Vitamin B	14
42	Unchar-3		Unknown Function	Uncharacterized	6
43	Single_gene_5			Uncharacterized	1
44	Gly-Ser-Thr			Amino Acid & Nucleotide Biosynthesis	14

6.2 Abgrenzung der Eigenleistung

Die in dieser Arbeit präsentierten Ergebnisse wurden von mir selbständig ohne andere als die hier aufgeführte Hilfe durchgeführt. Im Folgenden werden weitere an dieser Arbeit beteiligte Personen sowie deren experimentellen Beiträge genannt:

Dr. José Vicente Gomes-Filho (AG Randau, Philipps-Universität Marburg) :

Hat die Decapping Assays, die *in vitro* Transkription zur Generierung des Substrats und die Aufreinigung des Proteins hNudT5 für dieselben durchgeführt und die Bilder für die Abbildungen 2.8, 2.9 und 2.10 bereitgestellt. Hat den Sequenziervorgang zur Identifizierung der zirkulären SRP RNA durchgeführt und bei beiden Sequenziervorgängen (SRP RNA-Identifizierung und Nudix-Transkriptom) die anschließende Qualitätskontrolle, Datenprozessierung und Alignments durchgeführt, sowie die Coverage Plots und Reads für Abb. 2.2, die Heatmaps in Abb. 2.24 und S4 und die Dot Plots in Abb. 2.25 und S5 bereitgestellt.

6.3 Curriculum Vitae

Diese Seite enthält persönliche Daten. Sie ist deshalb nicht Bestandteil der Online-Veröffentlichung.

Diese Seite enthält persönliche Daten. Sie ist deshalb nicht Bestandteil der Online-Veröffentlichung.

6.4 Acknowledgements

Zuallererst möchte ich mich bedanken bei Prof. Dr. Lennart Randau, für die Möglichkeit mein Dissertationsprojekt in seinem Labor durchführen zu dürfen, sowie für die herausragende Betreuung und die anhaltende Unterstützung meiner Arbeit.

Weiterhin bedanke ich mich bei Prof. Dr. Michael Bölker für die Übernahme des Zweitgutachtens, sowie bei den Mitgliedern meiner Prüfungskommission, Prof. Dr. Julia Weigand und Prof. Dr. Martin Thanbichler. Außerdem möchte ich mich bei den Mitgliedern meines Thesis Advisory Committees, Prof. Dr. Anke Becker und Prof. Dr. Gert Bange, für die Ratschläge und Unterstützung im Verlaufe des Projektes bedanken.

Ein großer Dank gilt meinem Kollegen Dr. José Vicente Gomes Filho, für die großartige Unterstützung von Anfang an, die vielen anregenden Diskussion (zu wissenschaftlichen und nicht-wissenschaftlichen Themen) und eine insgesamt tolle Zusammenarbeit, in deren Verlauf ich so viel gelernt habe.

Bedanken möchte ich mich außerdem bei allen weiteren Kolleg*innen der AG Randau, aktuellen und ehemaligen, insbesondere bei Julia Wiegel und Hanna Müller Esparza, für ihre Freundschaft, Geduld und Hilfsbereitschaft. Die kollegiale und freundschaftliche Arbeitsatmosphäre zu der ihr alle jeden Tag beiträgt, hat diese Zeit besonders geprägt und ich hätte mit keiner anderen Gruppe zweimal innerhalb eines Jahres umziehen wollen!

Zu guter Letzt möchte ich mich bei meiner Familie und Freunden bedanken, sowie den Kolleg*innen und Freunden aus benachbarten AGs, für Aufmunterung oder Ablenkung (je nachdem was nötig war) und die anhaltenden Unterstützung dieses Vorhabens vor allem in seiner finalen Phase. Ich danke euch allen!